THE GEOLOGY AND MINERALIZATION OF THE ANTLER MINE AND VICINITY, MOHAVE COUNTY, ARIZONA

by

Syver Wakeman More

A Thesis Submitted to the Faculty of the

DEPARTMENT OF GEOSCIENCES

In Partial Fulfillment of the Requirements
For the Degree of

MASTER OF SCIENCE

In the Graduate College

THE UNIVERSITY OF ARIZONA

1 9 8 0

STATEMENT BY AUTHOR

This thesis has been submitted in partial fulfillment of requirements for an advanced degree at The University of Arizona and is deposited in the University Library to be made available to borrowers under rules of the Library.

Brief quotations from this thesis are allowable without special permission, provided that accurate acknowledgment of source is made. Requests for permission for extended quotation from or reproduction of this manuscript in whole or in part may be granted by the head of the major department or the Dean of the Graduate College when in his judgment the proposed use of the material is in the interests of scholarship. In all other instances, however, permission must be obtained from the author.

SIGNED: Lynn W. More

APPROVAL BY THESIS DIRECTOR

This thesis has been approved on the date shown below:

John M Guilbert
J. M. GUILBERT
Professor of Geosciences

December 21, 1979
Date

ACKNOWLEDGMENTS

This study and the resulting thesis would not have been possible without the aid and support of many individuals and institutions. Mr. Clancy Wendt, Philips Uranium, introduced me to the field problem and shared several field days with me. Mr. Richard Dwelley, Standard Metals Corporation, permitted my access to the property, reports, and drillcore from the Antler Mine. Mr. Steve Tima, Bobcat Mining Company, permitted access to the Copper World Mine. Drs. Paul Gilmour and Arthur Still provided time and insight into the Antler property from their past experience with it. Several of the ideas presented in this thesis were first proposed by Paul or Art, and due credit is extended to both of them. I would also like to thank Mr. James Lukanuski and Mr. Richard Loring, Continental Oil Company, for their aid and encouragement.

Dr. John Guilbert, my thesis advisor, provided me with the impetus to expand my investigative horizons. His constructive criticism, patience, and humor has certainly helped me over the rough spots. Dr. Howard Stensrud has overlapped with me on many aspects of Hualapai geology, and I have profited greatly from our collaboration. Drs. Richard Beane, George Davis, and William Peters have assisted at various stages of the thesis and unhesitatingly provided counsel. Jerre, Spence, and Vence Cavalliere provided friendship, hospitality, beer, and recountings of the history of the region.

Special thanks go to my many fellow graduate students for their help and discussions, particularly Valerie Walker, Douglas Lane and William Webb. Finally, my appreciation is expressed to Philip Anderson, for his insights into Arizona Precambrian geology.

Support for this thesis was provided by a Duval Corporation Fellowship and a grant from the Department of Geosciences from the B. S. Butler fund. Continental Oil Company provided funds to offset field, analytical, thin section, and thesis preparation expenses. This thesis is dedicated to my wife, Judy, who has persevered and gone without so that I might complete this undertaking.

TABLE OF CONTENTS

		Page
	LIST OF ILLUSTRATIONS	viii
	LIST OF TABLES	x
	ABSTRACT	xi
1.	INTRODUCTION	1
	Purpose	3
	Methods	3
	Location	4
	Previous Work	6
2.	PRECAMBRIAN ROCKS	9
	Metamorphic Rocks	9
	Amphibolites	9
	Quartzofeldspathic Rocks	19
	Intrusive Rocks	33
	Cavalliere Granodiorite	35
	Antler Granite	36
	Pegmatites	37
	Diabase	38
	Injection Migmatitic Rocks	39
3.	STRUCTURAL GEOLOGY	41
	Boriana Canyon Structures	41
	Antler Mine Area Structures	42
	Copper World Mine Structures	44
	Structures in the Quartz-Mica Schists	45
	Faulting and Shearing	48
	Structures and Lithology in the Bulge	51
	Lithology	52
	Foliation Data	53
	Faulting	53
	Folding	55

TABLE OF CONTENTS--Continued

	Page
4. ECONOMIC GEOLOGY	56
Antler Mine	56
History	56
Surface Exposures	58
Mineralization and Alteration	60
Sulfide Mineralogy	61
Silicate Mineralogy	64
Copper World Mine	72
Cordierite-Anthophyllite Schists and Iron Formations in the Bulge	74
5. GEOCHEMISTRY	78
Analytical Methods	79
Protolith Geochemistry	80
Amphibolites	81
Quartzofeldspathic Rocks	88
Trace-Element Content of Ironstones and Ore Zone	95
Lead Isotope Data	96
"Pseudofragmental" Amphibolite	96
Chemical Nature of the Volcanism	98
6. METAMORPHISM	102
Metamorphic Rank	102
Origin of the Antler Granite	105
7. INTERPRETATION AND DISCUSSION	108
Volcanogene Model	109
Significance of Cordierite-Anthophyllite Assemblages	111
Metamorphism of Sulfides	114
Antler Synthesis	117
Structural Deformation	121
Evolution of the Bulge	122
Alternative Models	125
Conclusions	127
APPENDIX I: ELECTRON MICROPROBE DATA	129
APPENDIX II: MINERAL ABBREVIATIONS UTILIZED IN TEXT	131

TABLE OF CONTENTS--Continued

Page

APPENDIX III: WALLROCK AND FIBROUS SILICATE GEOCHEMICAL DATA 132

LIST OF REFERENCES 143

LIST OF ILLUSTRATIONS

Figure		Page
1.	Geologic Map of the Antler Mine and Vicinity, Mohave County, Arizona	in pocket
2.	Geologic Map of the Antler Mine and Vicinity, Mohave County, Arizona: Photo-linears	in pocket
3.	Location Map, Antler Mine Area, Mohave County, Arizona	5
4.	Simplified Geologic Map of Boriana Canyon	10
5.	Amphibolite Outcrops	13
6.	Spotted Amphibolite Outcrop	15
7.	Slabbed Specimens of Spotted Amphibolite Gneiss	17
8.	Fold Hinge or Fragment in Quartz-Biotite-(Potassium) Feldspar Schist	22
9.	Comparison of Textures in Quartz-Biotite Schists	27
10.	Conglomerate within Quartz-Mica Schist	31
11.	Photomicrographs of Microfolds	43
12.	Overturned, Isoclinal-to-Tight Folds in Quartz-Mica Schists	46
13.	Lower-Hemisphere, Stereographic Projection of Boriana Canyon Foliation Data, Exclusive of the Bulge	49
14.	Lower-Hemisphere Stereographic Projection of Bulge Foliation Data	54
15.	Cordierite-Anthophyllite Outcrop	65
16.	Photomicrographs of Cordierite-Anthophyllite	67
17.	Photomicrographs of Sillimanite	70
18.	Iron Formation Outcrop	75

LIST OF ILLUSTRATIONS--Continued

Figure		Page
19.	Plot of niggli c versus mg	82
20.	Plot of niggli c - 100 mg - al-alk	83
21.	Plot of niggli c - al-alk	85
22.	Plot of niggli k versus mg	86
23.	Plot of Cr and Ni versus niggli mg	87
24.	Plot of Ba and Sr versus niggli mg	89
25.	Plot of Zr and Cu versus niggli mg	90
26.	Plot of Co and $\frac{Co}{Ni}$ versus niggli mg	91
27.	Plot of Cr and Ni versus % TiO_2	92
28.	Classification of Volcanic Rocks by Silica Index	93
29.	AFM Plot for Antler Wallrocks	99
30.	Plot of Total Alkalies versus Silica for Antler Wallrocks	100
31.	Jensen Cation Plot for Antler Wallrocks	101
32.	Slabbed Specimen of Massive Sulfide Ore	115
33.	Schematic Illustration of the Structural Evolution of the Bulge: Fault Model	124

LIST OF TABLES

Table		Page
1.	Summary of Antler Ownership and Past Production Data	57
2.	Pb-Pb Isotope Ratios for Central Arizona Massive Sulfide Deposits	97
3.	Comparison of Antler Granite and I and S Type Granites	106
4.	Whole Rock Data for the Antler Mine Wallrocks	134
5.	Trace-Element Data for the Antler Mine Wallrocks	135
6.	Whole Rock Data for Iron Formations and Silicate Alteration	136
7.	Trace-Element Data for Iron Formations and Silicate Alteration	137
8.	Niggli Data for Antler Wallrocks	138
9.	Ternary Cation Percentage Data for Antler Wallrocks	139
10.	Listing of Silicate Alteration Assemblages	140

ABSTRACT

Generation of the volcanogenic massive sulfide ores of Boriana Canyon commenced approximately 1850 m.y. ago with the inception of tholeiitic bimodal volcanism in what appears to have been an intra-oceanic arc complex. Thin basalt-andesite flows on an unknown, presumably oceanic, basement were interspersed with subaerial outpourings of rhyolite tuff prior to deposition of a submarine felsic end stage marked by generation of chlorite and cogenetic massive sulfides and chert precipitated onto the seafloor. The stratiform Cu-Zn-Pb bodies were then buried by coeval tuffaceous and later pelitic sediments.

During the Mazatzal Revolution from 1715 to 1660 m.y., the sedimentary and volcanic rocks were metamorphosed during a deformational event in which a weak foliation was imparted to the rocks. A second major northwesterly-directed compressional event resulted in development of strong northeast foliation, tight-to-isoclinal northeast trending folds, steeply plunging lineations, and chevron folds, all contemporaneous with batholithic activity. Anatexis of tuffaceous and pelitic material generated a granitic melt emplaced along northeast structures. Later recurrent north-northwest block faulting, possibly post-Precambrian, cut the metamorphic-plutonic complex.

This major metamorphic event obliterated all primary lithologic features. The chloritically altered wallrocks of the ore horizon were

converted to cordierite-anthophyllite assemblages, while the massive sulfide bodies were plastically deformed. Petrochemistry reveals the parentage of amphibolites to be basalt-andesite-dacite, biotite schists to be rhyolite tuffs, and mica schists to be pelitic sediments.

CHAPTER 1

INTRODUCTION

The Antler and Copper World mines, located in Boriana Canyon in the Hualapai Mountains, are historically notable for their massive high-grade copper and zinc ores. These ore deposits, in a sequence of intensely deformed lower-to-middle amphibolite grade Precambrian quartzofeldspathic and amphibolitic gneisses and schists, have received little serious attention from either exploration firms or students of ore deposits. The erroneous interpretation that the deposits are small has led many managers to write off the bodies as economically unattractive under today's economics. Additional uncertainty as to the origin of the deposits discouraged further step-out exploration due to the lack of a conceptual genetic model.

In the last decade, workers in Precambrian terrains of central Arizona have redirected their mapping and research efforts toward formulation of a unifying theory for the geologic and plate tectonic evolution of the Precambrian of Arizona. Concurrent development of the submarine volcanogenic model for massive sulfide bodies from the Archean terrains of Canada to the Miocene terrains of Japan has led to a critical examination and reevaluation of genetic models proposed for several central Arizona massive sulfide deposits (Gilmour and Still, 1968; Anderson and Nash, 1972; Clayton and Baker, 1973;

Anderson and Guilbert, 1979). Individual studies of stratiform massive sulfide deposits in central Arizona have further corroborated the syngenetic volcanogenic theory of ore genesis (Brook, 1974; DeWitt, 1976; Larson, 1976; Webb, 1979).

These studies, however, have dealt with ore systems that have undergone moderate deformation and metamorphism, generally to the greenschist facies. Primary features such as bedding and relict textures in many cases are still preserved in the rocks, greatly facilitating genetic interpretation. In Boriana Canyon, folding and metamorphism have obscured most original stratigraphic and lithologic features within the rocks. Nevertheless, a comparison of the salient characteristics of host-rock lithology and orebody silicate-sulfide constitution at the Antler and Copper World mines with the same characteristics of Archean massive sulfide deposits suggests that the Boriana Canyon deposits are also the once-stratiform exhalative products of submarine volcanism.

The author has undertaken this thesis study with an eye towards understanding the ore environment and testing the involvement of volcanic and sedimentary processes as progenitors of the Boriana Canyon gneiss belt and its ores. It will be seen that future exploration for massive sulfide bodies in Boriana Canyon and elsewhere in the Hualapai Mountains clearly demands an understanding of the Precambrian rocks and their correlation with the Antler and Copper World deposits.

Purpose

The purpose of this study has been to delineate the lithology of the host rocks at the Antler and Copper World mines, to ascertain the igneous or sedimentary heritage of the rocks, and to report on the silicate and sulfide assemblages of the ore horizons. The focus of this investigation covers the swath of Precambrian metavolcanics and metasediments that form the floor and footslopes of Boriana Canyon. The younger east- and west-bounding granodioritic masses are not an integral part of the study. The tungsten- and copper-productive Boriana Mine located north of the thesis area was purposefully excluded from the study; even superficially, it represents an ore system distinct from that of the Antler and Copper World deposits.

The completed thesis study and geologic maps (Figures 1 and 2, in pocket) can be used as an evaluative guide for further exploration work not only in the largely unmapped Hualapai Mountains and northwestern Arizona Precambrian ranges, but by analogy in Proterozoic terrains elsewhere in the western Cordillera where deformation and metamorphism have resulted in similar structural and lithologic changes.

Methods

After an initial reconnaissance of the area, a fruitless literature study was undertaken to evaluate the thoughts of early workers. The current owners of the Antler Mine, Standard Metals Corporation, Lakewood, Colorado, were contacted, and they graciously

provided access to their mine records, maps, and diamond drill core from the most recent period of mining and exploration. Fascinating and illuminating discussions were held with Drs. Paul Gilmour and Arthur Still, consultants to Standard Metals during the 1966 to 1975 period of activity, and the author acknowledges his great debt to both of them. A 1966 consultants report on the Copper World Mine was provided by Steve Tima, Bobcat Mining Company, Phoenix, Arizona.

Field mapping at a scale of 1:6000 (1" = 500') was carried out using aerial photographs commissioned by the author over an intermittent period from March 1978 to January 1979. Some 230 samples of outcrop and drillcore were taken for thin-section and polished surface studies. Twenty outcrop and drillcore samples were collected for whole-rock analysis. Underground workings and the ore horizons are now inaccessible. Both mines, sealed off at their entrances, are flooded at depth, and the timbering has collapsed. Underground maps and cross-sections and the diamond drillcore help elucidate the third dimension of the deposits.

Location

The Boriana Canyon complex, and the Antler and Copper World mines, are located in the west-central Hualapai Mountains of Mohave County in northwestern Arizona and are situated within the Cedar Valley mining district. The area is approximately 34 km southeast of Kingman and 19 km east of Yucca (Figure 3). Portions of the Creamery Canyon and Wabayuma Peak 7½' quadrangles form the topographic base of the geologic map.

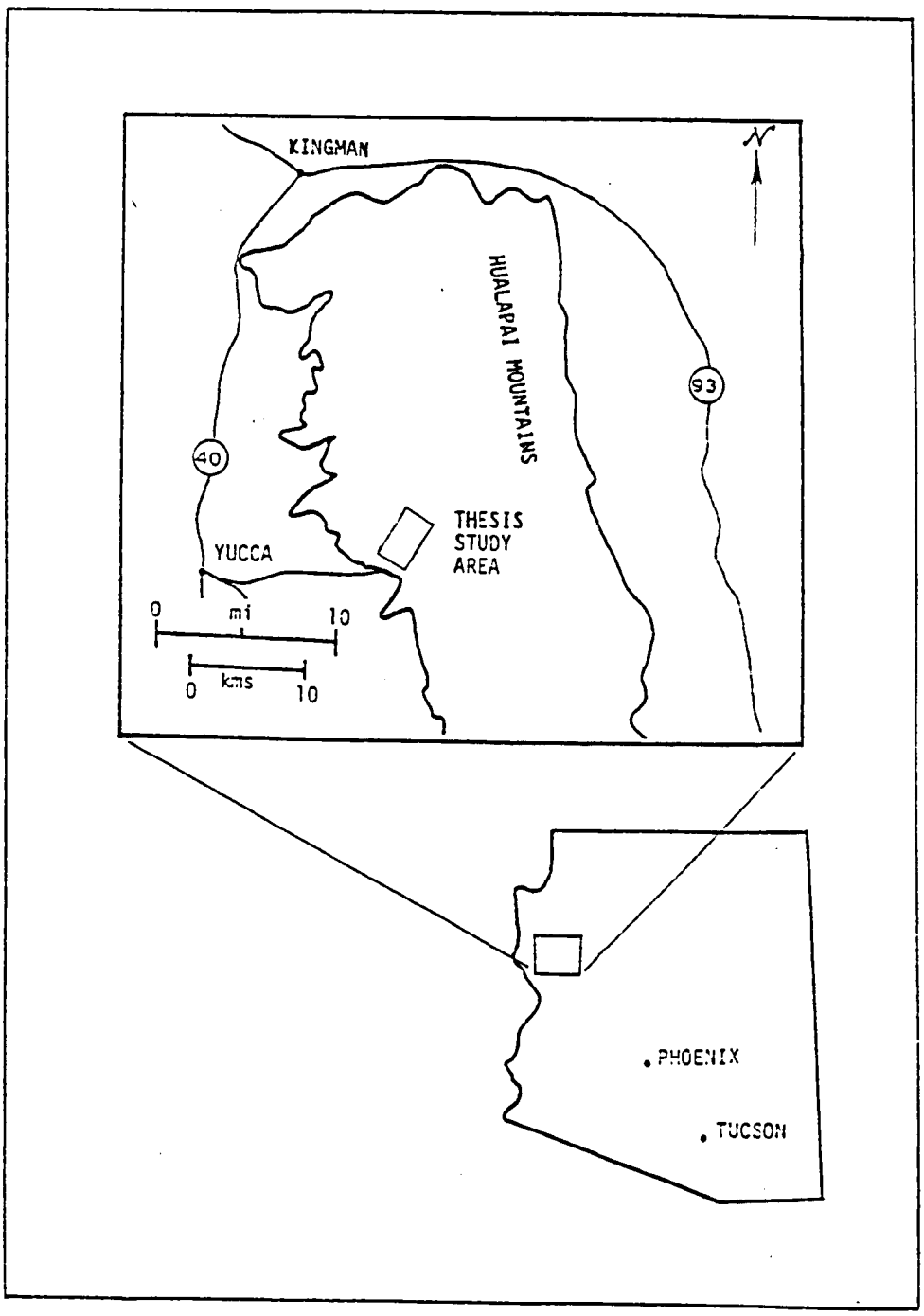

Figure 3. Location Map, Antler Mine Area, Mohave County, Arizona.

The thesis area, approximately 5.6 by 7.5 km, encompasses an area of about 42 km^2. Access to the study area is good, with a county-maintained road leading from Yucca to the Antler Mine. Above the Antler Mine toward the Boriana Mine the road narrows and is more susceptible to springtime thaws and summer rains. The side road leading up to the Copper World Mine is poor. A poorly maintained BLM trail road continues from the Boriana Mine over the Hualapai Mountains into Kingman. An unimproved drill road provides access to the Bulge area, described below.

The typical desert climate passes into semidesert in the higher parts. Rainfall averages 9-10" (23-25 cm) in the entrance flatlands. Vegetation in the southern reaches is a typical desert assemblage of cactus, cholla, creosote, ocotillo, and Joshua tree, grading into thick chaparral and mountain oak above the 4000' level to yellow pines along the high ridges. Elevation near the entrance of Boriana Canyon is approximately 3000', with elevations of 5600' above the Copper World Mine.

Previous Work

Sparse published literature dealing with the Antler Mine dates to the wartime years. Holt (1944) and Romslo and Wilson (1948) reported on the local geology and mining at the Antler Mine. Romslo and Wilson briefly intimated the mineralization was the product of hydrothermal fluids emanating from the intrusive granodiorite and selectively replacing the schist along foliation planes and in

fracture fillings. Another wartime report by Hobbs (1944) dealt with the Boriana Mine further up the canyon. Rasor (1946) reported on a loellingite occurrence at the Copper World Mine.

The geochronology of the Precambrian rocks at the northern end of the Hualapais in the Wheeler Pass vicinity was reported on by Kessler (1976). Research by H. Stensrud (personal communication, 1979) and P. Anderson (personal communication, 1979) on the regional aspects of the Precambrian geology of the central Hualapais is currently ongoing. Thus, except for reports in the files of exploration companies, there is virtually no literature on the deposits or the Precambrian geology.

The results of this geological investigation can be approximately divided into two sections, one devoted to description and the other to interpretation. In the first section, the lithology, structure, and mineralization of the Boriana Canyon gneiss belt is presented. The second section attempts to provide an interpretive reconstruction of the protolithologic setting and the genesis of the massive sulfide mineralization as deduced from geochemical and geological constraints.

The author has adopted several terms to designate those discrete lithologic bodies within the study area that are presently unnamed. The western batholith of granodiorite is hereby termed the Cavalliere granodiorite, in recognition of the Cavalliere Ranch situated nearby. The amphibolites and quartzofeldspathic schists are

informally referred to as the Boriana series, with no strict implications as to their true stratigraphic relations. The granite ridge off to the east side of the Antler Mine is termed the Antler granite. The amphibolite salient projecting into the batholith is aptly termed the Bulge, in keeping with earlier designations by Still and Gilmour.

CHAPTER 2

PRECAMBRIAN ROCKS

The rock types of the Antler area are categorized as:

1. Metamorphic: amphibolites and quartzofeldspathic schists, gneisses, and phyllites; pegmatites.
2. Intrusive: granodiorite and "anatectic" granite plutons; pegmatites; diabase.
3. Injection migmatitic: an interleaving of metamorphic and intrusive rocks.

Metamorphic Rocks

The metamorphic rocks comprise the largest outcrop area, occupying the lower bounding slopes on both sides of the canyon and the floor (Figures 1, in pocket, and 4). The ridge of Antler granite divides the western amphibolites and quartz-biotite-dominant gneisses and schists from the eastern quartz-mica schists. Lithologic contacts approximately parallel the N30°E-N40°E foliation trend; in the Bulge, the contacts of the semicircular gneiss units also remain sub-parallel to foliation.

Amphibolites

The amphibolites in the study area are defined as those gneisses or schists in which the percentage of amphibole minerals,

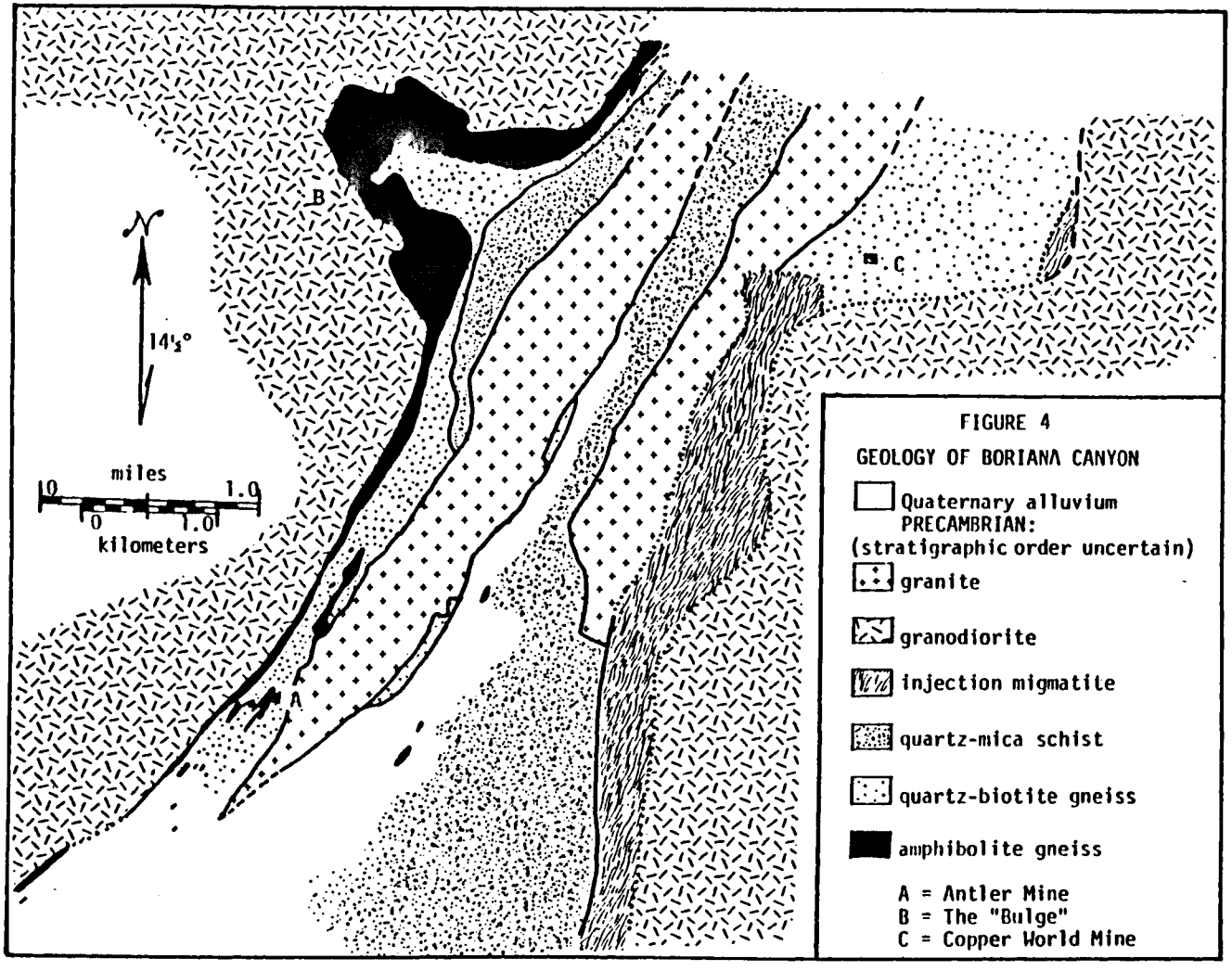

Figure 4. Simplified Geologic Map of Boriana Canyon.

chiefly hornblende, exceeds the percentage of other mafic minerals. Anthophyllite, biotite, and actinolite rocks are mapped as separate discrete lithologic sub-units and shown as such on the geologic map (Figure 1, in pocket).

Over 95% of the amphibolites occur along the margin of the Cavalliere granodiorite, in the Bulge, and along the margin of the quartz-mica schist. Several outliers of amphibolite occur east of the screen of Antler granite. Although amphibolite float has been found in the higher canyons to the east, no amphibolite outcrops have as yet been discovered in the eastern portions of Boriana Canyon.

The amphibolites may be further subdivided, either in outcrop or thin section, into two mineralogical subtypes:

1. hornblende-plagioclase amphibolite.
2. quartz-hornblende-feldspar amphibolite.

The hornblende-plagioclase amphibolite is dark brown to black, weathering to a dark grey to black rock with a massive to blocky habit. In thicker sections, particularly in the Bulge, the term hornfels might be equally applicable (Spry, 1969). At the Bulge, the units attain apparent thicknesses of 216 to 560 meters. Elsewhere, the hornblende-plagioclase gneisses are relatively thin, ranging from 10-20 meters to 45-60 meters. The definitive metamorphic assemblage for the unit is hornblende-plagioclase-epidote-quartz. Both fine and coarse-grained textural varieties are encountered,

along with rare porphyroblastic and "pseudofragmental" sections. All units have a well-developed gneissic texture.

With increasing felsic proportions the hornblende-plagioclase gneiss can grade into a quartz-hornblende-feldspar gneiss or schist (Figure 5). In outcrop the color of the more felsic amphibolite is medium to light grey, approaching cream white in some instances, and weathers to a medium to dark grey. The quartz-hornblende-feldspar units are fine- to medium-grained and more fissile than their hornblende-plagioclase counterparts. The hornblende grains are distinctively foliated, almost porphyroblastic. Separation of the two amphibolite sub-types in hand sample can be somewhat arbitrary at times. However, there appears to be a "break" in which a hornblende content of around 25% or less of the total mineral content is associated with sections of predominantly felsic schist. Assignment of samples to this category are thus made by hand sample determination.

Apparent thickness of the quartz-hornblende-feldspar amphibolite varies from 45 to 60 meters near the Antler Mine. The two amphibolites can grade into one another. Commonly a unit of hornblende-plagioclase amphibolite passes sharply or gradationally into 70- to 100-cm-thick sequences of quartz-hornblende-feldspar amphibolite interspersed with 10- to 50-cm layers of mafic amphibolite. This cyclical gradation in a given package tends towards a predominance of quartz-hornblende-feldspar, and finally to its takeover. In turn, the quartz-hornblende-feldspar can be cyclically gradational into quartz-biotite-(potassium)

Figure 5. Amphibolite Outcrops.

(a) Cyclical compositional layering of hornblende-plagioclase and quartz-hornblende-feldspar gneisses; unit dipping to northwest.

(b) Close-up of amphibolites. -- Location: Northeast of Antler Mine along gneiss-granodiorite contact.

A

B

Figure 5. Amphibolite Outcrops.

feldspar rocks. An arbitrary separation of amphibolite units is drawn when one type predominates over the other by 50%. Attention is directed to the small relative overall thickness of all amphibolite units relative to the quartzofeldspathic units on the geologic map (Figures 1, in pocket, and 4).

In addition to the fine and coarse-grained textural varieties of amphibolites, two other minor but distinctive sub-types of hornblende-plagioclase gneiss are found in Boriana Canyon. First, a thin and intermittent unit, with distinct 5 to 10 cm hornblende porphyroblasts elongated within foliation and set in a medium to coarse grained matrix, occurs in restricted sections. In the Bulge, garnet porphyroblasts rimmed with hornblende and plagioclase produce augen-like textures. The units are so thin that they have been combined on the geologic map with the units of hornblende-plagioclase gneiss. Secondly, a fine-grained unit of hornblende-plagioclase amphibolite spotted with elongated ovoids and wisps of leucocratic material is found above the Antler Mine. Maximum thickness of the unit is less than 1.5 m. The 5 by 15 cm clots impart a fragmental texture to weathered surfaces (Figure 6). The texture is suggestive of "clasts" caught up in the hornblende matrix. Thin sections across the sharp boundaries between the leucocratic knots and the hornblende matrix reveal the light colored material is not of felsic composition, but instead is composed of calcium-rich amphiboles and pyroxenes: actinolite-tremolite (70%), colorless diopside (10%),

Figure 6. Spotted Amphibolite Outcrop. -- Location: Hillside above Antler Mine.

epidote (5%), plagioclase An_{54} (3%), quartz (2%), muscovite (2%), carbonate (3%), and trace potassium feldspar and chlorite.

Slabbed specimens of this unusual amphibolite show the development of rootless folds paralleling foliation, with elongation of ovoids concordant with fold outlines (Figure 7), suggesting the leucocratic ovoids are not true clasts but stretched-out layers or segregations of a once-stratiform horizon within the amphibolite.

Petrography of the Amphibolites. In the following descriptions, the average mineral abundances measured or estimated in thin sections are given with the ranges observed from all thin sections of the designated unit. For conciseness, "hornblende-plagioclase amphibolite" will be abbreviated hp, "quartz-hornblende-feldspar amphibolite" will be shortened to qhf, and $\bar{x}$ represents "average."

Hornblende is the defining mineral for the amphibolites (at 25-75%, $\bar{x}$ = 54% in hp, and 8-25%, $\bar{x}$ = 13% in qhf). It is pleochroic from light brown to dark brown or blue green to light green, and is often prismatic with a subidioblastic to idioblastic habit. The 0.5 mm by 2.0 mm grains reach over 10 mm in porphyroblastic sections. Chlorite is developed as a retrograde product along cleavages. Hornblende commonly carries poikiloblasts of both quartz and opaque minerals. It cuts and embays plagioclase and quartz and is replaced by granules of epidote.

Plagioclase (at 5-30%, $\bar{x}$ = 13% in hp, and 20-45%, $\bar{x}$ = 32% in qhf) occurs as idioblastic crystals ranging in length from 0.3 mm to

Figure 7. Slabbed Specimens of Spotted Amphibolite Gneiss.

(a) "Pseudofragmental" leucocratic ovoids and porphyroblastic material.

(b) Detached noses and attenuated limbs of rootless (disharmonic) folds.

A

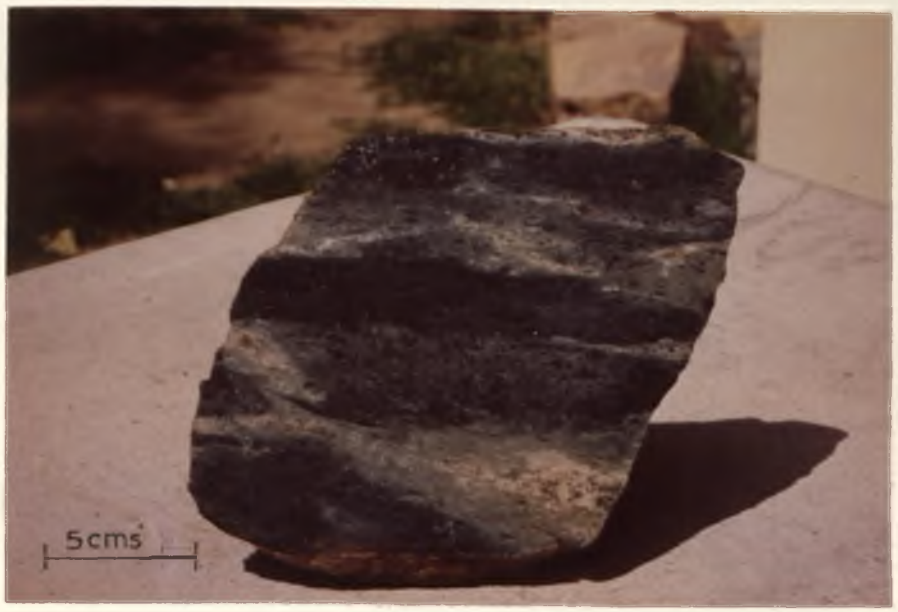

B

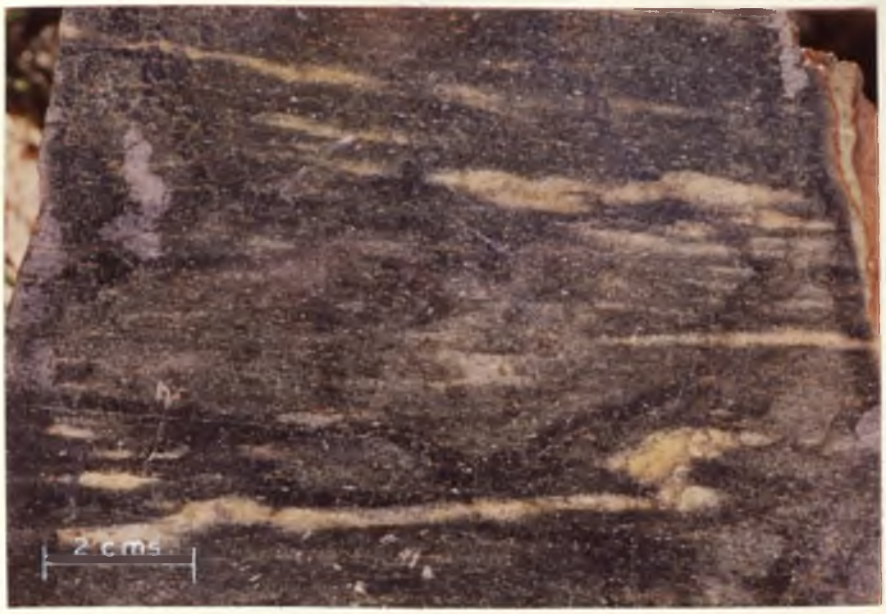

Figure 7. Slabbed Specimens of Spotted Amphibolite Gneiss.

1.2 mm. Plagioclase is often replaced by sericite and has fine (0.05-0.10 mm) needle-like inclusions of actinolite-tremolite. Undulose deformation twinning is prominent in many samples. Albite values range from An_{32} to An_{50} ($\bar{x} = An_{37}$) for the hornblende-plagioclase gneiss. For the quartz-hornblende-feldspar units, values range from An_{25} to An_{45} ($\bar{x} = An_{32}$).

Zoisite and epidote ($\bar{x}$ = 5%) occur as xenoblastic poikiloblastic ovoids from 0.1 mm to 0.2 mm in length. They replace hornblende, quartz, and, rarely, plagioclase.

Undulose, xenoblastic, 0.1 mm to 1.0 mm embayed quartz (hp: 2-25%, $\bar{x}$ = 7%; qhf: 2-50%, $\bar{x}$ = 30%) appears paragenetically oldest. In the more siliceous quartz-hornblende-feldspar amphibolites, quartz displays a granoblastic polygonal texture. Lesser minerals include idioblastic to subidioblastic clinopyroxene, mostly pale green diopside (2-30%); actinolite-tremolite (1-5%), biotite (1%); ilmenite and magnetite (1%); subidioblastic poikiloblastic garnet (trace); cummingtonite (trace) and hastingsite(?) (trace); and xenoblastic potassium feldspar (hp: 1%; qhf: 1%); and serpentine (trace). Calcite veinlets crosscut all minerals.

In summary, the metamorphic assemblages (see Appendix II for abbreviations) apparent in thin sections of the amphibolites, based on whether they are texturally primary or secondary in habit, are:

hp

Primary:

hb + plag An_{32-50} + qz + opq ± act-trem ± Kfs ± cpx ± biot ± cumm ± gt ± hast(?)

Secondary:

epid ± ser-musc + chl ± cal ± serp

qhf

Primary:

plag An_{25-45} + qz + hb + Kfs + opq ± biot ± cpx ± act-trem

Secondary:

epid + ser-musc + chl ± cal

Whole-rock analyses and protolith evaluations of these rocks will be presented in separate sections further along in the manuscript.

Quartzofeldspathic Rocks

In Boriana Canyon, quartzofeldspathic rocks are quartz and feldspar-dominant micaceous gneisses, schists, and phyllites. They comprise the largest proportion of the exposed metamorphic rocks. The quartzofeldspathic rocks are divided into quartz-biotite and quartz-muscovite groups, based on the hand specimen mica ratios. The validity of this mesoscopic separation of schist types by mica mineralogy is borne out in thin section examination, where feldspar differences are as pronounced. The term "quartz-mica schist" is a field term used to describe the quartz-muscovite schist, and does not include the quartz-biotite schists. Quartz-biotite rocks have

biotite as their dominant mica type, while quartz-mica schists contain muscovite which either exceeds or equals the percentage of biotite. Compositional overlap of the two groups poses occasional problems at the field mapping level, requiring either petrographic verification or arbitrary assignment based on the predominant rock type in the section. On a large scale, the distinction between the groups is emphasized by inspection of their overall distribution on the geologic map (Figures 1 and 2, in pocket). The thickest expression of quartz-biotite dominant rocks occurs west of the Antler granite, with only thin units of quartz-mica rocks encountered around the Antler Mine. East of the granitic screen the quartz-mica schists form a massive expanse along the canyon floor, with a few scattered locales of amphibolite and quartz-biotite dominant rocks near the granite ridge.

Quartz-biotite Dominant Rocks. At both the Antler and Copper World mines the quartz-biotite rocks form the apparent footwall and hangingwall of the massive sulfide ores. It is important to distinguish two separate and mappable sub-types within the group, namely, quartz-biotite schist and quartz-biotite-(potassium) feldspar schist/gneiss. The quartz-biotite schists are very fine to fine grained, buff tan to light grey weathering to a light to medium green grey, gneissic to schistose felsic rocks. They can be imperceptibly gradational into quartz-mica and quartz-biotite-(potassium) feldspar units, identification of which can sometimes only be resolved by

petrographic examination. In the vicinity of the Antler Mine the quartz-biotite rocks are anomalously siliceous (70-85% SiO_2). North of the mine the units, with an apparent thickness of 15-20 meters, thicken to 75 meters. At the Bulge, the quartz-biotite schists approach apparent thicknesses of 270 meters.

The quartz-biotite-(potassium) feldspar schists and gneisses are the more abundant of the two sub-types. They are very fine to fine grained, light tan to pale cream colored weathering to yellow buff tan to medium grey, gneissic to schistose felsic rocks. It has a blocky to fissile habit like the quartz-biotite schist. The 3 mm to 8 mm weakly chloritized biotite laths are flattened parallel to foliation and surrounded by haloes of indigenous limonite. In hand sample, the smeared biotite laths, their large size with respect to the fine grained groundmass, and the limonite staining are diagnostic.

The quartz-biotite-(potassium) feldspar units range from 28 to 75 meters in apparent thickness, reaching 190 meters in the Bulge. The section can overlap with quartz-hornblende-feldspar amphibolite, with 20-80 cm intervals of schist alternating with thinner amphibolite units. Careful inspection of weathered quartz-biotite-(potassium) feldspar outcrop reveals rare patches of apparent remnant "fragments." The drillcore penetrated several sections of gneiss possessing angular felsic "fragments" or isolated lenses non-concordant to foliation and penetrated by the last foliation phase. The "fragments" appear to form fold hinges (Figure 8). The "fragments" cannot be distinguished from the matrix in thin section.

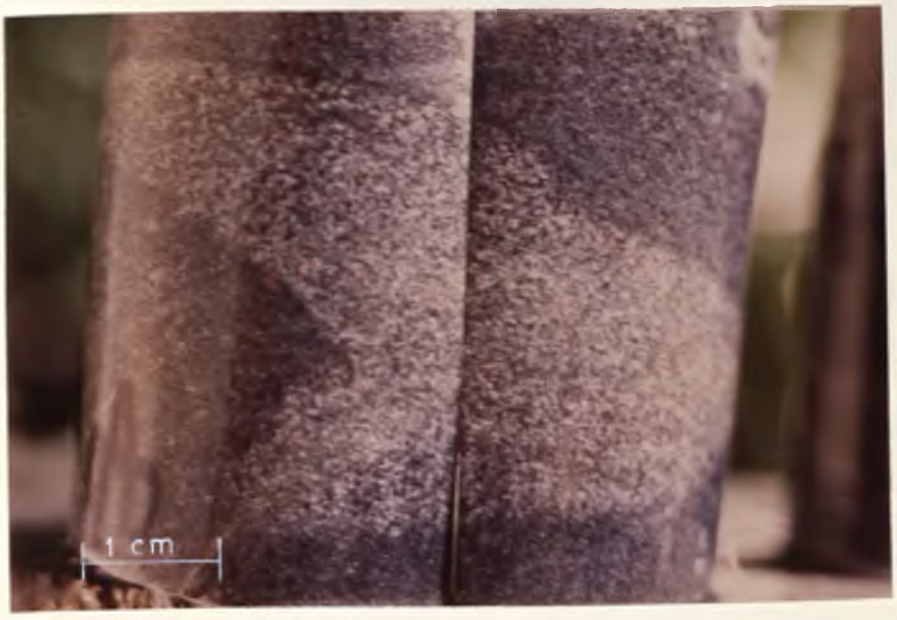

Figure 8. Fold Hinge or Fragment in Quartz-Biotite-(Potassium) Feldspar Schist. -- Slabbed specimen B6-1843.

In thin section, the quartz-biotite and quartz-biotite-(potassium) feldspar rocks are sufficiently dissimilar in both metamorphic texture and mineralogy to deserve separate descriptions.

Quartz-biotite Rocks: The prominent mineral by far is quartz. Grain sizes in some intercepts are uniformly distributed from 0.2 mm by 0.5 mm up to 1.2 mm by 2.3 mm. In other sections, particularly in apparent footwall samples, a bimodal grain distribution is perceived with a second set of larger grains of 0.3-0.8 mm by 0.8-1.2 mm size. The quartz grains are equigranular and xenoblastic, forming 120^{o} intersections and imparting a granoblastic equigranular polygonal texture to the rock. In the bimodally-distributed grain size samples the texture is granoblastic inequigranular polygonal or interlobate.

The quartz is often strained and undulose and can contain cloudy inclusions and poikiloblasts of apatite and opaque minerals. The foliation is defined by the slight elongation of the quartz grains and the laths of biotite trapped between them. The percentage of quartz within the quartz-biotite rocks falls into two groupings, dependent on the potassium feldspar content. In samples with a high potassium feldspar content, the average quartz content hovers around 58%, while in low potassium feldspar sections the quartz content averages between 75% and 85%.

Orthoclase is the common form of potassium feldspar in quartz-biotite rocks, although lesser microcline is found. The

orthoclase grains are xenoblastic and in the same general size range as quartz, typically 0.3 mm by 0.6 mm. Microcline can attain a subidioblastic habit and contains occasional perthitic intergrowths. Both feldspar types carry ovoid poikiloblasts of quartz and are embayed by quartz grains. The quartz-biotite rocks fall into either high (10-15 volume %) or low (trace to 5 volume %) potassium feldspar groupings.

Subidioblastic plagioclase grains have a wide size range from 0.2 mm to 0.9 mm. Pericline twinning is common. Albite values vary from An_4 to An_{16} ($\bar{x} = An_{10}$). Sericitization is common as a "dusting" and along twin planes and grain edges. Very fine poikiloblasts of actinolite are observed. Plagioclase comprises an average of 10% of the quartz-biotite rocks, with a range from 3% to 20%.

Both muscovite and biotite display subidioblastic to idioblastic habits. Fine laths of biotite vary from pleochroic light green to dark brown to ragged yellow brown remnants replaced by muscovite. The size range of biotite is from 0.2 mm to 2.0 mm, with common grain size around 0.4 mm. Zircon inclusions are common. Biotite cuts and embays quartz, potassium feldspar, and plagioclase and in turn is embayed by opaque, chiefly magnetite. Muscovite is an apparent alteration product of biotite and paragenetically the youngest. In habit it is seen as subidioblastic laths and slivers, with dimensions varying from 0.3 mm to 1.5 mm. The percentage of biotite in the rock varies from 7% to 25% ($\bar{x} = 12\%$), while muscovite varies from 1% to 13% ($\bar{x} = 3\%$).

Minor constituents include traces of fine (0.2 mm-0.8 mm) poikiloblastic garnet, subidioblastic hornblende, and ovoid epidote. Rare phlogopite is encountered, particularly near the ore horizons. Late-stage calcite veinlets crosscut all minerals.

The metamorphic assemblages for the quartz-biotite rocks are:

Primary:

qz + Kfs + plag An_{4-16} + biot $\pm$ gt $\pm$ hb $\pm$ phlog $\pm$ opq

Secondary:

epid $\pm$ ser-musc $\pm$ cal

Petrography of Quartz-biotite-(potassium) Feldspar Rocks: At the Antler Mine the quartz-biotite-(potassium) feldspar units form the present footwall and in most intercepts the present hangingwall of the massive sulfide bodies. The distinguishing characteristics which set the unit apart from the quartz-biotite rocks are the predominance of potassium feldspar, mostly microcline, coarse segregations of felsic and mafic minerals, and the disconnected lenses of slightly more felsic material ("pseudofragments") seen in rare drill core intercepts. The overwhelming predominance of quartz-biotite-(potassium) feldspar units both above and below the ore horizons is striking.

The quartz content of the quartz-biotite-(potassium) feldspar schists varies from 25% to 70% ($\bar{x}$ = 46%). The quartz is xenoblastic and heteroblastic, with a size range from 0.4 mm to 0.8 mm. Grain

boundaries are curved, embayed, and in several rare instances seriate. Poikiloblasts of potassium feldspar and biotite are common. Microcline is the predominant form of potassium feldspar in the units. In thin section it imparts a diagnostic texture to the rock by the mutual interference along grain boundaries that prevent development of 120° joins among quartz grains. The resulting texture is a granoblastic inequigranular interlobate to seriate fabric, contrasting with the granoblastic polygonal texture of the quartz-biotite schists (Figure 9). The pericline twinning of most of the microcline is a useful feature permitting the units to be separated by thin section examination.

Microcline is subidioblastic to xenoblastic in form. Grain sizes are bimodal, varying from 0.3 mm to 1.0 mm with means close to each end value. Microcline prominently embays quartz, with slightly rounded tongues and protrusions that lend an interlobate to amoeboid texture to the juxtaposition. Abundant poikiloblasts of quartz as ovoids and lesser stringlet and bead-type perthitic intergrowths are common. Microcline averages 39% of the quartz-biotite-(potassium) feldspar schists. Orthoclase is observed in some sections as small (0.2 mm-0.4 mm) xenoblastic granules.

Biotite forms subidioblastic laths from 0.3 mm to 1.5 mm in length. The color is pleochroic light to dark brown, approaching yellow brown in more iron-rich grains. Under uncrossed nicols, fine edges of opaque limonite can be seen skirting grains. Muscovite,

Figure 9. Comparison of Textures in Quartz-Biotite Schists.

(a) Quartz-biotite schist, B1-1346 (32X).

(b) Quartz-biotite-(potassium) feldspar schist, B2-1499.5 (32X).

A

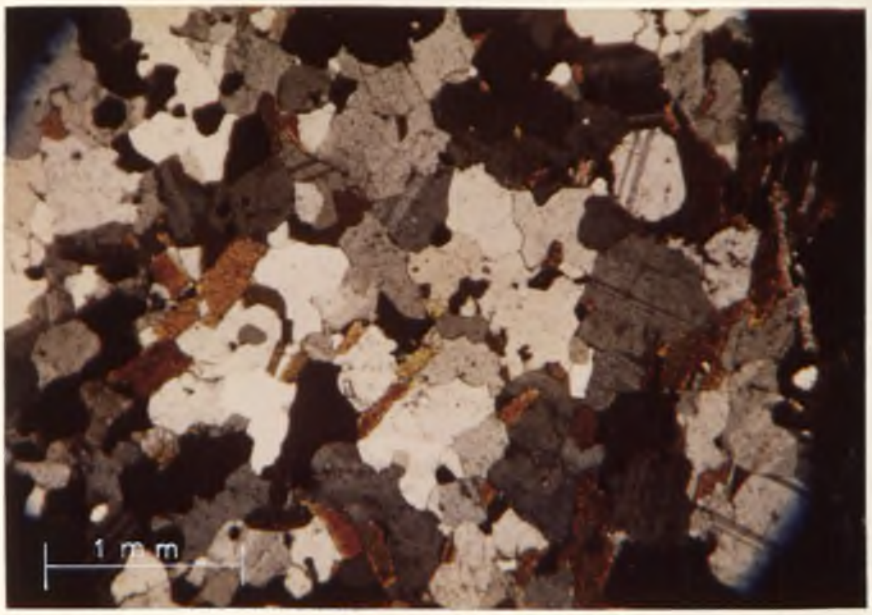

B

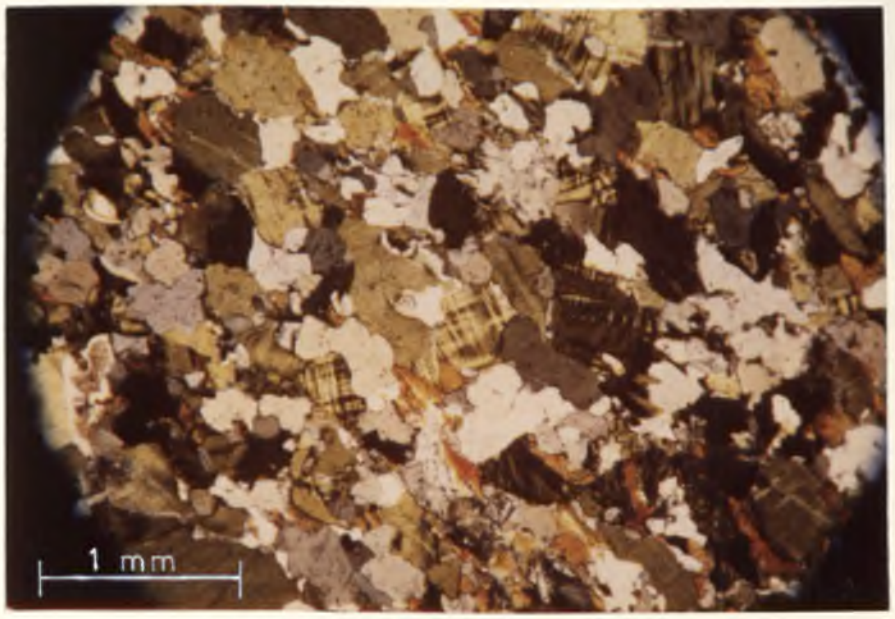

Figure 9. Comparison of Textures in Quartz-Biotite Schists.

developed as an apparent alteration product at the edges and along cleavages, totally replaces biotite grains in some instances.

Plagioclase crystals possess subidioblastic to xenoblastic shapes. Grain sizes are variable from 0.3 mm to 0.9 mm. Compositionally, the plagioclase lies towards the albitic oligoclase end, with values of An_{12} to An_{16}. Sericite replaces plagioclase as cloudy dustings of grains. The percentage of plagioclase in quartz-biotite-(potassium) feldspar rocks varies between 1% and 15% ($\bar{x}$ = 5%).

Epidote occurs as xenoblastic replacements in biotite and hornblende sites. Average grain size is approximately 0.1 mm. A positive correlation between epidote abundance and carbonate content is noted. Epidote group minerals range from trace to 15% ($\bar{x}$ = 1%). Lesser minerals include idioblastic magnetite, with values of trace to 5% in samples; rare subidioblastic garnet, rimmed with chlorite or sericite and carrying opaque and quartz poikiloblasts; and xenoblastic chlorite, both as an apparent alteration of biotite and as rare primary clumps interstitial to other minerals. Muscovite and sericite also appear as alteration products of plagioclase and biotite. Carbonate, chiefly as calcite, occurs as true grains within the matrix and as crosscutting surface veinlets. Trace apatite (in quartz grains), serpentine, and hornblende are encountered in several slides. Sillimanite occurs as fine (0.1-0.2 mm) idioblastic needles near the contact of the schist with the second wedge of Antler granite west of the Copper World Mine.

The defining metamorphic assemblages for the quartz-biotite-(potassium) feldspar rocks are:

Primary:

qz + Kfs + biot + plag An_{12-16} $\pm$ gt $\pm$ sill $\pm$ chl $\pm$ cal $\pm$ opq

Secondary:

epid $\pm$ ser-musc $\pm$ chl $\pm$ cal

Quartz-mica Rocks. Among the metamorphic rocks of Boriana Canyon the quartz-mica schists constitute the largest percentage of outcrop exposure. The quartz-mica rocks represent an assemblage of quartz + muscovite $\pm$ biotite $\pm$ chlorite. They are a very fine to fine grained, light green-grey weathering to grey, phyllitic to schistose series of micaceous rocks with a highly fissile to flaggy parting habit. East of the Antler granite ridge, the units are folded and cut by numerous northeast-trending pegmatites along axial planes. At the Antler Mine the quartz-mica schists are very narrow, on the order of several meters to perhaps fifteen to twenty meters in apparent thickness.

The quartz-mica sections on the eastern side contain biotite-rich sections that are difficult to distinguish in hand specimen from quartz-biotite schist. Traverses along stream beds reveal thin (20 cm-60 cm) biotite-dominant schist sections intercalated among quartz-mica rich sections. Resolution of boundaries can only be determined by petrographic means, and assignment of schist types is sometimes made according to the unit predominant in the vicinity.

Graded bedding, either normal or reverse, can be observed in several of the biotite-rich sections exposed by stream cuts (whole-rock sample #AM-7 is from such an exposure). Whether this is a true primary feature left intact through dynamic metamorphism or a phenomenon generated during deformation is conjectural. Although the large-scale sense of folding in the section is unresolved, the direction of younging is to the southeast if it is normal graded bedding or to the northwest if it is reverse.

Approximately 1330 meters east of the Antler Mine, a well-preserved conglomerate unit within the quartz-mica schist section is exposed (Figure 10). The unit has a true thickness of 20 meters and can be traced along strike for 60 meters. Bedding is approximately normal to foliation, striking N80°W and dipping 73° to the north. The matrix consists of quartz-mica schist material; the clasts are siliceous quartz-biotite and arenaceous(?) quartz-mica material. The rounded clasts, which average 5 cm in the long dimension, attain sizes of 9 to 15 cm by 7 cm. Clast size rapidly drops off to 2.5 to 7.5 mm and finer, eventually merging and disappearing into the fine-grained fissile quartz-mica schist which sandwiches the conglomerate unit on both sides. Quartz veins from 1 cm to 8 cm in thickness penetrate the finer clast conglomerates along northeast foliation planes, but do not cut the several meter wide coarse clast sections.

Petrography of the Quartz-Mica Rocks: The dominant mineral in the quartz-mica schists is quartz. Grains have a xenoblastic

Figure 10. Conglomerate within Quartz-Mica Schist.

(a) In outcrop.

(b) Slabbed specimen.

Location: 1330 meters east of Antler Mine.

A

B

Figure 10. Conglomerate within Quartz-Mica Schist.

form and are very fine, with sizes of 0.1 mm to 0.2 mm. Larger recrystallized grains along foliation planes reach sizes of 0.3 mm to 0.4 mm and, in veinlets, to 0.8 mm. Invariably the texture is granoblastic equigranular polygonal. Muscovite and biotite bound the quartz grains. The percentage of quartz averages 58%, with a range from 20% to 80%.

Muscovite is the defining mineral that separates the quartz-mica schists from the quartz-biotite schists. Subidioblastic to xenoblastic muscovite grains border, crosscut, and are intergrown with biotite. Very fine-grained specimens of friable quartz-mica schist contain muscovite grains of 0.1 mm to 0.2 mm size, while fissile mica-rich specimens contain muscovite laths intimately intergrown with 0.8 mm biotite. The micas are distributed such that the (110) or (010) faces define the foliation. Muscovite content varies from 5% to 40% ($\bar{x}$ = 16%). Biotite in this unit is similar to muscovite in habit and size range, but differs from the biotite found in the quartz-biotite schists. In outcrop it is bleached colorless to pale green or brown; in thin section it is pleochroic dark brown to yellow brown, noticeably "stringy" and ragged in habit, replaced by chlorite along cleavages, and intergrown with and replaced by muscovite. Elongated poikiloblasts of opaque material, mostly hematite, are common. The percentage of biotite in the quartz-mica units ranges from 8% to 35% ($\bar{x}$ = 16%).

The most notable difference between the quartz-mica and quartz-biotite assemblages lies in the virtual absence of plagioclase in quartz-mica rocks. Minor potassium feldspar is present in some samples.

Of the lesser minerals, xenoblastic epidote occurs in trace amounts in at least half of the samples. Hematite and magnetite constitute the opaque minerals, rarely exceeding 1%. Chlorite is weakly developed in the biotite grains.

Almandine garnet and andalusite assemblages which occur near the border of the quartz-mica schists with the injection migmatite zone were not examined in thin section. The quartz-mica units become more muscovite rich with the appearance of deep red-brown idioblastic garnet and large 10-cm andalusite grains in traverses to the east of the central portion of quartz-mica schist.

In summary, the mineral assemblages for the quartz-mica schists are:

Primary:

qz + musc + biot + opq $\pm$ Kfs $\pm$ gt $\pm$ and

Secondary:

musc $\pm$ epid $\pm$ chl

Intrusive Rocks

The intrusive rocks within the thesis area include the west-bounding Cavalliere granodiorite, the eastern quartz monzonite, the Antler granite, pegmatites, and an isolated diabase sill.

Putman and Burnham (1963) sampled and described what they termed the Boriana granodiorite in the west-central Hualapai Mountains, believing it to be a single batholith. H. Stensrud (personal communication, 1979) and P. Anderson (personal communication, 1979), however, have mapped portions of the Hualapai plutonic complex and show it to be composed of a number of closely-related but separate batholiths with mappable intrusive contacts. Putman and Burnham sampled at least two separate plutons in their traverse, but their analyses and conclusions implied only one.

Near the Boriana Canyon area at least three phases of the plutonic complex can be distinguished. Southwest of the thesis area a fine to medium-grained hornblende-bearing granodiorite phase is intruded by a coarsely porphyritic granitic through granodioritic phase. The latter unit, which appears compositionally to be more of a quartz monzonite to granodiorite, is hereafter referred to as a quartz monzonite on the geologic map (Figure 1, in pocket). The fine-grained granodiorite may possibly represent the border zone and the quartz monzonite the core zone of a single plutonic complex. The quartz monzonite occupies the eastern mountain ridge of the canyon and has not been extensively studied due to its distance from the Antler Mine metamorphic complex and its nebulous contacts into an injection migmatite zone. The Cavalliere granodiorite, on the other hand, is in direct contact with the amphibolite gneisses and and quartz-biotite dominant schists and thus has a more direct bearing on the deformational history of the area.

At the northern end of the 80 km long Hualapai plutonic complex, Kessler (1976) has obtained a Rb_{87}/Sr_{86} isochron of 1800 $\pm$ 470 m.y. for the "Granodiorite gneiss." His correlation of the unit with the Boriana granodiorite is now open to question. Since the oldest known rocks in Arizona are slightly under 2000 m.y., the large error in his data permits overlap of the Hualapai complex with the 1400-1700 m.y. plutonic episode common throughout the central Arizona province (Wilson, 1939) if the error is negative.

Cavalliere Granodiorite

The Cavalliere granodiorite is a light grey to pink grey, medium to coarse-grained, equigranular to porphyritic, weakly to moderately foliated massive rock. The unit weathers to form steep slopes and jutting cliffs. It is cut by numerous late-stage pegmatites concordant to the northeasterly foliation direction. A prominent northwesterly grain particularly evident in aerial photographs cuts the batholith. In the Boriana Canyon area, the Cavalliere granodiorite shows prominent foliation at N40^{o}E, dipping steeply to the northwest. The granodiorite is in knife-sharp contact with the amphibolite. In thin section, samples of the Cavalliere granodiorite are seen to consist of quartz (30-35%), plagioclase An_{27} (40-45%), microcline and minor perthite (8-10%), biotite (8-10%), and lesser epidote (0.5%-1%), sericite, hornblende, and opaque. Trace accessory minerals include diopside, sphene, zircon, apatite, and muscovite.

Compositionally, the Cavalliere granodiorite hovers on the quartz monzonite-granodiorite boundary, as do the other plutons in in the Hualapai complex. Age relations with the eastern quartz monzonite and the Wabayuma Peak complex to the north are equivocal. Age dating on the Hualapai plutonic complex by H. Stensrud (personal communication, 1979) is in process.

Antler Granite

Antler granite forms the prominent ridge that rises near the entrance to the Antler Mine and runs the length of the canyon to the northern limit of the Bulge, where it suddenly plunges under alluvial cover. A second wedge of Antler granite between the quartz-mica schists and the quartz-biotite-(potassium) feldspar schists near the Copper World Mine disappears to the south into the injection migmatite zone with ill-defined contacts difficult to trace.

The Antler granite is an intrusive body, and not a quartzo-feldspathic schist as earlier indicated by mine personnel. Near the mine, tonguings and protrusions of granite can be seen snaking into the quartz-biotite schists and hornblende-plagioclase gneisses, both in plan and vertical exposure. Knife-edge contacts of amphibolite and granite can be seen near the mine entrance. Biotitic xenoliths in the granite are elongated along foliation trends. To the north H. Stensrud (personal communication, 1979) reports blocks of quartz-mica schist incorporated in the Antler granite. Foliation in both

granite bodies retains the strong N30°E-N40°E trend, with dips steeply to the northwest at 70° to 80°.

In hand sample the Antler granite is a medium to coarse-grained, light to medium mottled tan grey weathering to a dark grey, well-foliated porphyritic rock. The granite is cut by concordant quartz veins from 2 cm to 30 cm in width and by quartz-muscovite pegmatites. Mineralogically the Antler granite is notable for its anomalous two-mica assemblage, for which biotite and muscovite contents can exceed 20% and 10% respectively.

By IUGS classification, the Antler granite is a true petrographic granite. An averaged compilation of mineral percentages from thin sections shows it to be composed of quartz (45%), microcline (30%), myremekitic plagioclase An_{13} (7%), biotite (12%), muscovite (5%) and opaque (0.25%). Accessory trace minerals include epidote, zircon, and surficial carbonate. At the edges of the granite ridge, the plagioclase index can jump to 15%, pushing portions of the body into the quartz-monzonite composition field.

For reasons that will be discussed more fully in a later chapter, the Antler granite is proposed to have been an S-type granite generated by anatexis of mica-rich sediments and tuffs.

Pegmatites

The pegmatites in Boriana Canyon cut all rock types and are widespread, particularly in the eastern half. All are concordant with foliation. In areas of extensive folding, pegmatites tend to occupy the axial cores of folds. Dimensionally the pegmatites range

from 0.5 meters to 60 meters and greater in thickness, with an average at 1 to 3 meters. Along strike they range from 5 meters to over 200 meters long. Mineralogically they consist of a simple assemblage of quartz, potassium feldspar, plagioclase, muscovite, biotite, and tourmaline. There is a suggested crude grouping of pegmatite assemblages, namely qz-biot-Kfs-musc within the Antler granite and plutonic complex, qz-Kfs-musc-biot-plag within quartz mica schists, qz-Kfs-tour-musc near the injection migmatite border, strained blue-grey qz-musc possibly metamorphically-derived bodies occupying axial cores of folds, and qz-Kfs-musc in the injection migmatite zone, interfingering with coarse-grained granitic bodies and quartz-mica - quartz-biotite schists.

On the hillside above the Antler Mine discontinuous pods of fractured pegmatite are strung out along the contact of the Cavalliere granodiorite and the amphibolite units. Concordant pegmatites away from the contact in the granodiorite suggest they are late-stage end members derived from the pluton and are either contemporaneous with or post-date the deformation. The pegmatites appear generally to be of igneous origin, and are best described as simple unzoned granitic pegmatites.

Diabase

A lone sill of diabase is exposed in the bottom of a stream-cut in the massive quartz-mica schist section. The unit is approximately 60 to 70 cm wide and can be traced along strike for approximately

forty meters. It is a fine-grained, dense, black rock that is structurally featureless. No alteration effects are evident on either side of the diabase. In thin section it is seen to consist of a fine, felty, ophitic intergrowth of plagioclase, augite, clinopyroxene, opaque, epidote, hornblende, sericite, and quartz. The other notable occurrence of diabase in Boriana Canyon consists of a large triangular sheet in the Cavalliere granodiorite west of the Boriana Mine.

Injection Migmatitic Rocks

The injection migmatite zone on the eastern side of Boriana Canyon represents a transition from quartz-mica schists into quartz-biotite schists through pegmatites and leucogranites and finally into quartz monzonite. The term "migmatite" is a field term chosen to represent a mix of mica schists and pegmatites that are too finely intermixed accurately to define at the mapping level. The migmatites are categorized as "injection migmatites," after Winkler's (1976) cautioning note to designate:

> ...such migmatites which have attained their migmatitic appearance by the injection of granitic magmas in the form of apophyses, smaller or larger dykes, etc., into a metamorphic country-rock. It is suggested to call such migmatites injection migmatites. These should be fully distinguished from in-situ migmatites, i.e. from such migmatites whose light-colored granitic portions are overwhelmingly not intrusive originating from an outside source, but have been formed within a high grade metamorphic gneiss or schist itself... (p. 278).

Foliation planes are the localizing structures for the narrow lit-par-lit injections and bulbous dikes of granitic and pegmatitic

material which intrude both quartz-biotite and quartz-mica schists. Leucogranitic dikes widen out to 50 meter wide zones with thin entrapped interleavings of mica schist.

Petrographic examination of the quartz-biotite - quartz-mica units shows the same general textures and size values as their western counterparts. Mineralogically the schists have undergone thermal alteration, as biotite is degraded to sillimanite and muscovite. Sillimanite needles are also found as inclusions in quartz grains. The gradational boundaries of the quartz-mica schist and the quartz monzonite with the injection migmatite zone are difficult to place. On the geologic map, the contacts are crudely placed from aerial photographs; they have not been extensively studied on the ground.

CHAPTER 3

STRUCTURAL GEOLOGY

The two broad structural elements in Boriana Canyon are the northeasterly-trending foliation, fold axes, and lithologic contacts within the Boriana series and the enigmatic northwesterly circular projection of amphibolite and quartz-biotite schist into the Cavalliere granodiorite called the Bulge. Each regime possesses unique structural character, so they will be treated separately.

Boriana Canyon Structures

Prominent steeply-dipping N30°-N40°E foliation is developed within both the Boriana series and the intrusives. The foliation is defined by platy alignment of amphiboles and phyllosilicates and by slight elongation of recrystallized quartz grains in more siliceous units. A very weak north-to-northeast(?) remnant foliation can be observed in rare sections within amphibolites near the Antler Mine.

Contacts among gneisses and schists are only approximately parallel to the northeasterly-striking foliation. Discrete lithologic units at the map level tend to merge into a compositionally different unit at a slight angle. The angle, variable in direction and magnitude and generally constituting a small departure from the lithologic

trend, signifies that the present foliation and original compositional layering are not necessarily coincident.

Along the western margin of the canyon, rootless folds on the scale of tens of centimeters are developed within the amphibolite units. The rootless folds are defined by 0.5 to 1.0 cm thick attenuated limbs and detached crescent-shaped noses, with axial planes parallel to foliation, that is, similar folds or Ramsay Class 2 or 3 folds (Ramsay, 1967). Attention is directed to the fold system southwest of the Antler Mine, which on the geologic map (Figure 1, in pocket) displays the same characteristics as one of rootless folds or transposition structures, but on a larger scale. Photomicrographs of silicate alteration from the ore horizons reveal tight to isoclinal and chevron microfolds (Figure 11).

Antler Mine Area Structures

Folding within the Boriana series is best demonstrated at the Antler Mine where the schist and gneiss units are trapped in a 250 meter wide zone between Antler granite and Cavalliere granodiorite. Amphibolite gneiss and quartzofeldspathic schist units are doubly-plunging, isoclinally folded, and overturned to the east. Southwest of the mine shaft, massive fibrous silicates occupy the nose and trough of the synformally folded units. Lineations, as defined by alignment of micaceous and amphibolitic minerals, demonstrate that the folds plunge to the southwest between 45° and 64°. North of the mine shaft the gneisses and schists are antiformally folded. In

Figure 11. Photomicrographs of Microfolds.

(a) Isoclinal-to-tight microfolds in muscovite-biotite, B7-1489 (100X).

(b) Chevron (kink) microfolds in muscovite-biotite, B7-1489 (100X).

A

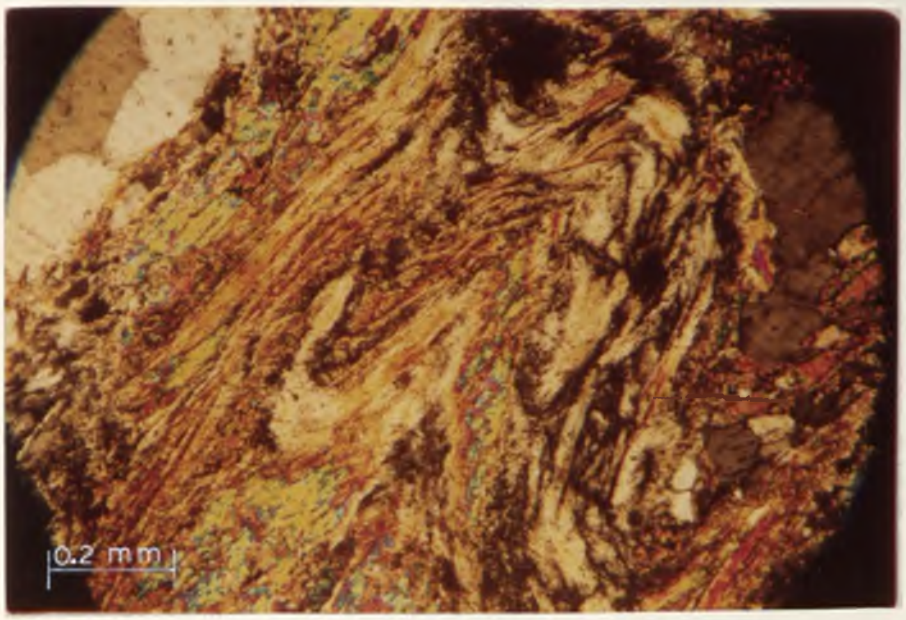

B

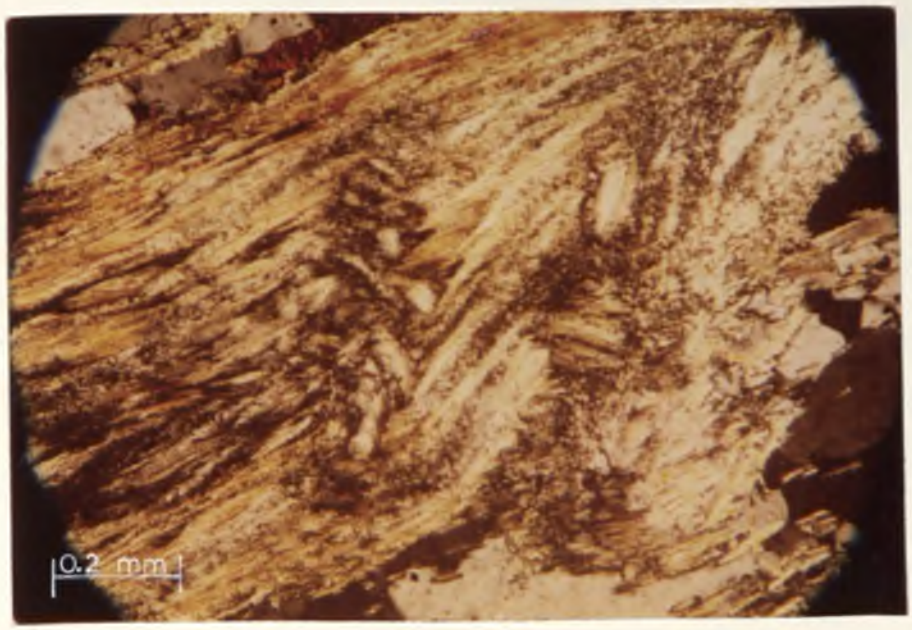

Figure 11. Photomicrographs of Microfolds.

the streamcut below the mine, measurements on overturned isoclinal to tight folds with axial plane cleavage show the antiform to plunge N0-10°E between 52° and 66°.

Still (1974) described the antiformal fold system in the ore horizons as a series of left-hand en-echelon folds variably plunging to the north between 50° and 63°, based on compilation of drill data and available maps. On the surface, however, evidence of a left-hand en-echelon fold system is not convincing. Instead, the ore bodies would appear, by projection of surface folds, to be part of a transposed, steeply-plunging, overturned, isoclinal-to-tight fold geometry. Further complications of poorly outcropping subsurface folding are quite probable, but confirmation and understanding await reopening of underground workings.

Copper World Mine Structures

The Copper World Mine, almost entirely within a thick section of quartz-biotite-(potassium) feldspar gneiss, does not evince the same degree of folding as at the Antler Mine. The lack of amphibolite marker horizons and the hillslope cover tend to mask any obvious fold exposures. Silman (1966) reported the locus of mineralization to be confined to the limbs and fold nose of a steeply-dipping northeasterly-plunging fold. The glory hole near the hilltop above the mine workings is situated within a limb of the overturned isoclinal fold and is coincident with a rare northeasterly fault zone.

The apparent similarity in fold style to the Antler Mine is striking. Transposition and shearing along a limb can account for the northeasterly fault zone and the strong shearing reported in the ore horizons. Mineralization diminishes to the northeast, and continuity has not been adequately tested to the southwest; northwesterly faults and photolinear "shears" slicing through the area suggest an off-setting relationship between southwestern and northeastern parts of the fold. More detailed mapping is needed in both mine workings and on the hillsides to delineate the intricacies of fold geometry.

Structures in the Quartz-Mica Schists

The structural character of the quartz-mica schist section in the central portion of Boriana Canyon is not as sharply displayed as it is at the Antler Mine; the homogeneity of the quartz-mica schists contrasts with the thin amphibolite and quartz-biotite schist units that so well delineate folds at the mine.

The structures in the well-foliated micaceous terrain consist of normal and southwesterly-plunging, isoclinal-to-tight, overturned folds. Synformal and antiformal fold limbs are overturned predominantly to the east, although a minority are overturned to the west. Some of the few fold exposures consist of weathering-resistant outcrops of siliceous quartz-mica schist (Figure 12). Plunge measurements from well-defined lineations vary between 30° and 70° to the southwest.

Figure 12. Overturned, Isoclinal-to-Tight Folds in Quartz-Mica Schists.

Exposures of fold closures are rare. The steeply-dipping northeasterly foliation is approximately concordant to the axial plane trends, and dips both to the northeast and northwest.

The greater portion of the central section of quartz mica schist is a flat to gently-rolling expanse of schist with a veneer of soil and rubble. Traverses across a level expanse of overturned isoclinal folds with no marker horizons reveal foliation surfaces with dips which vary by only a few degrees from one limb to the other within several meters. It is thus difficult accurately to gauge degree of folding in the section, except where streamcuts and siliceous outcrops fortuitously permit observation. Pegmatites, some metamorphically derived, tend to occupy the axial cores of folds and are abundant across the quartz-mica schist section. The pegmatite abundances, the changes in dip from northeast to northwest, and the intermittent fold exposures suggest the entire section to be isoclinally folded and overturned, predominantly to the east.

Approximately halfway up the canyon, a "necking" or narrowing of the injection migmatite-quartz monzonite mass into the mica-schist section can be seen (Figure 1, in pocket). Commensurate with this feature is a series of compressionally-induced synformal-antiformal folds exposed in deep stream cuts which parallel the northeast-trending fold axes. The folds, traceable for distance on the order of tens of meters before being obscured by cover, in some instances can be correlated between exposures for several hundred meters.

Lineations are poorly developed but indicate plunges to the southwest between 44° and 70°. Very fine chevron folds are developed in the folds, and wrap the present foliation about them, demonstrating that they are later than the present foliation.

Foliation data for the Boriana Canyon belt (Figure 13) demonstrate the northeasterly trend and the folded nature of the section, with steeply-dipping limbs represented by the two opposite clusterings of poles to foliation.

Faulting and Shearing

With the exception of several minor northeast-trending faults at both mines, shown as the Cholla Fault on level maps of the Antler Mine (Romslo and Wilson, 1948), faulting in Boriana Canyon is dominantly northwesterly-directed (Figures 1 and 2, in pocket). Along the eastern edge of the canyon, maximum apparent separation is 110 meters, while along the western margins it is on the order of 35 meters. The faults, recognized by the displacement of granodiorite/quartz monzonite against schist/gneiss along the margins, are difficult to trace into and through the metamorphic terrain due to cover and the plastic nature of the schist units. In more competent sections, fault traces are revealed by 3 to 20 meter wide goethite-stained silicified breccia zones. Mappable faults are dominantly steeply-dipping to vertical, left-lateral structures, although minor right-lateral faults are evidenced.

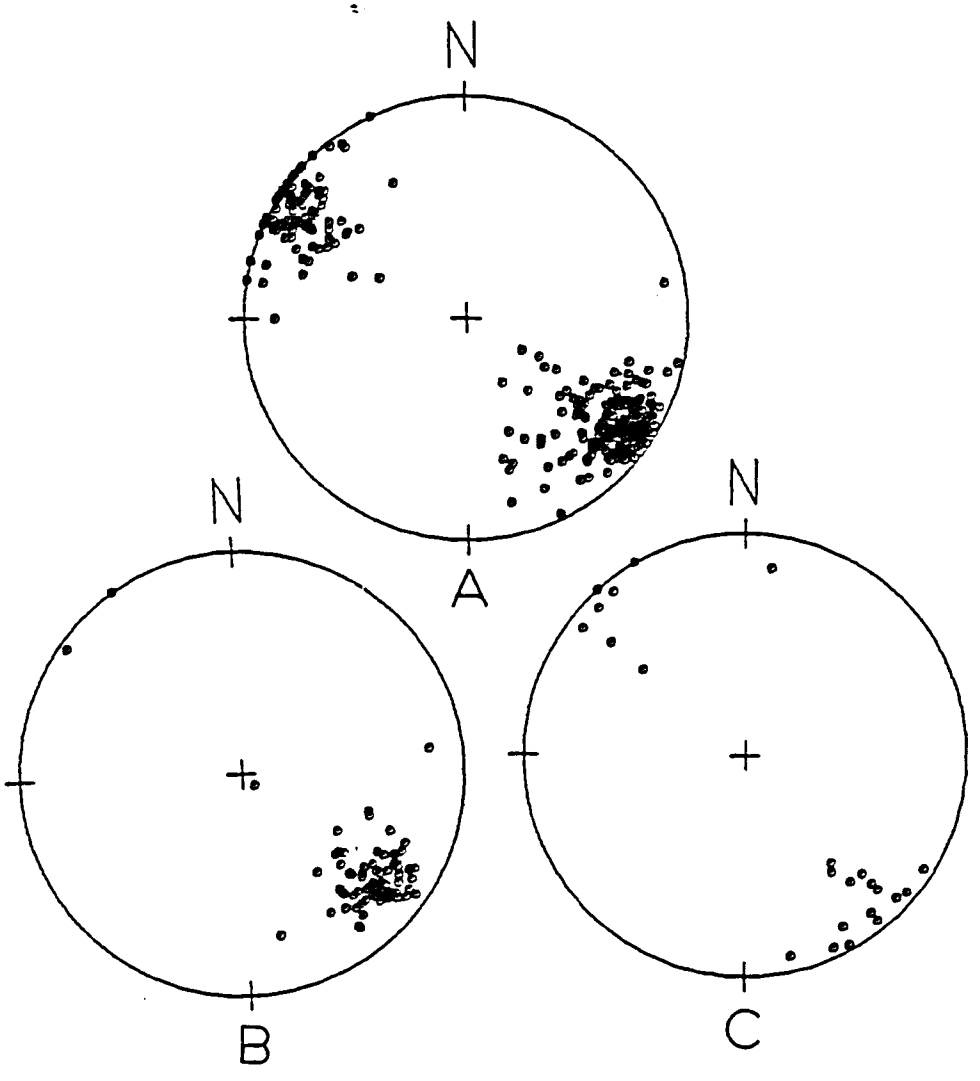

Figure 13. Lower-Hemisphere Stereographic Projection of Boriana Canyon Foliation Data, Exclusive of the Bulge. --
(a) Central portion of Boriana Canyon (267 points).
(b) Antler Mine vicinity (79 points).
(c) Copper World vicinity (23 points).

At the Antler Mine, Still (1974) showed the block situated between the northwesterly, steeply-dipping to vertical Saguaro and Ocotillo faults as downdropped with only minor lateral displacement. Across the faults the folds change from southwest-plunging to north-plunging structures. Approximately 300 meters northeast of the shaft a prominent left-lateral fault, here termed the Joshua Fault, can be traced through a boulder pile of Cavalliere granodiorite into gneiss and schist units. The eight-meter wide structure, exposed in a stream cut, strikes N40°W and dips 80° to the northwest. There are no horizons on which the degree of vertical displacement may be gauged. From the differences in continuity and projected widths of lithologic units on both sides of the Joshua Fault, it is apparent that the fault is another oblique-slip fault with a definite vertical component. Obvious folding disappears to the northeast across the faulting, suggesting that the block to the north is upthrown with respect to the southern block.

A number of linear northwesterly trending "shear" components, particularly evident across the western margins, are apparent in aerial photographs. The mapped faults in Boriana Canyon are coincident with the photo-linear features, which carry the sense of "shear" continuity across the canyon. Like the known faults, the photo-linears are geomorphically coincident with boulder-filled gullies, stream cuts, ridges, and saddles in the plutons and coincident with changes in outcrop width and lithologic continuity. On the map a 300 to

380 meter spacing of the photo-linears and faults is apparent along the western margins.

The outcrop pattern change and the similar disposition of mapped faults nearby leads one to the conclusion that photo-linear features are indeed an expression of the faulting, or shearing, picture within Boriana Canyon. North of the Joshua Fault the "shears" define further block faulting. Several amphibolite fold noses within the blocks thus indicate various levels of fold exposure, much in the manner of step faults. The "shears" or faults are not as well-defined in the massive quartz-mica schist section, but do pick up again in the eastern walls of injection migmatite-quartz monzonite.

Since hard physical evidence for actual displacement of the units is concealed by boulder talus and soil cover, the photo-linears are plotted separately on Figure 2 (in pocket) and presented as such. It is the conviction of the author, however, that the linears represent real but subtle faults of minor vertical and lateral displacement. Orebody extensions to the northeast or southwest of the present mine workings obviously will be affected by this minor faulting.

Structures and Lithology in the Bulge

The Bulge constitutes a puzzling structural anomaly in Boriana Canyon, as it represents a drastic deviation from the northeast structural trend. In map view it is seen as a thick semi-circular sequence of amphibolite and quartz-biotite schists projecting into

the Cavalliere granodiorite. Foliation in the gneisses and schist essentially parallels the outer semi-circular amphibolite-granodiorite contact; northeasterly foliation in the surrounding granodiorite abuts sharply against the amphibolite of the Bulge.

Lithology

Massive, almost hornfelsic, hornblende-plagioclase amphibolite in the Bulge has apparent thicknesses on the order of several hundred meters. Interspersed with it are lesser sections of quartz-hornblende feldspar schist, attaining a maximum apparent thickness of approximately 52 meters at one contact with quartz-biotite-(potassium) feldspar schist, but within the hornblende-plagioclase sequence is only 3 to 8 meters wide. Rare, thin, 0.5-3.0 meter porphyroblastic and 0.4 meter "pseudofragmentally" textured hornblende-plagioclase units are recognized. In thin section, the Bulge amphibolites texturally resemble their counterparts to the south. However, epidote is notably absent and garnet, magnetite, and actinolite-tremolite are noticeably more abundant.

Occupying the center, or inner circle, of the Bulge are quartz-biotite schists. Although quartz-biotite schist predominates over quartz-biotite-(potassium) feldspar schist, a good portion of the former petrographically may be quartz-biotite-(potassium) feldspar. Biotite and magnetite contents are slightly higher than in equivalent rocks outside the Bulge. Otherwise, the schists are identical to the quartz-biotite schists at the Antler Mine. It is

within quartz-biotite-(potassium) feldspar schist at or near its contact with amphibolite gneiss that iron formation and fibrous silicate masses are developed.

Foliation Data

The quartz-biotite schist units display a concentricity in foliation directions with foliation from the outer circle of amphibolite but with a great deal more scatter of poles. Lower-hemisphere stereographic projections of foliation data collected in the Bulge and granodiorite are presented (Figure 14) with a compilation of all foliation data for the Bulge (Figure 14a). The foliation values literally are seen to box the compass, illustrating the semi-circular course of the gneisses and schists as they carry into the Cavalliere granodiorite. Figures 14b and 14c represent data collected at locales from the westernmost extent of the amphibolites and along the southern edge of the Bulge. Foliation data in the amphibolites and in the granodiorite directly across the contact were collected at both locales to illustrate the sharp differences in foliation within the batholith and the gneisses.

Faulting

The southwest edge of the Bulge is bounded by a 10-15 meter wide, northwest-trending, sheared section of granodiorite. Across the shear zones, northeast foliation swings to the northwest, indicating an apparent left-lateral movement. The northern edge of the

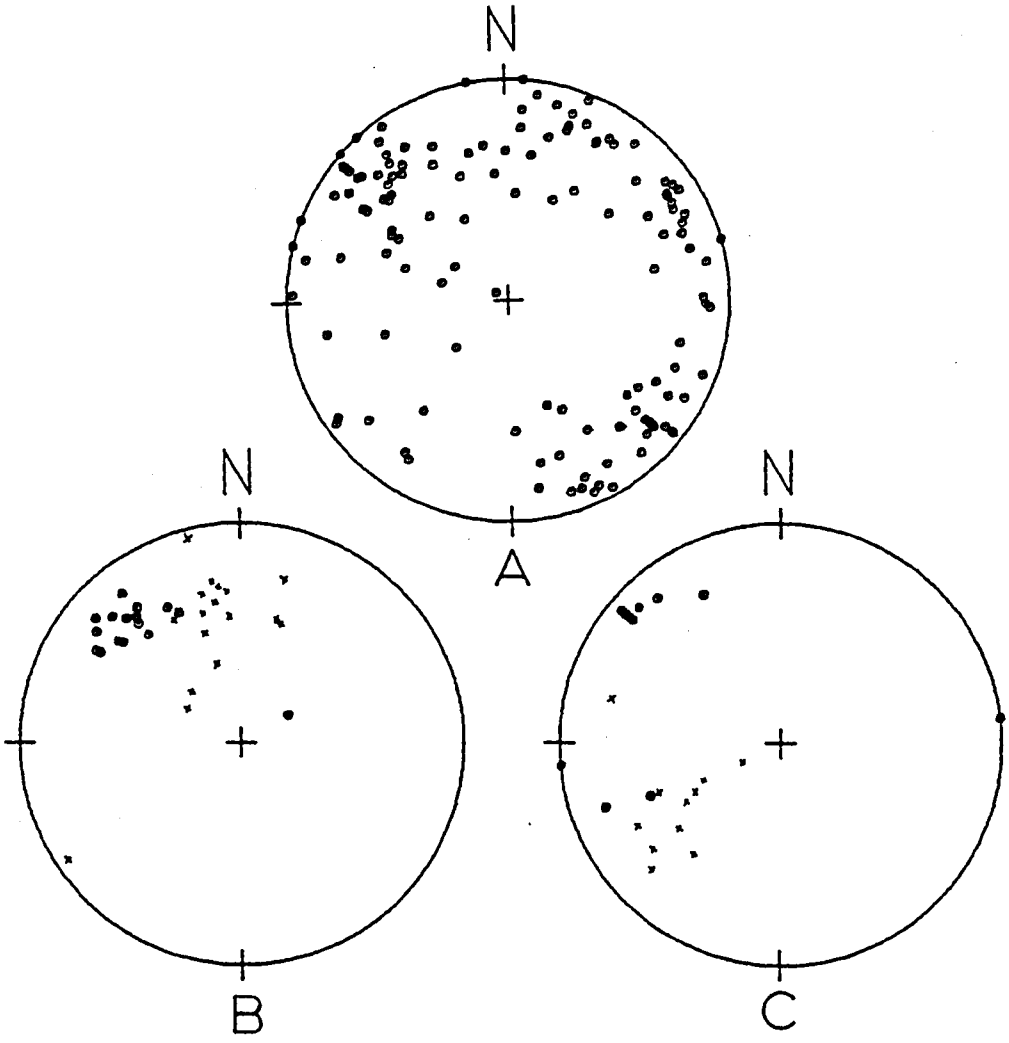

Figure 14. Lower-Hemisphere Stereographic Projection of Bulge Foliation Data.

(a) All gneisses and schists within the Bulge (137 points).

(b) Amphibolite versus granodiorite, westernmost locale. Circles = granodiorite, crosses = amphibolite (33 points).

(c) Amphibolite versus granodiorite, southern locale (23 points).

Bulge, obscured by talus, displays a west-northwest photo-linear shear component coincident with a minor shear zone that continues into Boriana Canyon. The Antler granite disappears, or is downfaulted, under cover at its juncture with the photo-linear, suggesting the photo-linear is a major structure.

Folding

Within the amphibolites it is possible to trace out attenuated limbs and detached noses of rootless folds and ptygmatic folding on a scale of tens of centimeters. Evidence for large-scale folding is not found until the Boriana Canyon structural regime is encountered where a series of synformal-antiformal folds are developed near the contact with granodiorite.

CHAPTER 4

ECONOMIC GEOLOGY

From an economic standpoint, the most significant aspect of Precambrian geology in Boriana Canyon is the occurrence of massive sulfide mineralization within the metamorphic sequence material. Mine production of high-grade copper and zinc ores in the area has so far been confined to the Antler and Copper World mines, where the original disocveries were guided by outcropping copper oxide mineralization. There are several other sites within the study area that bear potential for further discoveries. It is useful therefore to look at the sulfide and silicate constitution of the ore-bearing horizons and their relations to the wallrocks, and the occurrences of iron formations and fibrous silicate masses at the Bulge.

Antler Mine

History

Original discovery of Antler mineralization was recorded with the Antler claim in 1879 and in 1888 with the Spuyten-Duyvil claim (Romslo and Wilson, 1948). The Phelps Dodge Corporation later acquired the patented claims but undertook little development work. The property was intermittently active over the years, passing through a number of owners, operators, and lessors. A summary of ownership and production history (Table 1) is abstracted from Still (1974).

Table 1. Summary of Antler Ownership and Past Production Data. -- From Still, 1974.

Owner	Operator	Period	Production Tons	Grade
Phelps Dodge Corp. (to 1943)	--	1916-1929	1080	5-15% Cu (oxide)
	Mike and Peter Vukoye	1929	280	5-14% Cu (oxide)
Mike and Peter Vukoye (1943)	--	--	--	--
R. B. Strassburger (1943-?)	Silver Shield Mining & Milling Co.	12/43-2/44	400	12% Cu 2.5% Zn
	Arizona Antlers Mining Co.	7/44-7/47	6026	2.34% Cu, 8.38% Zn, 0.95 oz Ag, 0.69% Pb, 0.009 oz Au
	Faire Mining Corp.	3/48-3/49	945	4.11% Cu, 7.6% Zn, 1.11 oz Ag, 0.45% Pb, 0.009 oz Au
Yucca Mining & Milling Co. (?-3/66)	Yucca Mining & Milling Co.	3/49-5/53	35,284	2.54% Cu, 6.52% Zn
Standard Metals Corp. (3/66-present)	Standard Metals Corp.	2/70-12/70	34,236	3.26% Cu, 7.04% Zn, 1.23 oz Ag, 1.10 oz Pb, 0.0095 oz Au
		Total	78,251 tons @*	3.01% Cu, 6.22% Zn

*Grade based on 76,891 tons.

Standard Metals Corporation acquired the property in 1966 for feasibility and evaluation studies. Underground development work and mill construction were part of a program to reopen the mine at an initial 300 ton per day schedule. Mining commenced in February, 1970, and continued until December, 1970, when the operation was terminated due to economic and technical difficulties. Eight deep, exploratory, angled diamond drillholes explored the deeper ore extensions to the north of the present workings in 1974 and 1975. The currently inactive mine remains the property of Standard Metals.

Surface Exposures

Historically, early production from the Antler Mine was derived from high-grade, near-surface, oxidized ores. Smithsonite, antlerite (first described from this locality), azurite-malachite, and chalcanthite are noted. Copper staining is prevalent on the hillsides above the mine. Very little of the oxide ore remains, either on the dumps or in drillcore. Minor secondary covellite and bornite are reported by Romslo and Wilson (1948). All major production to date has been derived from the primary sulfide ores.

A short distance due northeast from the shaft, a thin unit of sulfide-bearing, ferruginous, quartzitic iron formation crops out on the hillside of quartz-biotite-(potassium) feldspar schist. The podiform unit averages 0.5 meters and reaches a maximum thickness of 0.8 meters. The unit can be followed along strike for approximately

twenty-five meters. The iron formation is approximately concordant with foliation within the schist. The magnetite content of the unit is low, averaging 12%. In fresh exposures pyrite can be discerned. Excavation along the present top of the iron formation reveals a 1.5 cm thick rim of massive biotite and an iron depletion for 10-15 cm into the ironstone.

Moving uphill from the iron formation, the biotite content in the schist increases perceptibly. At a point some 15 meters uphill from the iron formation, the schist unit is sheared and passes into a sheared podiform unit of massive actinolite-tremolite and talc stained with iron and copper oxides. The tremolite unit attains a maximum apparent thickness of 1.2 meters, tapering off to 0.4 meters. The N62^{o}E shearing dips 68^{o} to the northwest. A second anomalous unit of biotite schist encountered a short distance along strike and several meters uphill from the tremolite-talc body consists of garnetiferous quartz-biotite with fibrous silicates and copper and iron oxide staining. Across the hilltop the garnetiferous unit passes into amphibolite gneiss.

To the southeast of the Antler shaft, a thickened southwest-plunging synformal fold nose composed of cordierite, anthophyllite, almandine garnet, magnetite, and biotite is found on the high outcropping rise. The trough of fibrous silicates, which appears to be discontinuous at depth, can be traced into thin 0.5 to 2.0 meter units

of quartz-biotite schist and hornblende-plagioclase gneiss. The significance of this unusual assemblage will be treated below.

Mineralization and Alteration

Primary mineralization at depth is developed in thin irregular horizons from 0.6 to 12 meters thickness, with an overall average at 2.7 meters (data calculated from Gilmour, 1975). Along strike the sulfide mineralization persists for at least 730 meters, possibly more. South of the Antler shaft, the ore shoots are regular and narrow in plan view, the fold limbs becoming thicker into fold noses near the shaft where the major tonnage to date has been developed. The overall plunge of the orebody is approximately 63°, or 50° if a left-hand en-echelon fold interpretation is favored. In the deep drill holes B1 through B8, at least two separate intercepts of massive sulfide mineralization were encountered in several holes. Gilmour believes they are separate discrete horizons that may coalesce somewhere in the body, while Still interprets the dual intercepts as repetitions of the same folded horizon.

From drillcore examination, anthophyllite and biotite with variable chlorite pick up markedly along with disseminated pyrite, clots of magnetite, and quartz stringers as the ore zone is approached. In passing from a siliceous hangingwall of quartz-biotite schist (drill holes B1, second alteration horizon B2, B4) or quartz-biotite-(potassium) feldspar schist (first alteration horizon B2, B3, B6,

and B7), the appearance of the massive fibrous silicate rock is rather abrupt. The ore horizons consist of a mix of coarsened sulfides enmeshed in a matrix of cordierite, anthophyllite, biotite-phlogopite, actinolite-tremolite, muscovite, chlorite, garnet, sillimanite, carbonate, epidote, quartz, and trace cummingtonite-grunerite. Sulfides comprise a simple assemblage of pyrrhotite, sphalerite, chalcopyrite, pyrite with intergrown magnetite, and galena.

In all drillholes examined, abrupt termination of the sulfide horizon is marked by about 0.5 meters of brecciated or argillized sheared material against an unmineralized but weakly altered (phlogopite and epidote) siliceous footwall of quartz-biotite-(potassium) feldspar schist. The weak alteration dies out over a several meter span. Mineralization is commensurately sheared near this zone in several holes.

Sulfide Mineralogy

Distribution. Polished surfaces of samples selected from Standard Metals' "B" series of cores were made. As is normal in highly-deformed sulfide masses, no unusual phases other than the five major sulfide minerals observed mesoscopically are detectable. Electron microprobe analysis (D. Lane, personal communication, 1979) of sample B2-1425 confirms reflected-light observations; results are listed in Appendix I.

Sulfide minerals, primarily pyrite, are found scattered throughout the biotite schists but are most abundant in the fibrous silicate material. Pyrite increases from trace disseminations to 4% of the rock volume with the appearance of anthophyllite and phlogopite, and chalcopyrite and pyrrhotite appear as plastically-deformed elongated streaks or stringers. Several meters above the massive ore, 20-30% disseminated sulfides are encountered, although in drill hole B6 the disseminated sulfides are spread over a 12 meter interval. The massive ore constitutes from 20 to 100 volume percent of the rock. Sphalerite is the most abundant of the economically interesting sulfides, averaging 10 to 15 volume percent, with ores assaying 6.5-7% Zn. Chalcopyrite averages 10%, with copper assays averaging 3% Cu. Galena in amounts from nil to 1% Pb in the present upper portion of the ore horizons carries the silver values at the ratio 1% Pb:1 oz Ag. Gold values in the Antler and Copper World ores, unlike many other central Arizona deposits, are essentially nil. Varying abundances of pyrrhotite and lesser pyrite constitute the sulfide gangue mineralogy.

The lead increase at the top, or upper half, of the mineralized horizons was determined by assay (Gilmour, 1975). No systematic variation of copper to zinc ratio could be discerned from polished section observation. However, the split drill core remnants may have been mixed prior to inspection and sampling, an eventuality which would mask zonation.

Mineralogy. Pyrrhotite is the most abundant sulfide mineral. It is found as a pinkish-cream or brownish-pink colored, plastically-deformed mass with sharp to curved grain edges infilling and surrounding fractured euhedral pyrite grains and subhedral silicates, and as fine veinlets replacing anthophyllite along cross fractures. In some samples pyrrhotite contains inclusions of sphalerite, while in other samples sphalerite is the later mineral. Microprobe analysis shows only trace copper, cobalt, and arsenic levels in pyrrhotite.

Sphalerite and chalcopyrite are intimately intergrown, with mutually developed exsolution blebs. In massive sphalerite grains, chalcopyrite blebs are typically small at 0.01-0.06 mm; in massive chalcopyrite samples, sphalerite blebs range between 0.05 mm and 0.15 mm. In reflected light, chalcopyrite exhibits a consistent brass-yellow color, suggesting that selenium at least is not present. Sphalerite maintains a consistent dark-grey color and contains rare dodecahedral pits. Microprobe analysis of sphalerite grains shows approximately 8% to 9% iron substitution for zinc.

Pyrite is the less common form of iron sulfide at the Antler Mine and the most common form at the Copper World. It occurs as pale yellow euhedral cubes from 2 mm to 5 mm that are fractured and filled with ductile pyrrhotite, galena, and chalcopyrite. In some samples it has a ragged or corroded form. Ovoid to lathlike silicate inclusions are common. Fine 0.1-0.2 mm grains of magnetite are

intergrown with pyrite. Where they are in contact with pyrrhotite, they place the equilibrium assemblage at the po-mag-py triple point.

Galena is the scarcest of the sulfide minerals, occurring as smeared, very fine, grey-white, pitted granules coexisting with other ductile sulfides. Microprobe analysis reveals 0.03% silver substitution.

Silicate Mineralogy

Selected core samples of wallrock and massive fibrous silicate were collected from drillholes B1, B2, B3, B4, B6, and B7. Surface samples of fibrous silicate rock were also collected from above the Antler Mine and at the Bulge. In hand sample, the fibrous silicate material is a 2-15 cm, coarse-grained, red-brown through green to white and colorless, bladed acicular to rosette intergrowths of phyllosilicates, amphiboles, and aluminosilicates (Figure 15). Prismatic minerals are commonly aligned concordant to foliation in the surrounding wallrocks, although anthophyllite rosettes can cut across foliation.

Petrography. Anthophyllite is the most common silicate mineral encountered in the apparent hangingwall of the sulfides. Grains are idioblastic lath-like to prismatic and rosette to asbestiform in habit, ranging in size to greater than 15 cm. Under uncrossed nicols it is pleochroic pale-green to colorless, and commonly contains sulfide inclusions. It is replaced by chlorite, cuts biotite-phlogopite, and is interpenetrant into cordierite and garnet.

Figure 15. Cordierite-Anthophyllite Outcrop. -- Location: Northern-most fibrous silicate body at the Bulge.

Anthophyllite, sometimes over 80 volume percent of the slide, is often cross-fractured at 6-10° off extinction, with occasional replacement by pyrrhotite along fractures. Anthophyllite and sulfide-rich sections show sulfide-silicate interactions with growth of cummingtonite-grunerite within pyrrhotite, that is, iron-rich amphibole in the presence of excess iron. Gedrite, the aluminous variety of anthophyllite, occurs in deeper portions of the fibrous silicate mass (drillhole B6).

Cordierite and anthophyllite are minerals diagnostic of thermally-metamorphosed chlorite alteration assemblages (de Rosen-Spence, 1969). In thin section, cordierite shows cross veinlets of chlorite and sericite, and abundant inclusions of magnetite and amphiboles, especially anthophyllite (Figure 16). In habit, cordierite is xenoblastic with interlobate and straight edge boundaries. Lamellar twinning is rare. In thin section, cordierite reaches 6 mm, although in outcrop it is found in grains up to 2 cm. Along edges and fractures it is encircled and replaced by fine felty chlorite, often intergrown with serpentine. Anthophyllite is the only texturally primary mineral that cuts and penetrates cordierite. It is only locally present in the ore horizons, where it can constitute up to 55% of the slide.

Microprobe analysis (V. Walker, personal communication, 1979) of a sample of cordierite collected on the hillside above the Antler shaft from an iron-rich locale still shows a magnesium-dominant

Figure 16. Photomicrographs of Cordierite-Anthophyllite.

(a) B6-1908 (32X).

(b) #123 (northernmost fibrous silicate body at the Bulge). Note iron-depletion halo around anthophyllite, and distinctive crossfracturing in both anthophyllite and cordierite (32X).

A

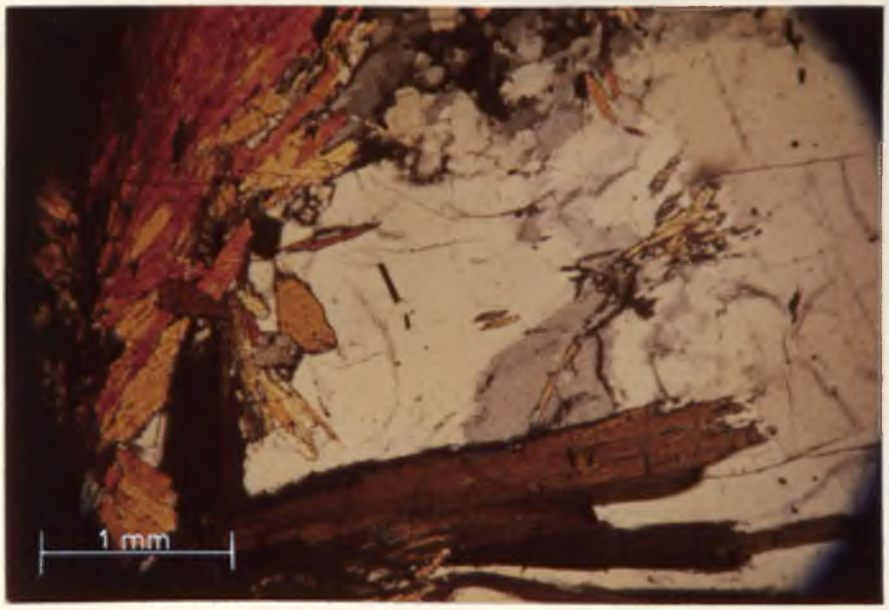

B

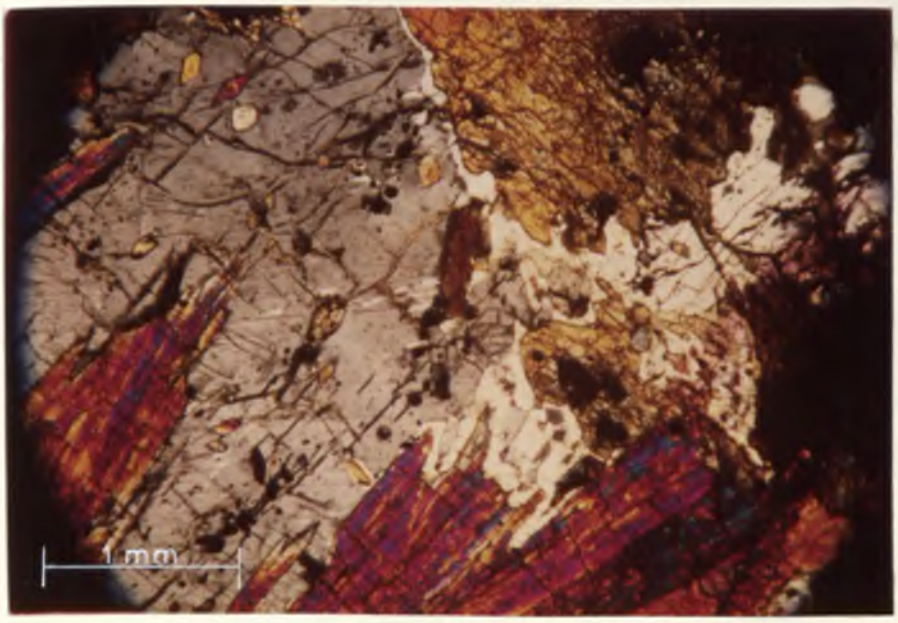

Figure 16. Photomicrographs of Cordierite-Anthophyllite.

composition at $(Mg_{1.32}\ Fe^{2+}_{0.69})\ Al_{3.96}\ Si_{5.02}\ O_{18}$, a composition close to stoichiometric.

The actinolite-tremolite amphiboles occur as idioblastic columnar to prismatic laths up to 5 cm, are commonly twinned, and in plane light appear colorless to pale green. They embay sulfides and appear younger than phlogopite and anthophyllite. The ferriferous middle member actinolite is more common in mineralized sections. Abundance of the minerals varies, but is generally low in anthophyllite-dominated sections and high in carbonate-epidote-rich sections.

Biotite and phlogopite both occur as 0.3 mm to more than 3.0 mm, subidioblastic to idioblastic columnar to prismatic laths. Biotite is pleochroic from light-green to brown, while phlogopite is colorless to pale-green. Biotite is more apt to contain ovoid poikiloblasts of quartz and magnetite. The pair embays quartz, sulfides, garnet, plagioclase, actinolite, and is either later than or contemporaneous with anthophyllite.

Chlorite appears to be an alteration product of anthophyllite and cordierite, although in a few sections it appears as a primary mineral. It has a fine to felty texture, and can be intergrown with or occur near to serpentine. Chlorite is mostly prochlorite (ripidolite), although pennine appears in a few samples.

Garnet appears discontinuously throughout the massive fibrous silicate zone, but is best developed in the iron and alumina-rich portions of the orebody. It has a subidioblastic to xenoblastic and

spongey habit, containing abundant rounded poikiloblasts of quartz and laths of biotite. In thin section, garnet ranges from 0.8 mm to 2.6 mm, while in outcrop it can reach 10 mm or more. Garnet is colorless to pale pink in thin section, and is commonly rimmed with chlorite and biotite. Four electron microprobe runs (D. Lane, personal communication, 1979) of a garnet collected from the massive garnetiferous outcrop of fibrous silicate above the Antler Mine shows it at $Alm_{0.77}$ $Pyr_{0.17}$ $Sps_{0.03}$ $Gr_{0.03}$ to be mostly almandine, with some pyrope and much less spessartine and grandite component. In addition, chlorite, hercynite, and ilmenite inclusions were noted. The garnets from this locale contain abundant tubular fluid inclusions discernible under high magnification.

Quartz occurs as 0.3 to 0.6 mm xenoblastic grains, containing poikiloblasts of opaques, biotite, actinolite and sillimanite. Quartz is both an alteration product and a remnant constituent of the wallrocks, along with remnant potassium feldspar and plagioclase.

Sillimanite occurs as 0.05-0.15 mm-long tubular needles or rods in alumina-rich portions of the orebodies (Figure 17). It is a replacement in quartz, actinolite-tremolite, biotite-phlogopite, muscovite, and chlorite. Overall sillimanite averages 0.5%, although in one thin section it constitutes 5% of the sample.

Fine felty serpentine, possibly talc, is often present with actinolite-tremolite, and is an apparent breakdown of magnesium-bearing minerals, although in several slides it has primary textural relations.

Figure 17. Photomicrographs of Sillimanite.

(a) Sillimanite with quartz, chlorite, phlogopite, serpentine, and anthophyllite, massive sulfide horizon B6-2056 (100X).

(b) Sillimanite with biotite-phlogopite and quartz, B2-1406 (100X).

A

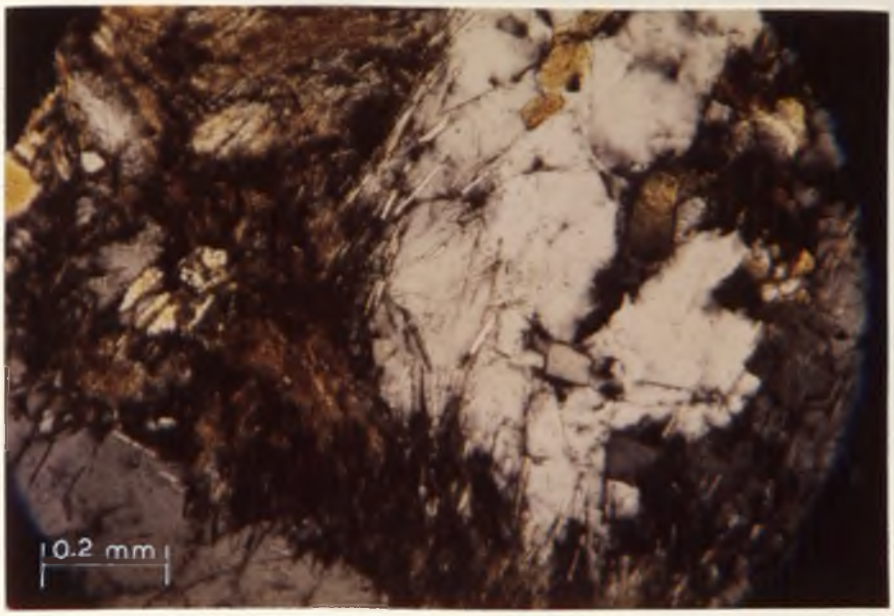

B

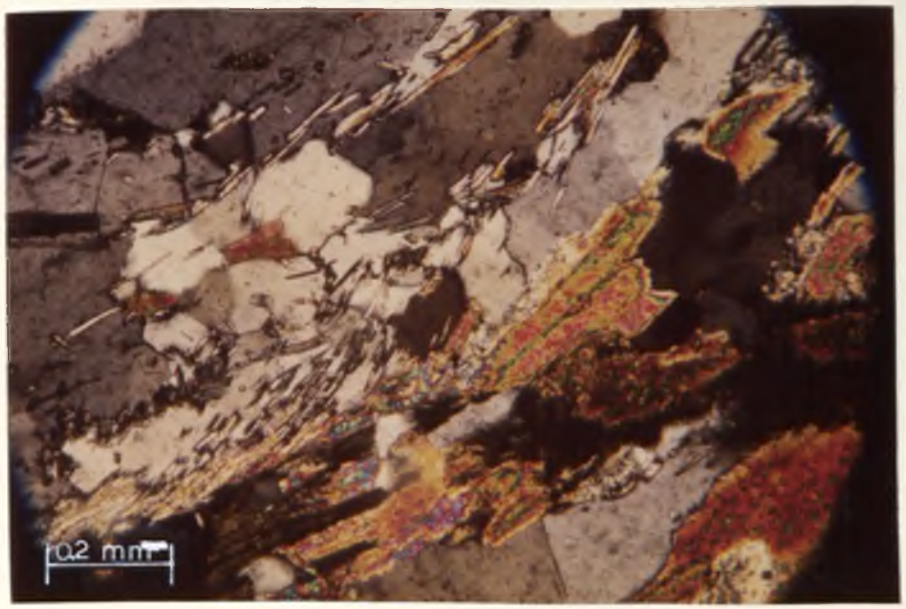

Figure 17. Photomicrographs of Sillimanite.

It rims and replaces amphiboles and cordierite, and has a fine columnar to needle-like aggregate habit.

Calcite is the common carbonate mineral encountered, with ankerite noted in one instance. The carbonate occurs as 0.5-1.0 mm disseminated grains. Carbonate is most abundant in deeper sections with actinolite-tremolite and epidote.

Muscovite occurs at sporadic intervals as both a primary and secondary mineral and can constitute from trace to 30% of the slide. In habit it is idioblastic to subidioblastic, varying from 0.1 mm to more than 1.5 mm.

Silicate Zonation. The fibrous silicate zone in B6 is 50 meters in drill core section (not necessarily true thickness) and can be divided into two chemically distinct assemblages. The 'upper' zone consists of cordierite-anthophyllite-biotite while the 'lower' zone is composed of actinolite-tremolite-carbonate-epidote-sillimanite-biotite-phlogopite-serpentine-anthophyllite. Although it is difficult to correlate assemblages from hole to hole due to uncertainties of fold reconstruction, it appears that the fibrous silicate assemblage in surrounding drillholes is more akin to the upper zone assemblage of B6.

There appears to be an inverse correlation between cordierite and biotite, as cordierite is only developed appreciably in association with anthophyllite without biotite. Where cordierite is absent, biotite and anthophyllite are the characteristic magnesian phases.

Further downhole in B6, phlogopite and actinolite content increase with the rare appearance of gedrite, the aluminous variety of anthophyllite, mixed with normal anthophyllite. A rise in carbonate and actinolite-tremolite content is paralleled by the appearance of serpentine, sillimanite, epidote, and rare cummingtonite. Within the disseminated sulfide zone, where actinolite-tremolite dominate the silicate assemblage, carbonate constitutes over 50% of the rock over a 2 to 3 meter interval.

A listing of the fibrous silicate assemblages in drillholes B1, B2, B3, B6, and B7 is presented for comparison in Appendix III. In drillhole B6 the bulk chemical change in the fibrous silicates is illustrated by the change in Ca + Al + Fe + K from the present top of the horizon (1895') to the bottom of the massive sulfide ore zone (2052-2056'). Magnesium-dominant minerals are constant down to the carbonate horizon (2026') where the iron, calcium, aluminum, and potassium components abruptly pick up. The change will be discussed more fully in later chapters, and is attributable to differences in the protolithic chlorite-wallrock starting compositions.

Copper World Mine

The history of the Copper World Mine is less well known. The mine was presumably founded in the early part of the century, but the only available mine production data begins in the 1940s. Forrester (1963) reports an estimated 16,074 tons of ore averaging

3.55% Cu, 10.29% Zn, 0.66 oz Ag, and 0.0017 oz Au hoisted in the period from 1944-1959. In 1963, the Bobcat (Copper World) property was donated to the University of Arizona, who leased it to several operators over the next 14 years. The mine was sold to Steve Tima, Phoenix, Arizona, who holds the currently inactive mine.

The mineralization and associated fibrous silicates at the Copper World Mine are virtually identical to the sulfide mineralization and silicate assemblage developed at the Antler Mine. In the little drill core available for examination, Copper World sulfide mineralogy consists of the same simple sulfide suite, with the exception that pyrite exceeds pyrrhotite. Arsenian sulfide minerals have been reported from the Copper World (Rasor, 1946), but were not seen either in dump samples or in drillcore. Fibrous silicates consist of anthophyllite, tremolite, biotite-phlogopite, sillimanite, quartz, chlorite, magnetite, and carbonate, some dump samples showing calcite exceeding 12%. Cordierite was not seen in core or thin section, but is expected since the thin sections only show the high biotite-anthophyllite pairing. Although tremolite was not encountered in thin section, Rasor reports tremolite constitutes a major portion of the silicate gangue mineralogy. This is consistent with the high calcite contents seen in dump samples.

Silman (1966) notes the presence of a "persistent, narrow chert" unit along the present base of the massive sulfide horizon, but offers no clues to its iron content or its affinities to a

pegmatite or to a true "chert" horizon. Wallrocks in the Copper World Mine are quartz-biotite-(potassium) feldspar schist and lesser quartz-biotite schist. Amphibolite units are not in evidence on the surface, nor are they mentioned in mine reports.

Questions remain as to continuity of sulfide mineralization to the southwest, orebody geometry, and silicate-sulfide zonation. Nevertheless, the lithologic, mineralogic, and structural characteristics demonstrate a commonality of the Copper World and Antler mines.

Cordierite-Anthophyllite Schists and Iron Formations in the Bulge

A number of podiform iron formations and fibrous silicate bodies are found in the quartz-biotite-(potassium) feldspar schist near its contact with the amphibolite at the Bulge. Their similarity in setting and mineralogy suggests a close tie with the Antler and Copper World deposits.

The bodies of iron formation consist of thin discontinuous lenses or pods of ferruginous quartzitic material. In outcrop, the iron formations are reddish-brown, resistant bodies that approximately conform to the foliation and contacts of the quartz-biotite-(potassium) feldspar schist and hornblende-plagioclase gneiss units (Figure 18). Slightly iron-depleted layers within the quartzose rock impart a faint banding effect to weathered surfaces. Fresh exposures of the units reveal a texturally homogeneous, recrystallized "black" mass of vitreous quartzite with a notable magnetic response. Along strike,

Figure 18. Iron Formation Outcrop. -- Location: Northernmost iron formation unit near Bulge drill road.

the ironstones attain 25 meter lengths comparable to the unit at the Antler Mine. The northernmost exposure of ironstone pinches and swells to a maximum thickness of 2.2 meters, while the other units vary from 0.3 to 1.1 meters in thickness.

In thin section, the ironstone is seen to consist of a granoblastic equigranular interlobate mosaic of xenoblastic quartz (0.3-0.5 mm), idioblastic magnetite (0.1-0.3 mm), xenoblastic hematite (0.6 mm), and minor shreddy stilpnomelane(?) and hornblende. The long axes of minerals are parallel to wallrock foliation. Microscopic apatite (10-30 microns) is present to perhaps 0.5%. Trace stilpnomelane(?) as a shreddy mass between grains eludes positive identification. Hornblende is particularly abundant (up to 12%) in the upper sections towards the amphibolite contact. No garnets were observed either in outcrop or in thin section.

Two fibrous silicate masses are also found at or near the biotite schist-amphibolite contact. In one case an ironstone unit is located within the schist unit and several meters below the fibrous silicate mass. The massive fibrous silicate bodies are discontinuous, slightly podiform, and concordant overall to wallrock foliation and lithologic contacts. The westernmost silicate unit attains a thickness of 12 meters, while at the other locale it averages between 1 and 2 meters width, and is persistent along strike for 20-30 meters.

In thin section, the textural relations of the silicates are similar to the Antler Mine samples. The copper and iron-oxide stained

fibrous silicate bodies consist of an assemblage of cordierite-anthophyllite-magnetite with or without chloritoid, biotite, chlorite, trace cummingtonite and subordinate actinolite-tremolite. Magnetite is more prevalent toward the amphibolite contact.

CHAPTER 5

GEOCHEMISTRY

In an attempt quantitatively to refine hypotheses concerning protolith identity of the Boriana gneiss-schist complex, samples of the various units were collected for major and trace-element analysis. The rationale is that regional metamorphism is essentially a closed isochemical system in which there are neither additions nor removals of components during metamorphism except perhaps for the loss of some volatiles and the redistribution of alkalies and SiO_2.

Complications can and do arise, if there are synkinematic plutons in proximity to metamorphic wallrocks, by the metasomatic introduction of fluids with alkalies from the pluton. Most current researchers, particularly in Canada, do not consider alkali metasomatism a major problem unless plutons exhibit evidence of large-scale fluid flow. Neither the Antler granite or Cavalliere granodiorite show signs of hydrothermal alteration.

The use of whole-rock and trace element data in distinguishing the igneous versus sedimentary origin of amphibolites was pioneered by Leake (1964) and Evans and Leake (1960). Leake's work was augmented by Van De Kamp (1968), who extended the method to cover metasedimentary rocks. Seymour and MacLean (1977) successfully applied these

techniques in the interpretation of the possible metavolcanic protolith wallrocks of the massive sulfide bodies at Montauban Les Mines, Quebec.

This technique was chosen, both for its economy and relative simplicity, to provide chemical evidence necessary for interpretation of the origin of the Antler wallrocks. The reader is urged to consult the benchmark papers for a more thorough discussion of the rationale and methods involved.

Analytical Methods

Fresh samples of schists, gneisses, ironstones, and fibrous silicate rocks were collected from outcrop and drillhole B6. After preliminary crushing, the splits were sent to Barringer Research, Inc., Englewood, Colorado, for further preparation and forwarding to Toronto, Canada, laboratories.

After hydrofluoric acid leaching the samples were analyzed by Barringer's "radio frequency induction coupled plasma emission spectroscopy" system, which theoretically allows simultaneous scanning for 24 elements at detection levels equal to or better than that offered by conventional atomic absorption spectroscopy methods. Analytical errors can result from liquid to solution dilution factors, dissolution techniques, and matrix effects introduced by atypical samples high in iron, calcium, strontium, or barium. The samples were rerun by wet-chemical means to obtain ferrous iron (Fe^{2+}) data. It became apparent that trace-element data were reproducible, but

that major-oxide analyses were open to question. Spot checks on several samples showed the silica and total iron analyses unacceptable. Therefore, the wallrock samples were reanalyzed by X-Ray Assay Laboratories, Toronto, by X-ray fluorescence methods with excellent results.

The analytical results, sample locations, the calculated niggli values for each sample and thin section fibrous silicate assemblages are listed in Appendix III. The major oxide analyses for the iron formations and fibrous silicate materials and mineralization should be regarded with caution, as these samples were not reanalyzed due to economic limitations. Several wallrock samples which proved upon thin section analysis to be slightly altered are not included in Appendix III or in the plots.

Protolith Geochemistry

In interpreting whole-rock data from the Antler Mine it is important to note that absolute values of individual elements are not as informative as relative values of oxide components. On Leake's (1964) and Van De Kamp's (1968) diagrams, it is trends of variation exhibited by relative values that help distinguish heritages of amphibolite and quartzofeldspathic units. The analyses are thus recalculated to provide niggli values, which simply relate the relative molecular proportions of the oxides in the rock, for al, c, mg, k, and alk by methods outlined in Barth (1962). Plots of

niggli numbers against one another and against log plots of trace-element values in ppm allow graphical separation of orthogneisses, those rocks derived from igneous material, and paragneisses, those rocks with sedimentary protoliths.

Amphibolites

Amphibolites represent either metamorphosed basalt-andesites or dolomitic pelites. A plot of niggli c versus mg for the Karroo dolerites of South Africa essentially defines a differentiation curve for a basaltic magma, a general decrease in niggli mg (molecular proportions of Mg:Mg + Fe^{2+} + Fe^{3+} + Mn) as a function of differentiation. Amphibolites of worldwide pelitic-carbonate origin show a clustering of points, characterized by low c and moderate mg values, which defines a pelite or semi-pelite field, and hence enables distinction of basalt or andesite protoliths from pelite-carbonate mixtures.

Only four Boriana amphibolites were analyzed due to financial limitations. As Leake points out, a large number of amphibolite analyses are desirable as systematic variation trends can be more clearly discerned. Nevertheless, in Figure 19 the four amphibolites plot close to the Karroo differentiation curve, suggesting an igneous origin.

A ternary plot of niggli c - 100 mg - (al-alk) for the same Karroo dolerites and pelitic gneisses also produces a differentiation curve and defines a pelite-semi-pelite field (Figure 20). Limestone

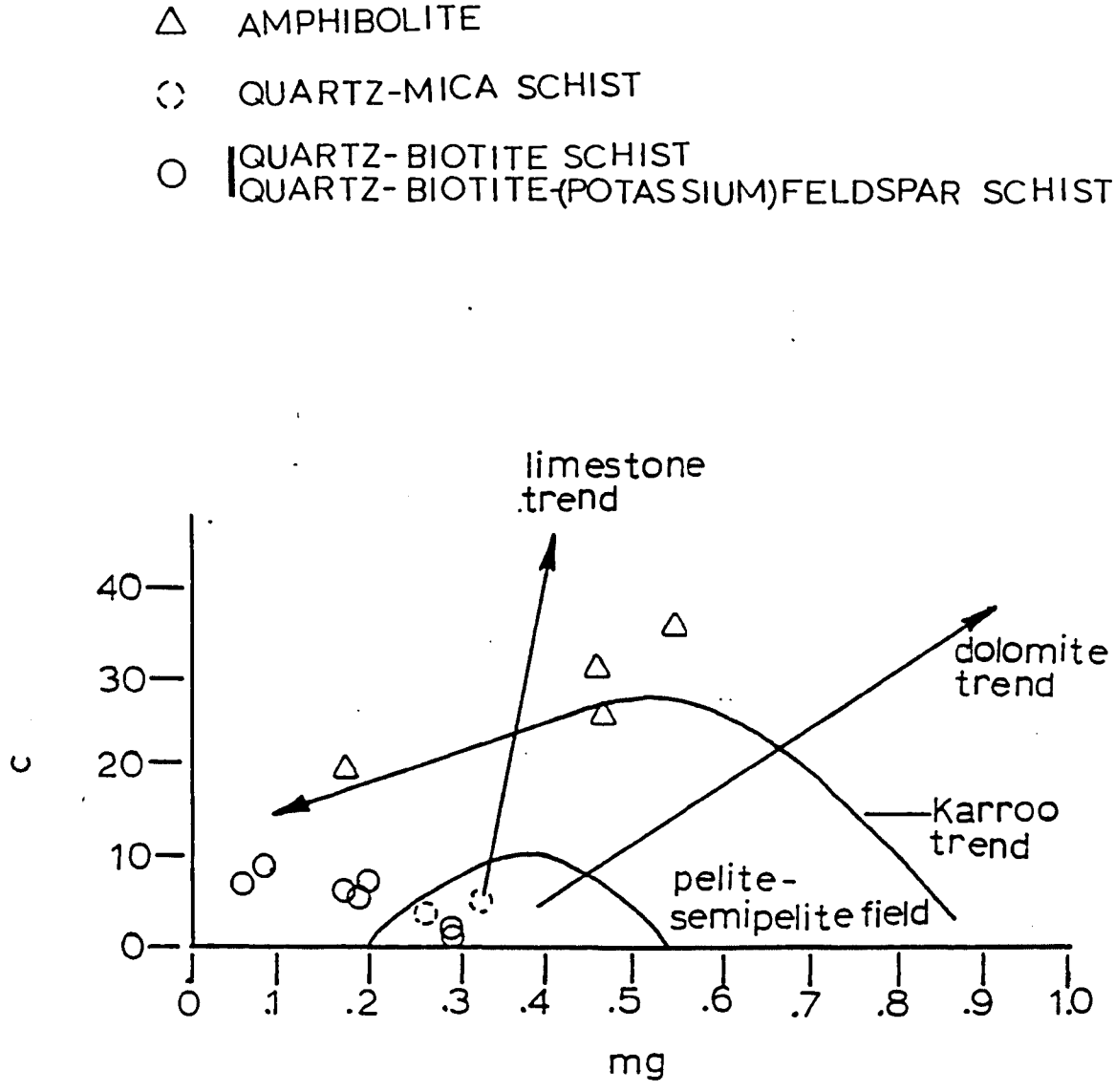

Figure 19. Plot of niggli c versus mg.

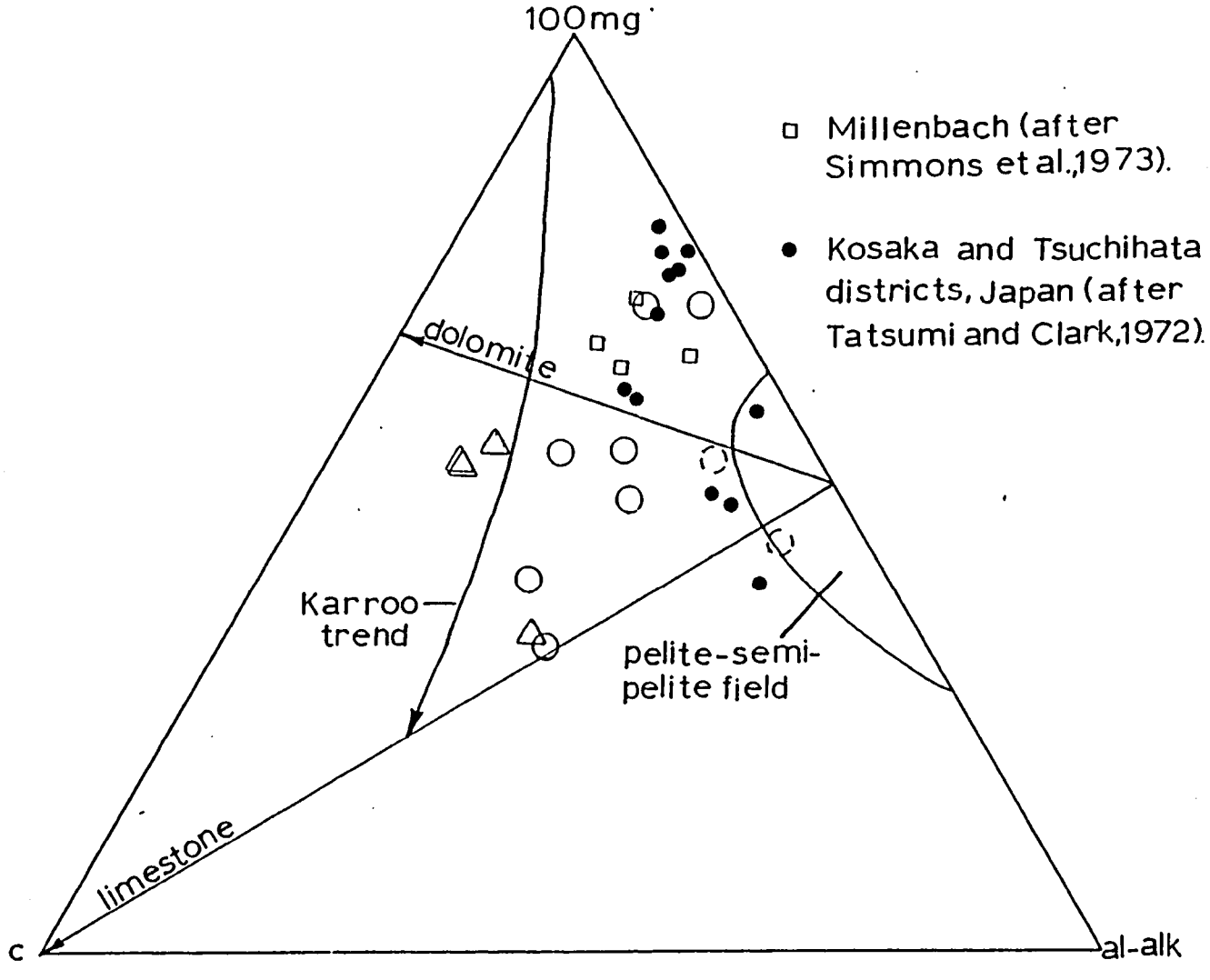

Figure 20. Plot of niggli c - 100 mg - al-alk. -- See Figure 19 for symbols.

and dolomite trend lines aid in recognition of carbonate-pelite mixture trends in an amphibolite series. Three of the four Boriana amphibolites display a marked clustering near the differentiation curve, while one sample shows sedimentary tendencies attributable to its rhyodacite silica composition and probable tuffaceous origin. A third plot of niggli c versus (al-alk) for Karroo dolerites and pelite gneisses defines a broad igneous field and a pelite field (Figure 21). Limestone and dolomite trend lines are indicated. All four of the Boriana amphibolites plot within the igneous field and near the dolomite trend line.

A final plot of niggli mg versus k for the same variety of rocks defines a broad pelite field (Figure 22). Boriana amphibolites plot decidedly outside the pelite boundary.

In trace-element plots, Leake found plots of niggli mg versus chromium and nickel the most reliable indicators of igneous origin. In igneous rocks, there exists a positive correlation between the three parameters. During basaltic magma differentiation, decrease in niggli mg is paralleled by a decrease in chromium and nickel. In pelite and pelite-dolomite mixtures the low proportion of dolomite to pelite is associated with generally higher chromium and nickel values.

In Figure 23 niggli mg is plotted against Cr and Ni, using the pelite-igneous boundaries suggested by Leake. Three of the four amphibolites plot in the pelite field near the igneous boundary.

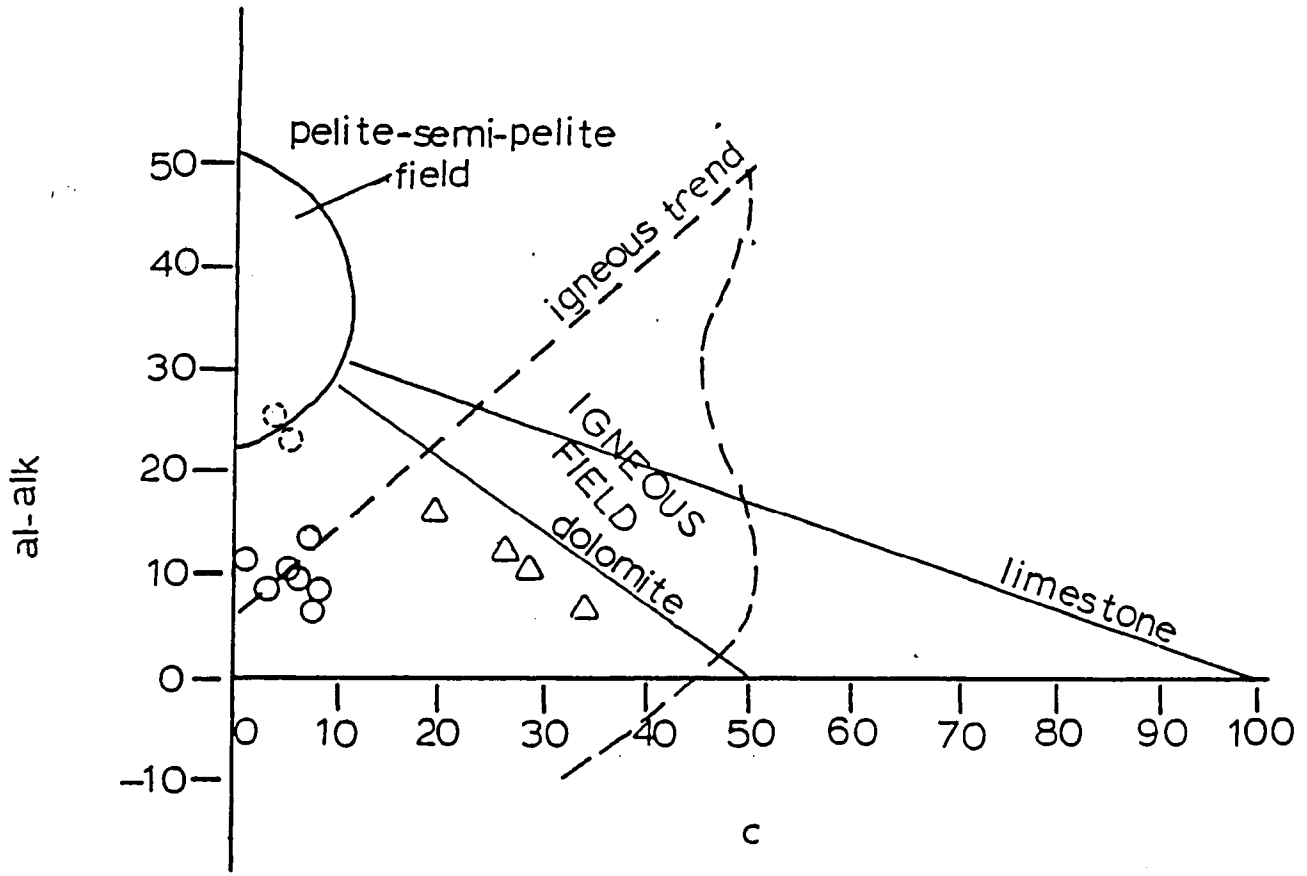

Figure 21. Plot of niggli c - al-alk. -- See Figure 19 for symbols.

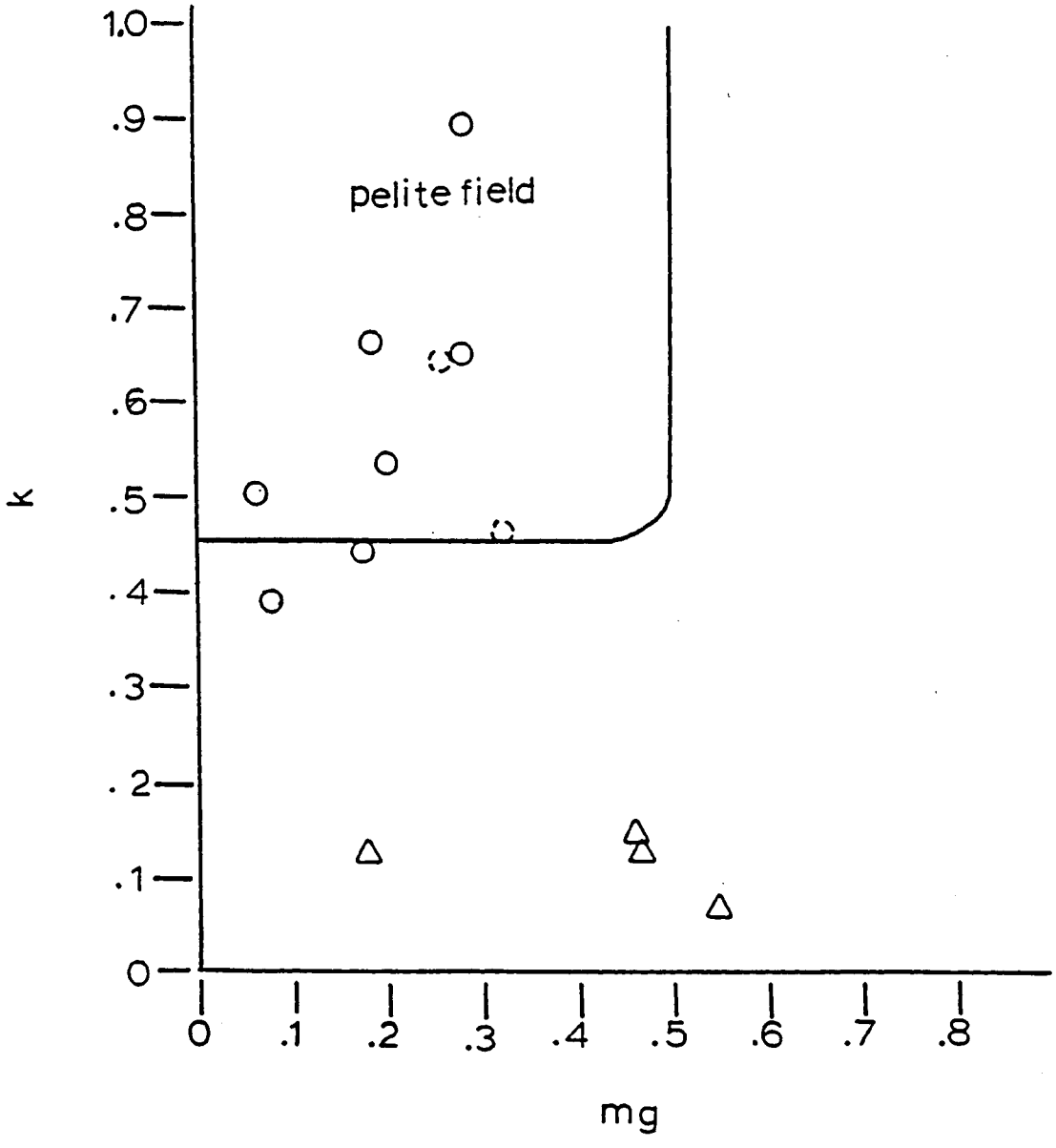

Figure 22. Plot of niggli k versus mg. -- See Figure 19 for symbols.

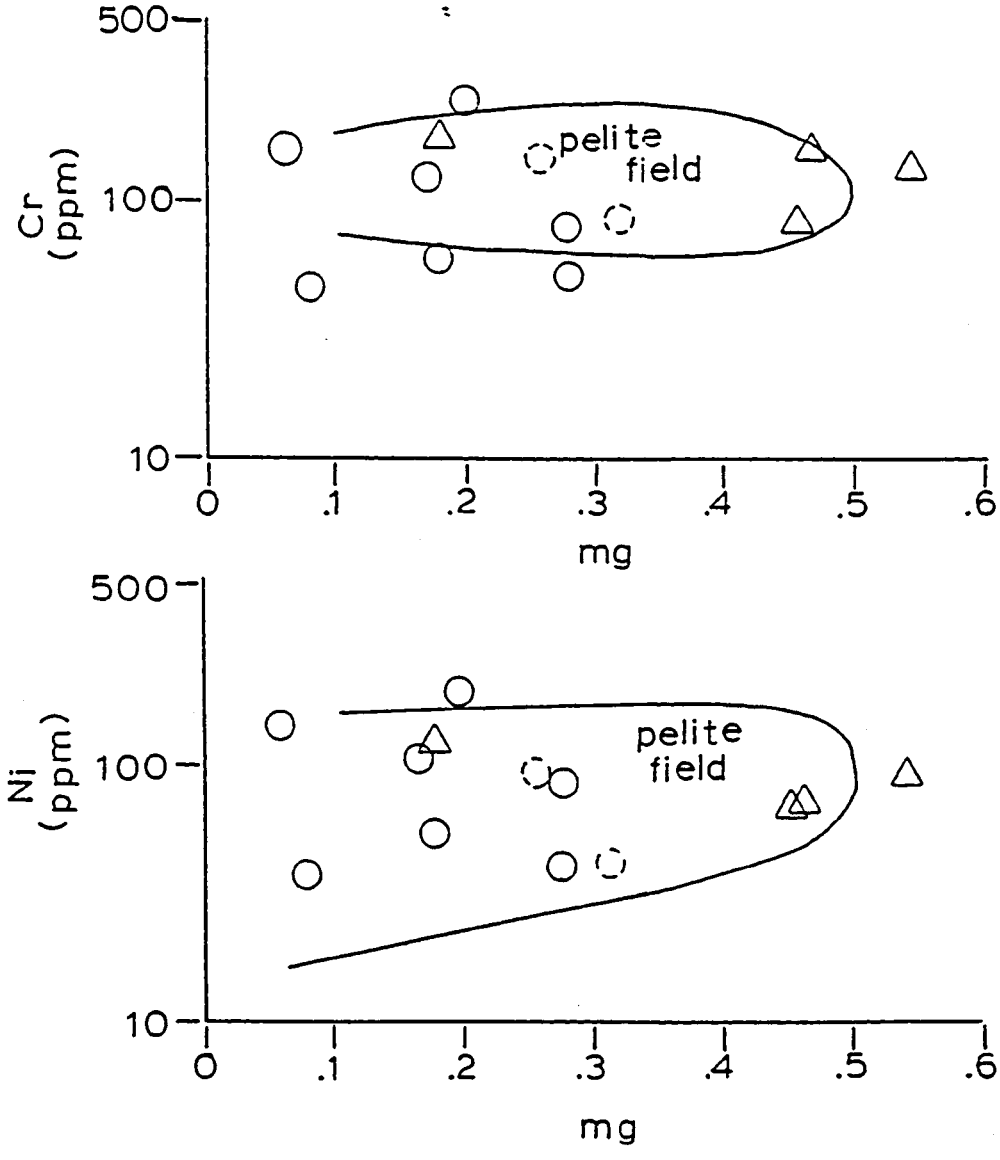

Figure 23. Plot of Cr and Ni versus niggli mg. -- See Figure 19 for symbols.

The one amphibolite sample with a low niggli mg value of 0.18 plots with the sediments, again attributable to a tuffaceous heritage and possible contamination with sedimentary components. The niggli mg values for the other amphibolites (0.46, 0.47, and 0.55) plot a little lower than the Canadian samples (0.6-0.7), but are close enough to indicate an igneous heritage.

Of less certain value are plots of niggli mg versus Ba, Sr, Zr, Cu, Co, and $\frac{Co}{Ni}$ and % TiO_2 versus Cr and Ni, with approximate field limits from Leake (Figures 24-27). These trace element plots indicate a pelitic or igneous heritage with no internally consistent pattern.

From whole-rock data, the Boriana amphibolites appear to have had igneous protoliths. From their silica contents they represent metamorphosed basalt-andesite-rhyodacite tholeiitic rocks, using the classifications suggested by Spitz and Darling (1975) and Gelinas et al. (1977) (Figure 28). The trace-element data is permissive of an igneous origin, but not conclusive.

Quartzofeldspathic Rocks

Determination of protoliths of quartzofeldspathic rocks from whole-rock data is not as clear-cut as for the amphibolites. The reader is urged to consult Van De Kamp (1968) and Seymour and MacLean (1977) for a more thorough discussion of the problems involved. In short, the degree of sedimentary involvement in a tuffaceous volcanic regime makes it difficult to separate greywackes or arkoses

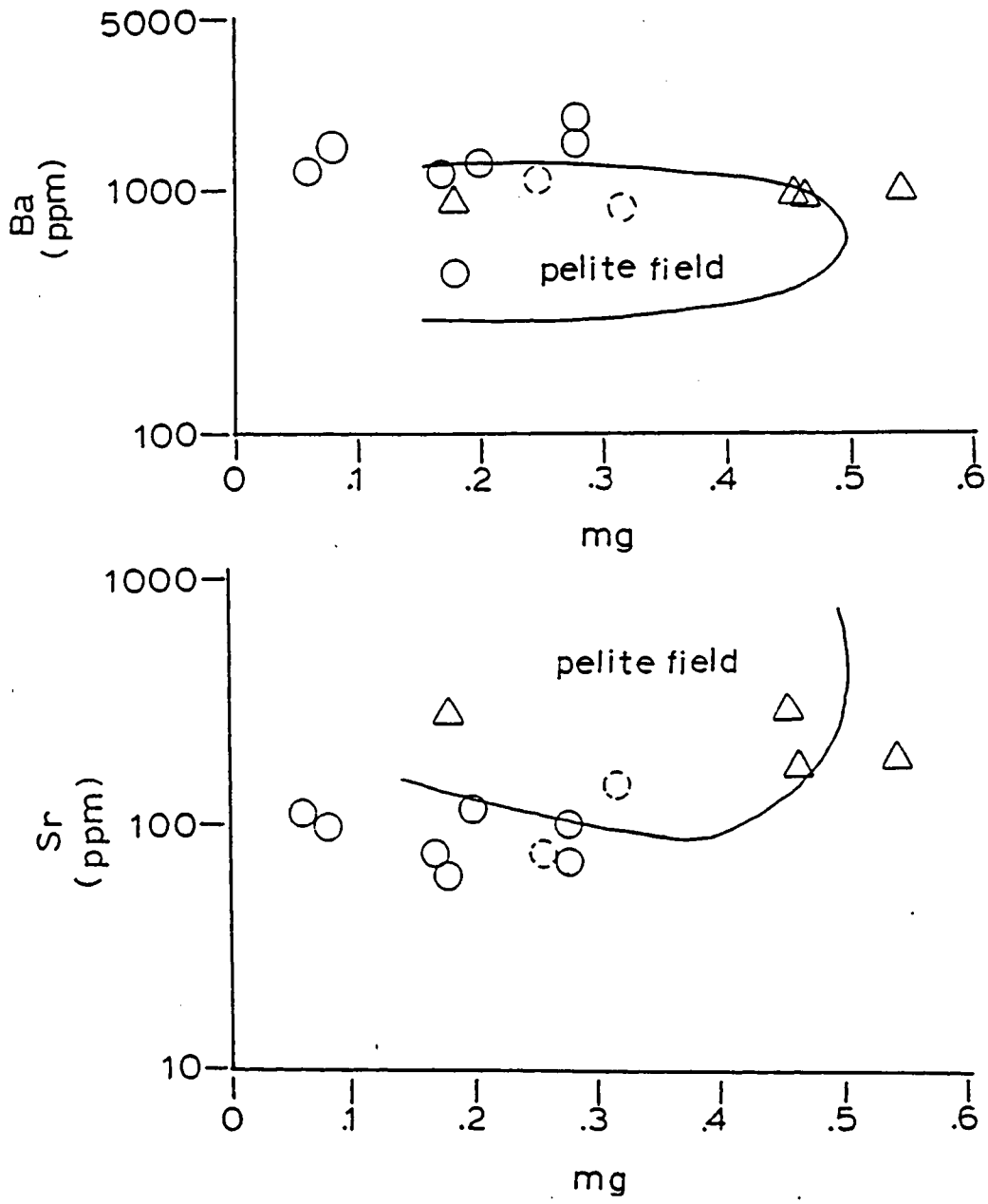

Figure 24. Plot of Ba and Sr versus niggli mg. -- See Figure 19 for symbols.

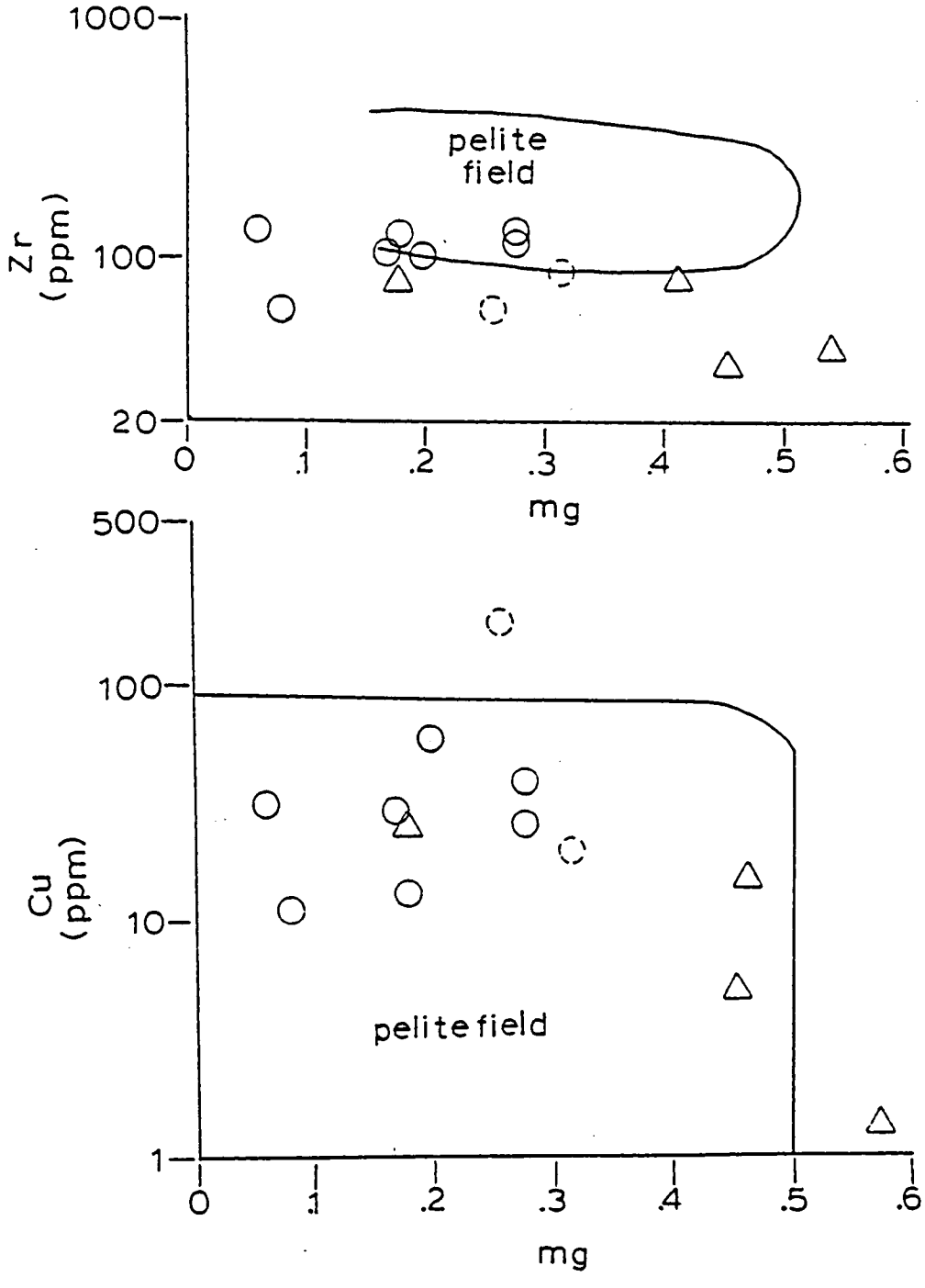

Figure 25. Plot of Zr and Cu versus niggli mg. -- See Figure 19 for symbols.

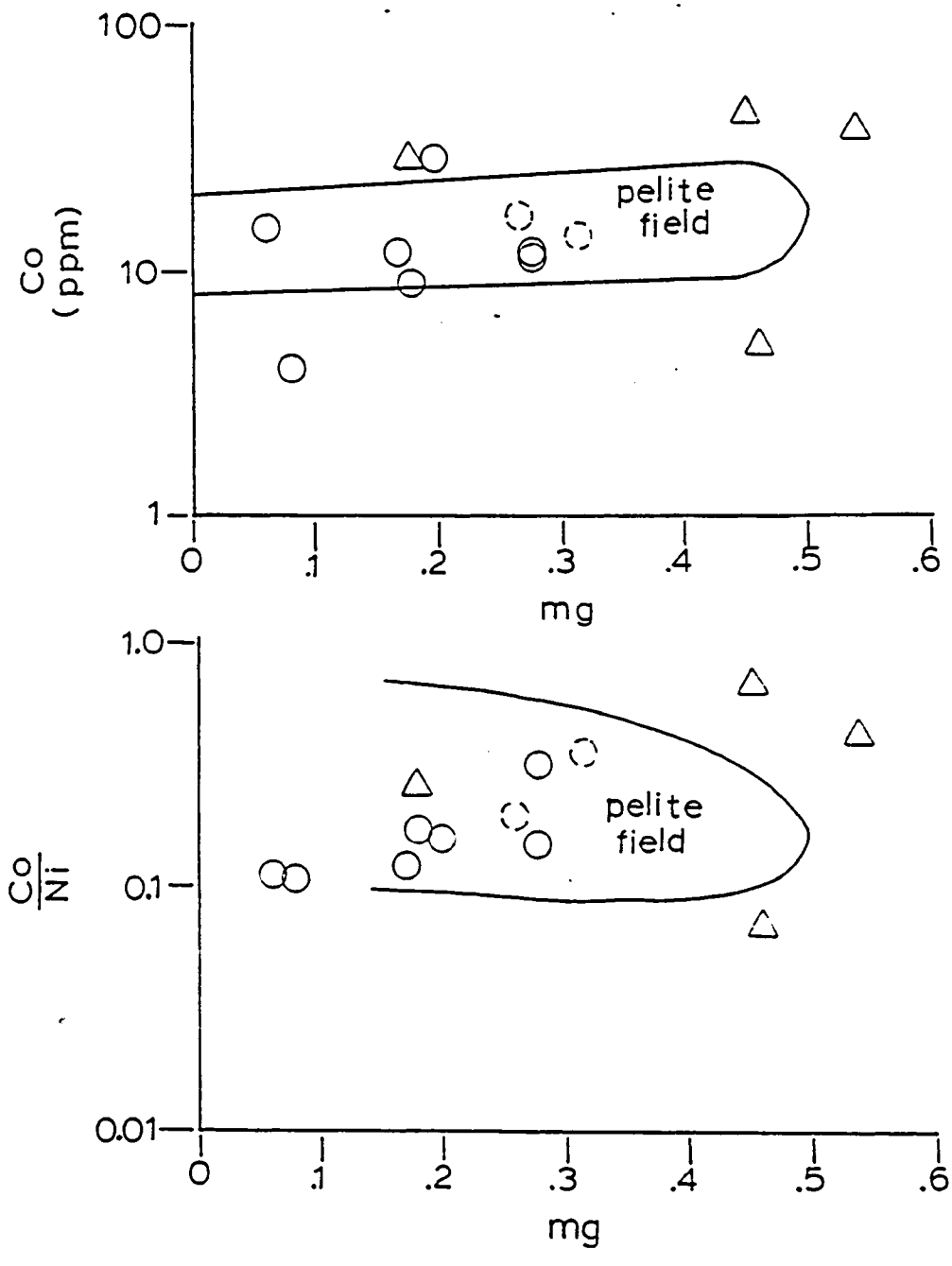

Figure 26. Plot of Co and $\frac{Co}{Ni}$ versus niggli mg. -- See Figure 19 for symbols.

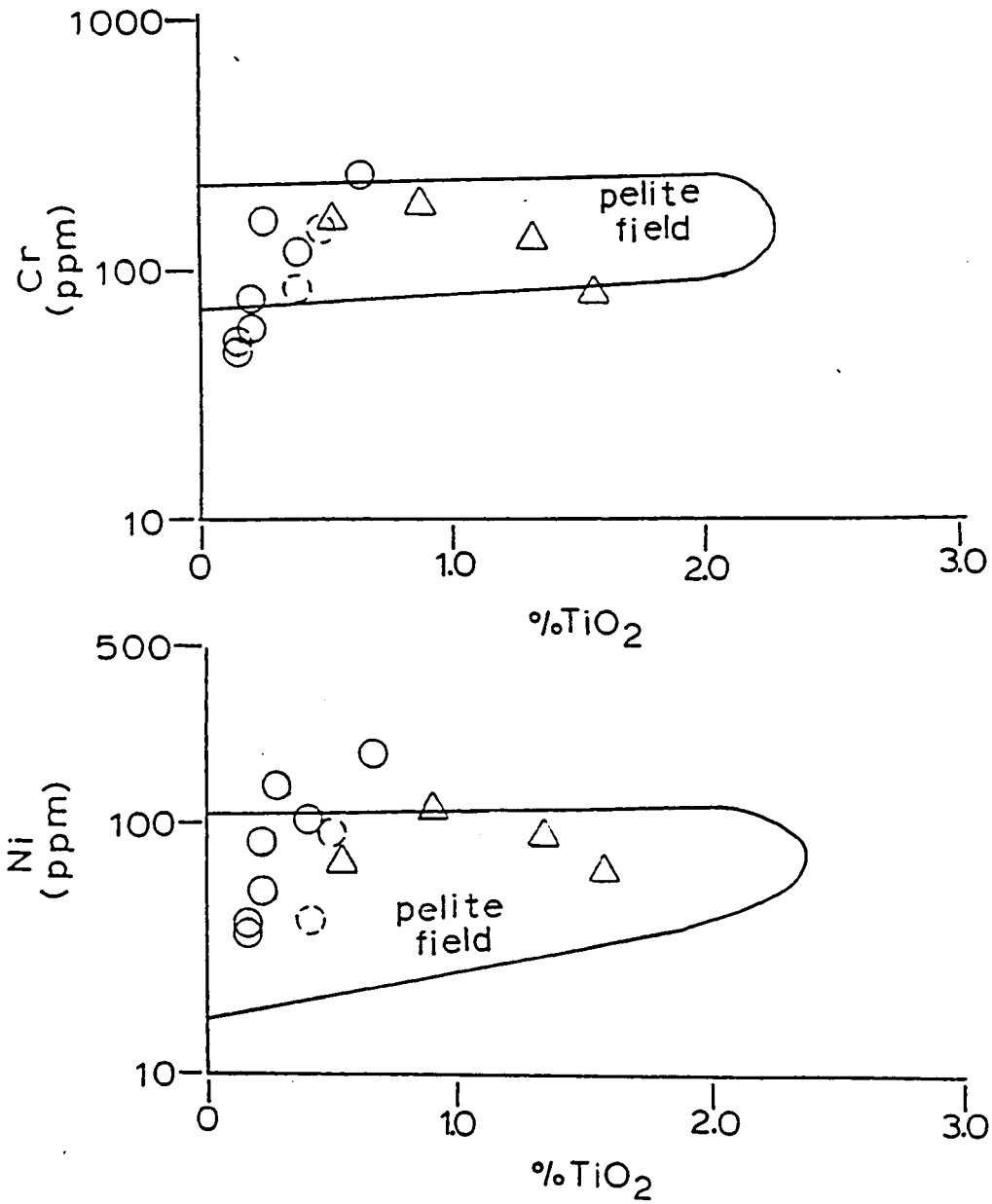

Figure 27. Plot of Cr and Ni versus % TiO_2. -- See Figure 19 for symbols.

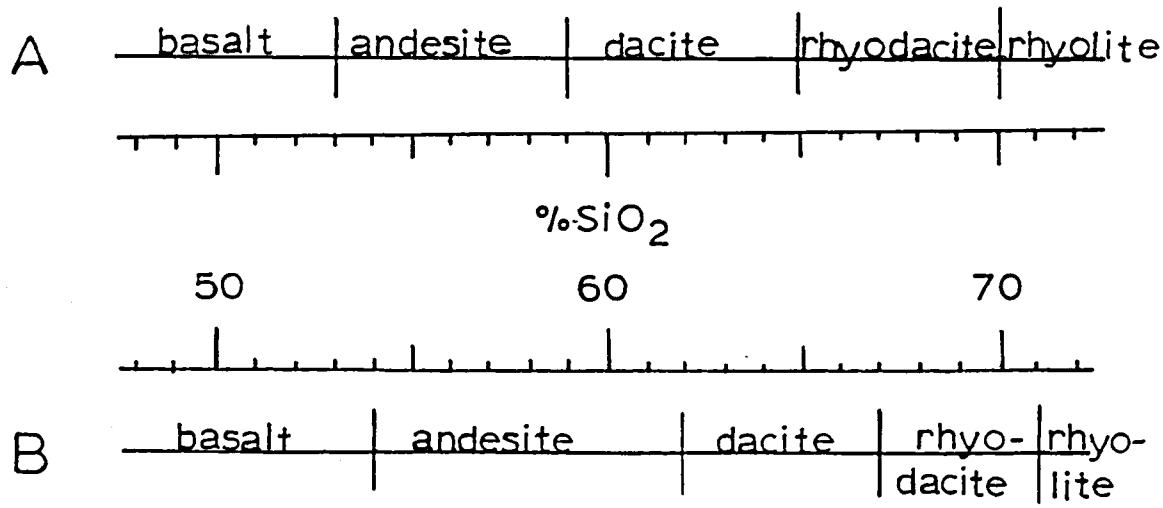

Figure 28. Classification of Volcanic Rocks by Silica Index. --
(a) After Spitz and Darling (1975).
(b) After Gelinas et al. (1977).

from felsic volcanics based solely on whole-rock geochemistry. Additionally, the loss of alkalies and CaO during hydrothermal processes leads to peraluminous silicic wallrocks chemically resembling sediments.

Plots of niggli values of felsic volcanic wallrocks from Canadian and Kuroko deposits reveal clusterings of sample points lying between the differentiation curves and pelite fields. Associated sediments also plot at or near the pelite field in the same manner as pelite-carbonate mixtures do for amphibolites. Felsic metavolcanics termed leptites by Seymour and MacLean (1977) thus possess mixed sedimentary and igneous heritages.

Figures 19-22 reveal the leptitic character of Boriana quartz-biotite-(potassium) feldspar and quartz-biotite schists, while the two quartz-mica schists plot consistently at or close to the pelite field. The similar disposition of Millenbach and Kuroko metavolcanics is shown in Fgiure 20, where they bracket the leptite field. Trace-element plots (Figures 23-27) expectedly demonstrate sedimentary involvement in the felsic wallrocks.

Whole rock data of felsic Antler wallrocks compared with those of other massive sulfide deposits with known or interpreted felsic volcanic affiliation, permits an igneous protolith interpretation. The variability of both whole-rock and trace-element data and lack of clear-cut trends is confirmation of the mixed volcanic and sedimentary genesis of the felsic wallrocks. By silica index,

all of the quartz-biotite-(potassium) feldspar schists in the canyon are rhyolitic to rhyodacitic in origin, if the interpreted volcanic protoliths are correct. The silica contents for the quartz-biotite schists also permit an interpretation of derivation from rhyolitic tuffs. The high quartz content of some quartz-biotite schists (70-85%) and the variable potassium feldspar contents lend themselves to a suggestive metaarkose-to-metaarenite protolith interpretation.

Trace-Element Content of Ironstones and Ore Zone

Two of the iron formations in the Bulge were sampled to determine anomalous trace element signatures, as found by Stanton (1976) in his study of banded iron formations at Broken Hill, New South Wales.

The ironstones do not reveal (Appendix III) any diagnostic, atypical concentrations of metals. The relatively small areal extent of the iron formations admittedly limits the effectiveness of the technique, but iron formation float has been spotted north of the Boriana Mine (Stensrud, personal communication, 1979). If outcrops are found, they may provide a better comparison of regional metals zonation. The major oxide analyses, regarded with caution, show high levels of CaO, Na_2O, MgO, and K_2O in sample AM-6, attributable to the high hornblende content of the iron formation.

Trace-element data for the wallrocks and ore zone reveal anomalous arsenic levels (7 to 125 times clarke), using Krauskopf's (1967) average abundance levels for the protolithic rock units.

Lead Isotope Data

A sample of galena from the Antler Mine was submitted to B. R. Doe, U.S. Geological Survey, Denver, for determination of lead isotope ratios for the Antler, United Verde (Jerome), and Old Dick (Bagdad) massive sulfide deposits (Table 2). Mauger (1973) obtained a lead-lead model age of 1725 $\pm$ 200 m.y. from galena collected at the Old Dick Mine. Stensrud (personal communication, 1979) has obtained a tentative date of 1850 m.y. for Antler ores, using Doe's analyses. Nevertheless, the closeness of the isotope ratios from the three ore deposits places the Antler within the Central Arizona massive sulfide epoch of 1.7-1.8 billion years.

"Pseudofragmental" Amphibolite

Spotted hornblende-plagioclase amphibolite containing leucocratic ovoids at the Antler site represents a basalt-andesite unit with thin intercalations of dolomite and pelite. The calcic nature of actinolite-tremolite, plagioclase (An_{54}), diopside, carbonate, and epidote knots and wisps places the units within the pelite fields on niggli diagrams (Figures 19-22). The elongated or "necked" geometry of the ovoids and the rootless folds seen in slabbed specimens (Figure 7) indicate structural transposition of the amphibolite units in a manner akin to boudinage. The porphyroblastic sections of the same amphibolite unit may be in part due to recrystallized glass components or relict amygdules, although nucleation and

Table 2. Pb-Pb Isotope Ratios for Central Arizona Massive Sulfide Deposits. -- Data from B. R. Doe.

	$\frac{Pb^{206}}{Pb^{204}}$	$\frac{Pb^{207}}{Pb^{204}}$	$\frac{Pb^{208}}{Pb^{204}}$
Antler Mine, Hualapai Mtns.	15.876	15.347	35.463
Old Dick, Bagdad	15.805	15.318	35.422
United Verde, Jerome	15.725	15.270	35.344

growth phenomena and compositional factors might equally account for the features.

Chemical Nature of the Volcanism

It is possible to determine the type of volcanism demanded by whole rock geochemistry by simple plots of the various components, assuming correct protolithic interpretations and negligible effects of alkali metasomatism. Using Kuno's (1953) dividing line between tholeiitic and calc-alkaline fields on AFM diagrams (alkalies, iron, and magnesium), the Boriana series rocks straddle the tholeiite and calc-alkaline boundary, indicating a mix of the two but with a majority falling within the tholeiite field (Figure 29). A second plot of total alkalies ($Na_2O + K_2O$) versus silica after Kuno (1966) also shows a scatter of points, equally divided between calc-alkaline and tholeiite fields (Figure 30).

A more useful and reliable plot is provided by Jensen cation plots (Jensen, 1976), which relate cation percentages of Al_2O_3, $FeO + Fe_2O_3 + TiO_2$, and MgO and allow recognition of differentiation trends for komatiitic, tholeiitic, and calc-alkalic volcanics (Figure 31). In Jensen's ternary plot, alumina is substituted for alkalies since alkalies tend to be more easily leached or exchanged than alumina. The preponderance of samples again shows a definite tholeiitic affinity, with only slight calc-alkaline tendencies.

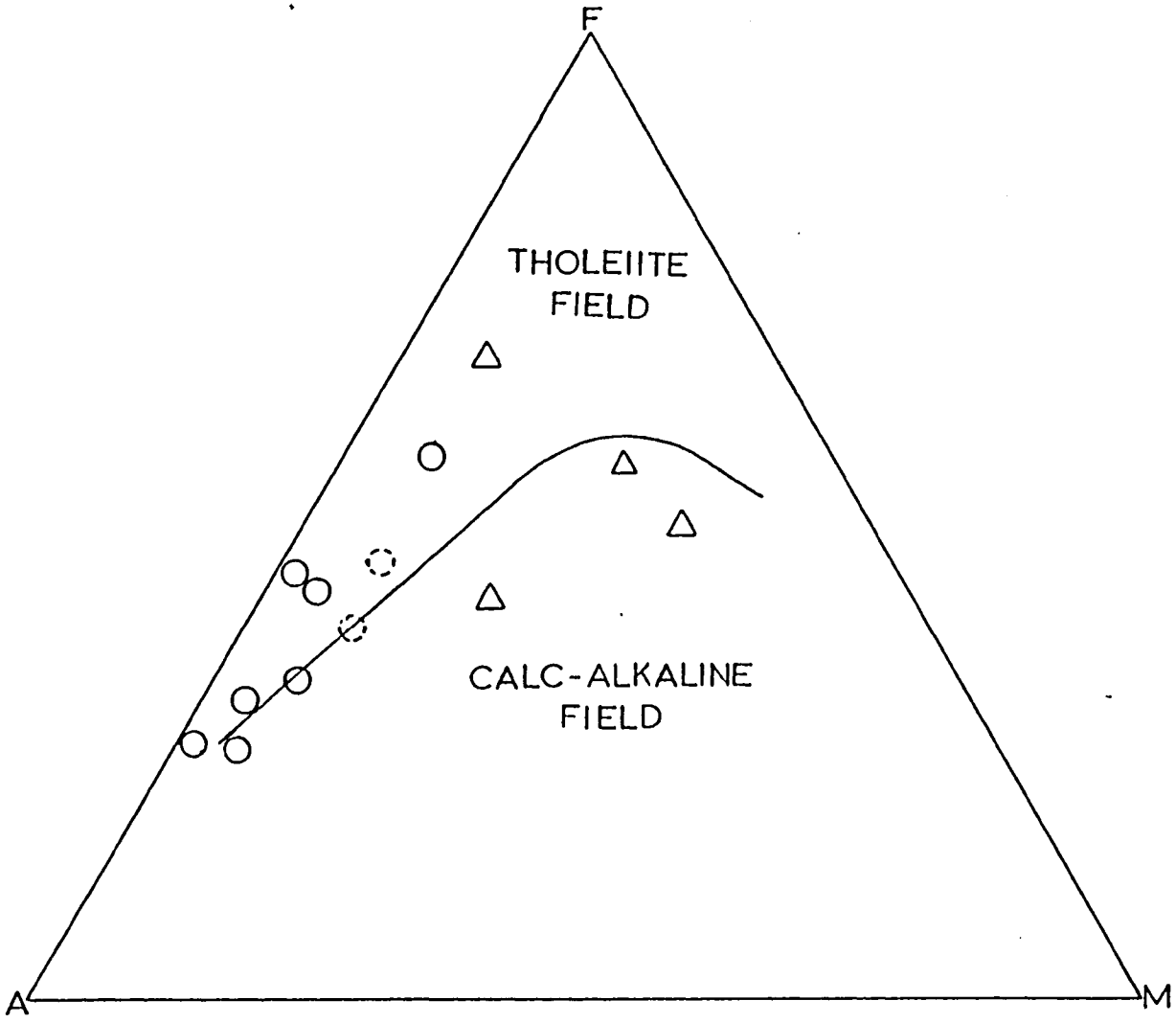

Figure 29. AFM Plot for Antler Wallrocks. -- See Figure 19 for symbols.

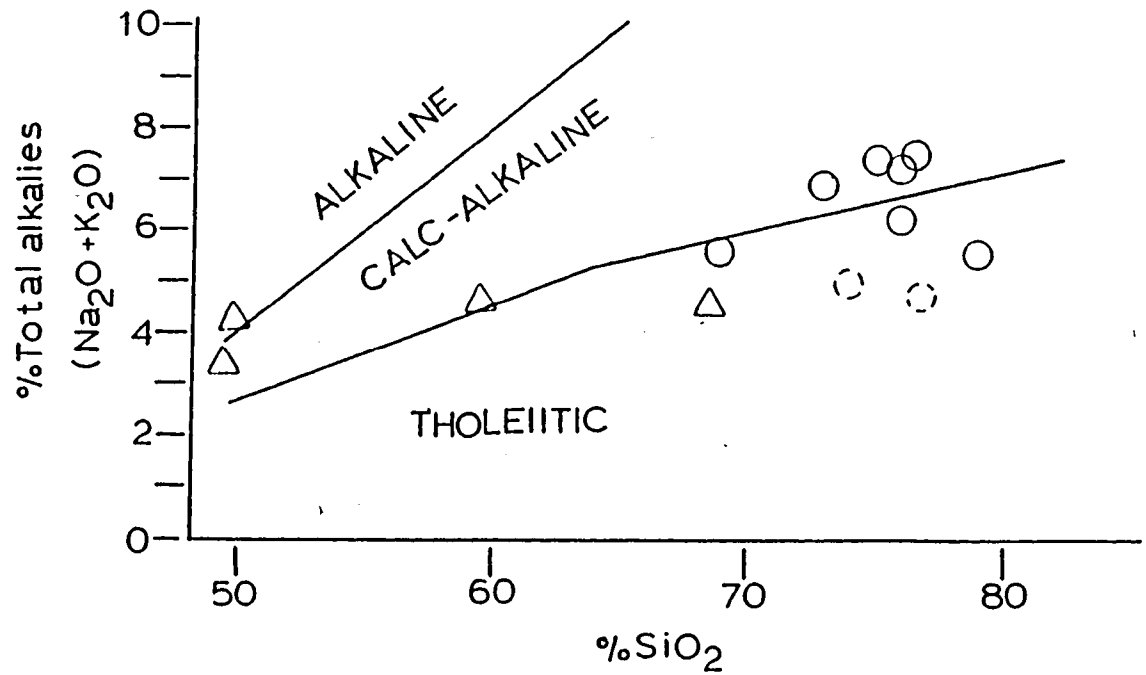

Figure 30. Plot of Total Alkalies versus Silica for Antler Wallrocks. -- See Figure 19 for symbols.

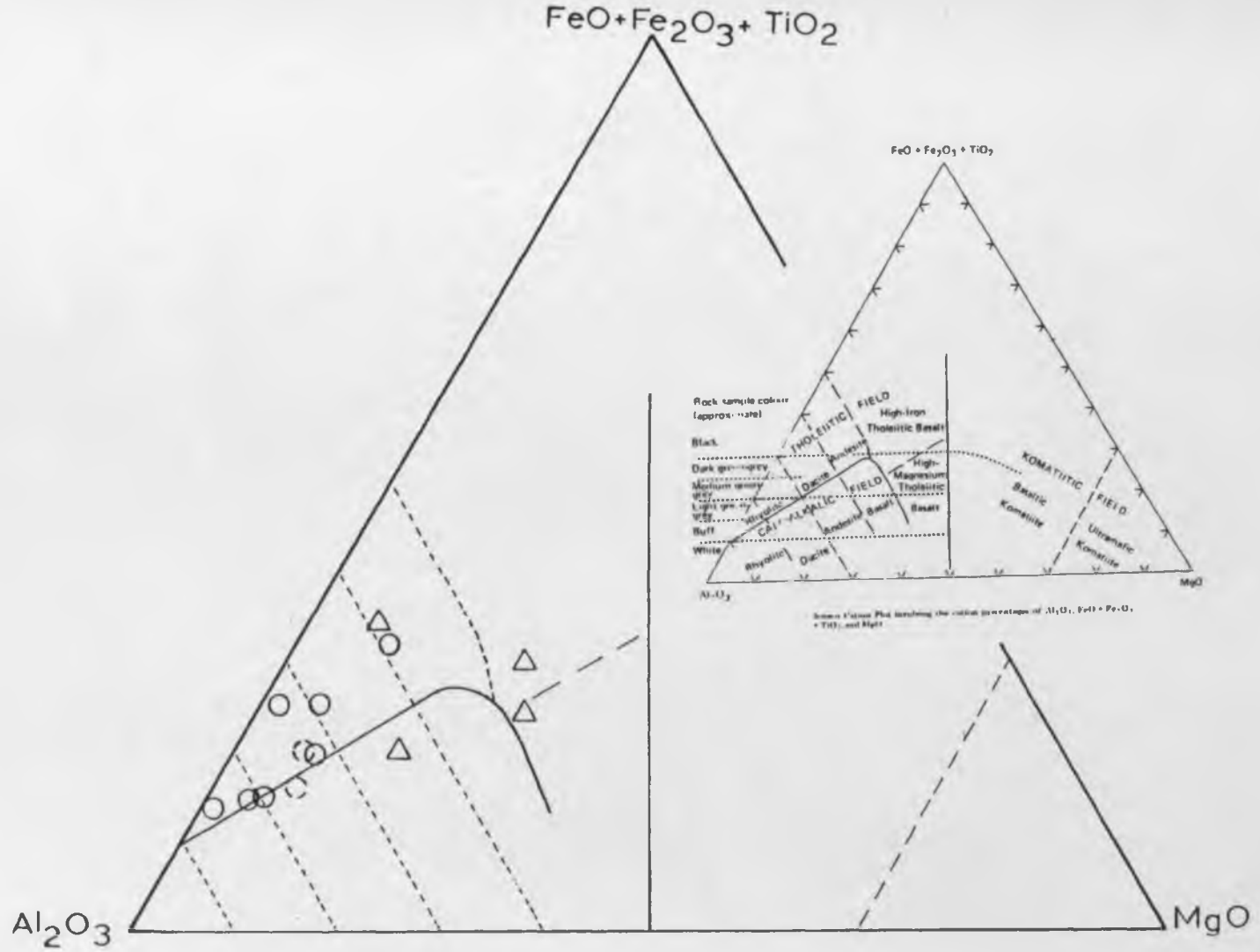

Figure 31. Jensen Cation Plot for Antler Wallrocks. -- See Figure 19 for symbols.

CHAPTER 6

METAMORPHISM

Volcanic and sedimentary rocks in the Antler Mine vicinity have been refolded and thermally metamorphosed, producing the present suite of hornblende gneisses and biotite and mica schists. Differing grades of metamorphism are apparent from differing mineral assemblages.

Metamorphic Rank

Definition of metamorphic rank depends on the classification on the geologist's bookshelf that finds preference. Winkler's latest revision (1976) provides upper and lower limits to temperature and pressure attained during metamorphism. A number of finer petrologic divisions for grade classification are presented in Fraser and Heywood (1978). Assemblages observed in quartz-mica schists (biotite + muscovite) best fit Winkler's low grade classification, approximately equal to greenschist facies. The absence of cordierite and chloritoid in the metapelites rules out medium grade assignment. The defining assemblage for the upper limits of low grade metamorphism in metapelites is:

(stilpnomelane + muscovite) - out

(biotite + muscovite) - in

The apparent absence of stilpnomelane indicates the following possible reaction:

stilpnomelane + phengite = biotite + quartz + chlorite + H_2O

Winkler indicates the temperatures for this transformation are 430°-$445^{\circ} \pm 10^{\circ}C$ between 1 and 4 kilobars, although solid solution is not accounted for.

Moving eastward from the central mass of metasediments toward the injection migmatite zone, the appearance of almandine garnet and andalusite indicates conditions of increasing temperature (Winkler, p. 214). The following reactions in pelitic rocks as suggested by Winkler may account for the garnet and andalusite:

chl + biot + qz = biot + alm-rich gt + H_2O

chl + musc + epid = biot + alm-rich gt + H_2O

chl'oid + chl + qz = alm gt + H_2O

chl + musc + qz = biot + alm gt + H_2O

iron-rich chl + musc + qz = biot + alm-rich gt + Al_2SiO_3 + H_2O

Experimentally-derived temperatures of $500^{\circ}C$ at 4 kilobars and $600^{\circ}C$ at 5 kilobars for the last reaction are reported by Winkler.

For rocks of original basalt to andesite composition, Winkler sets out the following mineralogic transformations during high-grade, medium-grade, and upper low-grade metamorphism:

1. clinopyroxene + hypersthene + pigeonite $\pm$ olivine = hornblende + almandine garnet;

2. plagioclase An_x = plagioclase An_{x-y} + clinozoisite $\pm$ epidote, such that with decreasing temperature the calcic component of plagioclase decreases while the amount of clinozoisite-epidote increases;
3. in low-grade metamorphism only, the coexistence of albite or oligoclase with hornblende, clinozoisite $\pm$ epidote, garnet, quartz and chlorite is indicated.

The Boriana amphibolites fall into the medium to high grade zone. The presence of diopsidic pyroxene in several thin sections indicates that portions of the amphibolite section are within the high grade zone, while pyroxene-free amphibolites with andesine plagioclase compositions place the majority of amphibolites within the medium grade zone. The upper temperature limits of medium-grade rank set by the breakdown of muscovite in the presence of plagioclase and quartz are 565°C to 680°C at pressures of 1 to 4 kilobars.

Cordierite thus far has only been found in the massive fibrous silicate near the contact of the gneisses and schists with the batholithic rocks, and is a local contact effect as opposed to a regional metamorphic effect. Hence the ore zone at both deposits and the fibrous silicate bodies at the Bulge also fall into the medium grade category. Alternatively, Nielsen's (1978) assemblage grouping places the ore horizon at the cordierite isograd, and with the appearance of sillimanite, at the first sillimanite isograd, of the lower amphibolite facies, bordering on the upper amphibolite facies.

In shallow contact metamorphism in which cordierite is found, pressures are generally low and range from 0.5 to 6 kilobars. Using sphalerite unmixing as a geobarometer on 3 samples from the Antler Mine, Stensrud (personal communication, 1979) has obtained tentative results indicating pressures of 5, 5, and 7 kilobars. These pressures appear somewhat higher than might be expected and should be regarded with caution. The presence of cordierite and sillimanite in drillhole B6 implies high temperatures and low pressures on the order of 1-3 kilobars, according to Winkler (1967).

Origin of the Antler Granite

The northeasterly elongate nature of the Antler granite and its screening position between amphibolites and biotite schists and the quartz-mica schists indicates a profound structural control on the body during emplacement. The two-mica composition of the granite is also anomalous and suggests an anatectic origin of the pluton.

Chappell and White (1974) provide an excellent summary of the chemical and petrographic differences between I-type igneous-derived and S-type sedimentary-derived granites. The differences between the I and S types and the Antler granite are listed in Table 3. The authors point out that

> ...these chemical properties result from the removal of sodium into sea water (or evaporites) during sedimentary fractionation, and calcium into carbonates, with subsequent relative enrichment of the main sedimentary pile in aluminum. S-type granites come from a source that has been subjected to this prior chemical fractionation... (p. 173).

Table 3. Comparison of Antler Granite and I and S Type Granites. -- (after Chappell and White)

	I-type	S-type	Antler granite
Chemical parameters	High sodium- Na_2O > 3.2% in felsic varieties > 2.2% in mafic varieties	Low sodium - Na_2O < 3.2% in rocks with 5% K_2O < 2.2% in rocks with 2% K_2O	Low sodium- Na_2O = 0.9% in rocks with K_2O = 6.3%
	Mol $Al_2O_3/(Na_2O+K_2O+CaO)$ 1.1	>1.1	1.2
	CIPW normative diopside or 1% normative corundum	>1% normative corundum	> 1% normative corundum
	Broad spectrum of compositions from felsic to mafic	Relatively restricted in composition to high SiO_2 types	→ 75% SiO_2
	Regular inter-element variations within plutons; linear or near linear variation diagrams	Variation diagrams more irregular	No data
Petrographic properties	Hornblende common in more mafic types, generally present in felsic varieties	Hornblende absent; muscovite common in felsic types; up to 35% biotite in more mafic S-types.	Felsic variety, with muscovite = 5%, biotite - 12%
	Sphene is common accessory mineral	Monazite is common accessory mineral	Not yet observed, but pleochroic haloes around zircon in biotite and allanite are common.
		Cordierite and garnet in xenoliths or granites themselves	Not yet observed
Radiometric properties	$Sr^{87}/^{86}$ ratios 0.704-0.706	$Sr^{87}/^{86}$ ratios : 0.708	No data
	Isochrons give a regular linear set of points	Isochrons show a scatter of points within a broad envelope	No data
Field relationships	Mafic hornblende-bearing xenoliths of igneous appearance	Hornblende-bearing xenoliths are rare, metasedimentary xenoliths are common	Metasedimentary xenoliths north of thesis area, biotite-rich xenoliths in thesis area.
	In composite (both I and S) intrusions are usually later in intrusive sequence, with massive or dominant primary foliation	Early in intrusive sequence, with strong secondary foliation	Strong secondary foliation.
	Associated with tungsten and porphyry-type copper and molybdenum deposits	Tin mineralization confined to highly silicic granites	

Using averaged thin section abundances, low Na_2O is revealed by normative plagioclase and composition, and high SiO_2 by quartz, plagioclase, potassium feldspar, and micas.

Comparison of the salient features of the granite with Chapell and White's criteria leads to the conclusion the Antler granite bodies were generated by anatectic melting of metapelites. Winkler (Cahpter 18) provides a thorough discussion of the process of anatexis. In summary, the temperatures required to begin partial melting of paragneisses in the presence of water are at the upper end of high-grade metamorphism: 700°C at 2 kilobars and 680°C at 4 kilobars. Using quartz-mica-feldspar schists as source material the process can begin at 650°C without H_2O on the strength of contained hydroxl components. Separation of the silicic component from the crystalline component of the melt above the solidus then occurs, dependent on the temperature of the melt and H_2O content.

Presumably generation of the melt, from biotite and mica schists as source materials, was structurally induced. The diffuse intermingling of the granite wedge near the Copper World Mine with pegmatites, and strong secondary foliation within the intrusives suggests that emplacement of granite bodies was contemporaneous with batholithic activity.

CHAPTER 7

INTERPRETATION AND DISCUSSION

The syngenetic volcanogenic model for generation of many of the world's massive sulfide deposits has been extensively studied and reported on for the deposit group in the last 15 years (Oftedahl, 1958; Gilmour, 1965; Goodwin, 1965; Horikoshi, 1969; Ridler, 1970; Matsukuma and Horikoshi, 1970; Gilmour, 1971; Hutchinson et al., 1971; Tatsumi and Clark, 1971; Sangster, 1972; Hutchinson, 1973; Constantinou and Govett, 1973; Sillitoe, 1973; Spence and de Rosen-Spence, 1975). In short, volcanigenesis provides a more tenable model than does the Lindgrenist epigenetic hydrothermal model of selective replacement, satisfactorily accounting for the geochemical and lithological features of mineralization and wallrock alteration for many massive sulfide deposits. The literature now abounds with individual case studies of proximal, distal, and basinal deposits related to known or hypothesized volcanic centers and their relative tectonic settings. It is useful therefore briefly to review the conceptual model of a volcanogene system and the production of chloritic alteration and metal sulfides, based on reconstruction of Archean deposits and their unfolded stratigraphy, and correlations with the younger, relatively undeformed, Kuroko deposits.

Volcanogene Model

A simplistic model of the volcanogene system begins with the inception of bimodal submarine volcanism, derived from differentiation of a tholeiitic basaltic magma, regionally progressing from tholeiitic at the series base to calc-alkaline in the upper cycle (Gelinas et al., 1977). Within the waning stages of felsic volcanism, usually within the upper calc-alkaline cycle, shattering of the subaerial vent or complex marked by the effusion of pyroclastic rhyolite debris occurs. Ingress of seawater into and below the now-permeable pile results in development of a convective circulation cell with consequent seawater-wallrock interaction and the leaching of alkalies and calcium from the volcanic wallrocks. Magnesium in the seawater reacts with the peraluminous remainder of the wallrock, producing chloritically altered wallrocks. The geometry of the alteration zone follows the fracture pattern or permeability channels, assuming a "pipe"-like or inverted cone-shaped form. A weaker "halo" of sericitic alteration is commonly developed around the pipe. Chlorite can also assume a stratiform geometry, by transport as a gelatinous mass away from the vent complex and deposition in the flanking basins or depressions.

During convective recirculation, seawater in the system undergoes a decrease in oxidation state and pH, and an increase in temperature with increasing depth and proximity to the heat source (Large, 1977). Iron reduces oceanic sulfate to produce sulfides.

Copper, zinc, and lead are perhaps wholly or partly derived from leaching of wallrocks of varying lithologies. In the lower less-permeable sections of the volcanic pile sulfides are deposited as veinlets and disseminations in the chloritically altered wallrocks. The metals in the upper portion of the complex remain integrally within the pipe as sulfides or are carried as chloride complexes outwards from the vent as a dense saline mass and are localized into topographic lows along with coprecipitated chlorite. Upon dilution and cooling, stability of chloride complexes degenerates, with resultant deposition of metal sulfides. Zonation of sulfides is attributable either to relative stability of complexes as they break down or by inception of a self-potential galvanic cell generated within the metals (Govett and Whitehead, 1974).

According to Sangster's (1972) description, silica, with or without chlorite, is deposited late in the sequence and can be intimately deposited with the metal sulfides, or borne out into the surrounding basins for great distances to be precipitated as a chemical sediment. Such sedimentation commonly caps the sequence, and the basalt-rhyolite eruptive cycle can begin anew.

The Antler ores may have formed in a similar manner. It is difficult to establish the regional geology through the Hualapais and nearby ranges due to the intense deformation and the little that remains of the metavolcanics and metasediments. Anderson and Guilbert (1979) and Anderson (personal communication, 1979) have provided a

tentative regional reconstruction of the Proterozoic belts of central Arizona. Their studies indicate that the Hualapai belt falls well within the proposed oceanic arc evolutionary epoch for the central Arizona belts and, by correlation to the New River-Prescott-Jerome-Bagdad belts, is permissive of a volcanogene environment necessary for generation of massive sulfides.

From geochemistry and field evidence it is seen the Antler wallrocks are metavolcanics and metasediments, i.e., they are not solely sedimentary in origin. Their mixed heritage is important in genetically separating the deposits from Precambrian basinal deposits like the MacArthur River-type deposits or Zambian Belt-type near-shore diagenetic-syngenetic deposits. Amphibolites represent a series of metamorphosed basalt-andesite-dacite flows and tuffs; quartz-biotite-(potassium) feldspar schist represents metarhyolite tuffs and rare flows; quartz-biotite schist represents a metaarkose to metaarenite, possibly derived from rhyolitic tuffs; and quartz-mica schist, with its conglomerate unit and sections with graded bedding, represents a metapelite.

Significance of Cordierite-Anthophyllite Assemblages

A distinctive feature of the Antler orebody that sets it apart from other central Arizona massive sulfide orebodies is the unique fibrous silicate assemblage associated with sulfide mineralization. The cordierite-anthophyllite-biotite metamorphic assemblage

is a common associate of metamorphosed massive sulfide deposits, as at Rouyn, Noranda (de Rosen-Spence, 1969); Montauban Les Mines, Quebec (Seymour and MacLean, 1977); Gullbridge, Newfoundland (Upadhyay and Smitheringale, 1972); Notre Dame Bay deposit, Newfoundland (Bachinski, 1976); Coronation Mine, Saskatchewan (Whitmore, 1969); Falun deposits of central Sweden (Magnusson, 1960); Outokumpo, Finland (Vahatalo, 1953); and the Blue Hill district, Maine (Lindgren, 1933).

In more recent reports, petrographic and geochemical evidence has been convincingly marshalled to demonstrate generation of cordierite-anthophyllite assemblages by thermal metamorphism of pre-existing chloritic assemblages.

The following reaction illustrates the transformation:

$$\text{chlorite} + \text{quartz} = \text{anthophyllite} + \text{cordierite} + H_2O \qquad (1)$$

In his study of the Notre Dame Bay deposits, Newfoundland, Bachinski (1976) noted a change in iron relative to magnesium within chlorites from periphery to center of the pipes subjacent to ore zones, a phenomenon observed at many volcano-related massive sulfide occurrences, and attributed the Mg:Fe zonation to sulfide-chlorite interactions during metamorphism. Reaction 1 can be rewritten to account for sulfide-silicate reactions as:

$$\text{chlorite} + \text{quartz} + \text{pyrite} = \text{cordierite}\cdot H_2O + \text{anthophyllite} + \text{pyrrhotite} + \text{magnetite} + H_2O \qquad (1a)$$

The actinolite-dominant horizon in drillhole B6 can also be generated by the addition of appreciable calcite, dolomite, sericite, and potassium feldspar components with chlorite, using the classic mineral reactions commonly listed in mineralogical texts, and compatible with the observed assemblages:

chlorite + calcite + quartz = clinozoisite + actinolite + CO_2 + H_2O (2)

dolomite + quartz + H_2O = tremolite + calcite + CO_2 (3)

dolomite + microcline + H_2O = phlogopite + calcite + CO_2 (4)

dolomite + sericite = phlogopite + calcite + corundum + CO_2 (5)

corundum + quartz = sillimanite (6)

Necessity for calcium and magnesium in these reactions is easily afforded by a carbonate component in the section. While carbonation is an associate of chloritic alteration in Archean deposits, it is nevertheless a minor constituent. Interpretative sedimentary carbonate, along with tuffs or arkosic sediments, is required with chlorite to complete the reactions.

MacRae (1974), however, has been able to produce cordierite-anthophyllite and cordierite-andalusite assemblages experimentally by sulfurization of basalt at high temperatures (700°C), with the progressive removal of Fe and Ca to form pyrite and anhydrite. Such a model, however, requires maintenance of high f_{S_2} requiring

initial finely disseminated pyrite in a thick basalt pile. At the Antler, the present thickness of the amphibolites, even allowing for drastic tectonic thinning of units, would appear insufficient to account for the mass of components necessary to form cordierite and anthophyllite. And to have derived the required iron and magnesium from straight isochemical metamoprhism of a volcanic pile would require an initial wallrock composition of ultramafic proportions, which are not seen in the Hualapai Mountains. The more reasonable explanation for the Antler fibrous silicate assemblage lies in isochemical thermal metamorphism of pre-existing chlorite.

Metamorphism of Sulfides

Sulfides are relatively coarse grained as a consequence of folding and thermal incursion. Antler ore samples reveal a contorted and foliated fabric, showing plastic flowage of ductile sulfides about silicate knots and embrittled pyrite grains (Figure 32). Transposition of the ore zone and wallrocks resulted in thinning of sulfide horizons along limbs by dislocation of units on either side of the plastic sulfide mass. Pyrrhotite, sphalerite, chalcopyrite, and galena, which can plastically deform at 300°C and 2 kilobars pressure (Clark and Kelly, 1973; Salmon, Clark, and Kelly, 1974), were subjected to temperatures in excess of 500°C at the Antler Mine based on observed assemblages. Thermal input from emplacement and crystallization of the Cavalliere granodiorite and

Figure 32. Slabbed Specimen of Massive Sulfide Ore.

Note sulfide flowage about silicate knots. Specimen from Antler dump.

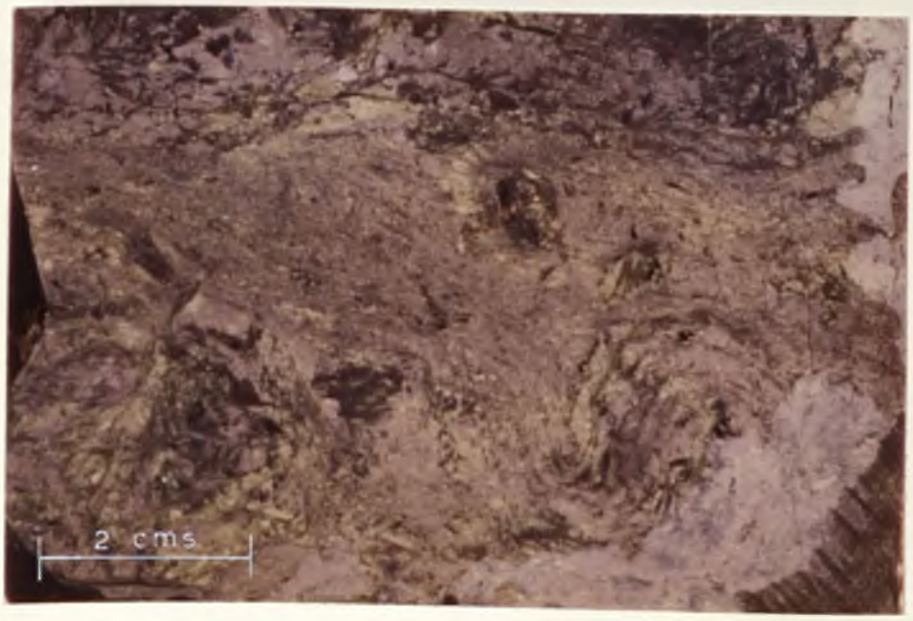

Figure 32. Slabbed Specimen of Massive Sulfide Ore.

Antler granite produced a coarsening of finely-disseminated sulfide grains and mineralogical phase changes by solid state transformation.

The predominance of pyrrhotite over pyrite is a common occurrence in highly metamorphosed massive sulfide deposits (MacDonald, 1967; Vokes, 1969; Sangster, 1972; Stanton, 1972; Mookerjee, 1976). Pyrite can be converted to pyrrhotite and magnetite by breakdown into iron and sulfur; if f_{O_2} is sufficiently high, iron combines with oxygen to form magnetite. Excess sulfur combines with remaining iron and possibly with iron-bearing chlorites, biotite, cordierite, and amphiboles to produce pyrrhotite plus iron-depleted silicates such as phlogopite. The presence of coexisting pyrrhotite and pyrite with magnetite in the Antler ores indicates that equilibrium was attained at or near the po-mag-py triple point.

The consistently high lead values near the present top of ore intercepts can only be accounted for by a primary zoning of lead prior to deformation. To invoke a migration of galena at such high prevailing temperatures and pressures (500°C and 1-4 kilobars) requires maintenance of a zone of lower permeability above the ore horizons contemporaneous with deformation (see Vokes, 1969, p. 134 and Clark et al., 1974, p. 15). Further, any transfer of components by injection "squeezing" or migration would result in features discernible as detached or elongated crosscutting lenses of galena concordant to foliation. It is more reasonable to call on a primary zoning or depositional layering of lead, as it appears to have remained intact relative to copper and zinc through deformation.

Some migration of components in the ore zone did occur during deformation. Large 5-10 cm gem-quality metacrysts of labradorite occur in pegmatites reported from the ore body. Vokes (1969) notes that migration of sulfides into structural troughs and crests can be accompanied by a transfer of alteration or wallrock constituents to produce quartz and feldspar pegmatites; both pegmatite types are found in the Antler ore horizons.

Antler Synthesis

Whether the Antler metavolcanics represent a lower predominantly tholeiitic cycle of volcanism or an upper predominantly calc-alkaline cycle with some minor tholeiitic pulses is difficult to determine, due to the lack of regional correlatives (see Anderson and Guilbert, 1979). Additionally, the number of basalt-rhyolite cycles in the area is unknown. Massive sulfide generation is generally more abundant in the upper calc-alkaline cycle of Arizona Proterozoic volcanic systems. Not enough regional data are available, however, to indicate whether a dual cycle of tholeiitic-calc-alkaline volcanism or a single tholeiitic cycle was erupted. Based on the preponderance of samples which fall within the tholeiitic field on the Jensen cation plot, bias is towards assignment of the Antler wallrocks to a single tholeiitic cycle.

It is reasonable to correlate the metavolcanic-metasedimentary setting of the central Hualapais with the Prescott-Jerome-Bagdad volcanic-sedimentary belts, and postulate an intraoceanic arc setting

in the 1850-1730 m.y. interval. Generation of a differentiating tholeiitic parent magma produced a volcanic complex of bimodally-erupted basalts and rhyolites, possibly on an oceanic basement, with sediments shed into surrounding basins. The Boriana series formed within this arc complex.

The volcanic complex is interpreted to have been off to the south or southwest of the present mine site, as there are no large structures in the canyon outside of the Bulge that are suggestive of a remnant metamorphosed volcanic pile. To the north toward the Boriana Mine, the quartz-mica schist metasediments become progressively more pelitic, indicating a basinal trend from the south or southwest. The thinness of the amphibolites suggests the basalt-andesite flows were not part of a shield, or volcanic edifice. They were probably deposited in a submarine environment, as suggested by the spotted amphibolite unit above the mine. The pelite-carbonate mixture comprising the leucocratic knots within the spotted amphibolite unit above the mine was intercalated in at least one flow. The cycle of basalt-andesite flows was followed by deposition of dacite-rhyolite tuffs and lesser interspersed sediments, the protoliths respectively of quartz-biotite and quartz-mica schists.

The "fragmental" nature of the quartz-biotite-(potassium) feldspar gneiss described on pages 21, 25 is equivocal. Angular fragments produced during final stages of explosive felsic volcanism are common in rhyolite horizons near the ore zones of many massive

sulfide deposits (Sangster, 1972). Rhyolite tuffs in which "fragments" are found at the Antler are certainly permissive of a "millrock" corollary. However, the folded geometry of the fragments (Figure 8) suggests structural thinning of a finely-laminated horizon within the rhyolite tuff, as in a submarine setting. The detached fold noses and elongated lenses within the units were structurally developed in the same manner as proposed for the spotted amphibolite unit.

Deposition of chlorite and sulfides was coeval with tuffaceous outpourings, flowing down from or precipitated near to a vent complex as a stratiform-to-podiform and strata-bound body, and buried by later tuffaceous and sedimentary accumulations. Some distance away, other masses of chlorite and sulfides settled into depressions to constitute the eventual Copper World lodes. Slight variations in the paleotopography allowed for interconnected, sometimes coalescing orebodies at the Antler site.

It may also be argued that orebodies and chlorite masses were part of an alteration pipe that was later tectonically flattened and transposed (Jenks, 1971) during deformation. However, the carbonate-rich section of the proto-chloritic alteration in B6 must still be accounted for. The slight lead zoning lends credence to a once-stratiform geometry.

Iron-rich, pyritiferous chert exhalites followed deposition of the sulfide bodies. At the Bulge, deposition of chert was closely

allied with chlorite bodies, as both occur at the same time stratigraphic horizon signified by the break from basaltic-andesitic into rhyolitic volcanism.

How many more cycles of basalt-andesite-rhyolite volcanism ensued is uncertain. However, if the sequence was from basaltic to rhyolitic volcanism with the younging direction in the Bulge to the southeast, then further accumulations of tuffs buried the exhalites. In turn, the tuffs were overlain by tuffaceous and pelitic sediments.

The Antler deposit is a proximal deposit, in the volcanogene sense of the word, although it has some distal qualities (Large, 1977; Anderson and Guilbert, 1979):

1. Metal content: copper-zinc rich, low lead values.
2. Alteration: uncertain geometry, interpreted as stratiform.
3. Iron species: pyrrhotite-dominant, lesser pyrite. Magnetite in apparent hangingwall.
4. Form: uncertain geometry, interpreted as stratiform. Stringer mineralization probably obscured by structure.
5. Metal Zoning: obscured, but higher lead values apparent in hangingwall.
6. Volcanic Setting: within a pile of volcanic tuffs with thin basalts, possibly fragmentals.

The Copper World Mine also is a proximal deposit, but the predominance of pyrite over pyrrhotite and tuffaceous rhyolites over

mixed volcanics indicates a slightly more distal setting than its counterpart. By Hutchinson's (1973) classification, both deposits fall into the Type I-Noranda-Mattagami copper-zinc massive sulfide category. Both occur within the more felsic portions of a bimodal volcanic pile and contain cogenetic exhalites precipitated at a basalt-rhyolite interface.

Structural Deformation

The northeasterly structural trend of Boriana Canyon is consistent with Precambrian terrains of the New River-Black Canyon, Bagdad, Prescott-Jerome, and Payson belts. Wilson (1939) described the regional Mazatzal Revolution deformational event producing northeast-trending foliation and fold axes. Silver (1965) and Anderson and Silver (1976) have dated the Mazatzal Revolution, placing the event between 1715 $\pm$ 15 m.y. and 1660 $\pm$ 15 m.y. However, Wilson originally confined the Mazatzal Revolution to the 1400 m.y. batholithic epoch of central Arizona. Silver and Anderson's dates of about 1700 m.y. dates possibly reflect an earlier deformational event and should be recognized as such.

The slight remnant foliation faintly discernible discordant to present foliation was produced during an early period of deformation. The weak schistosity is of uncertain and variable orientation but probably was concordant to bedding. Strong northwesterly compression followed and was contemporaneous with emplacement of the Cavalliere

granodiorite. Strong northeast-trending foliation and tight-to-isoclinal folds, with northeast axial trends, were produced. Transposition was concurrent with the folding. Progressive flexural-slip folding of a once-layered sequence led to attenuation of limbs and detachment of fold noses, producing isolated lenses, or pseudobedding, paralleling foliation (Whitten, 1966) and chevron, or kink, folding. Anatectic generation of the Antler granite proceeded, emplaced along a preexisting or coeval northeast basement break. Schistosity also developed in batholithic rocks and the Antler granite bodies. Lineations were produced by intersection of foliation with folds. At the Antler, the doubly plunging fold system and steeply-plunging lineations possibly were induced by relative "sinking" of the Antler section with respect to relative "rising" of the Cavalliere granodiorite and Antler granite bodies to the west and east.

A much later, possibly Mesozoic, period of northwest block faulting resulted in a series of progressive step faults across Boriana Canyon.

Evolution of the Bulge

Two models for the structural evolution of the Bulge are suggested by its overall fold-like form and shearing along edges: a fault model, and a pinch-and-swell fold model. In the first model, the volcanics and sediments were foliated during early deformation. Activation of west-northwest and northwest fault zones during later

deformation and batholithic activity produced both a left-lateral relative shear movement along the present southern edges and right-lateral movement along the northern edges, folding the units into their semi-circular course much in the manner of a drag-fold (Figure 33). Elevation of the triangular plate during batholithic encroachment along the faults, or flowage of the pluton about the mass, resulted in only weak transmittal of late-stage deforming stresses during later deformation. Overlap of the Bulge into the canyon produced northeast-trending foliation, grading into northwesterly foliation. Post-deformational reactivation and minor uplift or readjustment of the triangular plate was concurrent with development of step faulting to the south.

A second and perhaps more viable alternative is to compare Boriana Canyon with the "pinched-in" synclinal zones of Mesozoic sediments within the crystalline basement massifs of the alps (Ramsay, 1967). The metamorphic complex would appear in cross-section as a thin synclinal wedge of schist/gneiss entrapped within the granodiorite-quartz monzonite batholith. Consistent with this interpretation are mullion-type structures or folds generated by compressional deformation.

The interface between two layers of differing viscosities, corresponding to granodiorite and schist/gneiss in this case, becomes dynamically unstable with application of a principal compressive strain either normal or parallel to bedding. Perturbations along

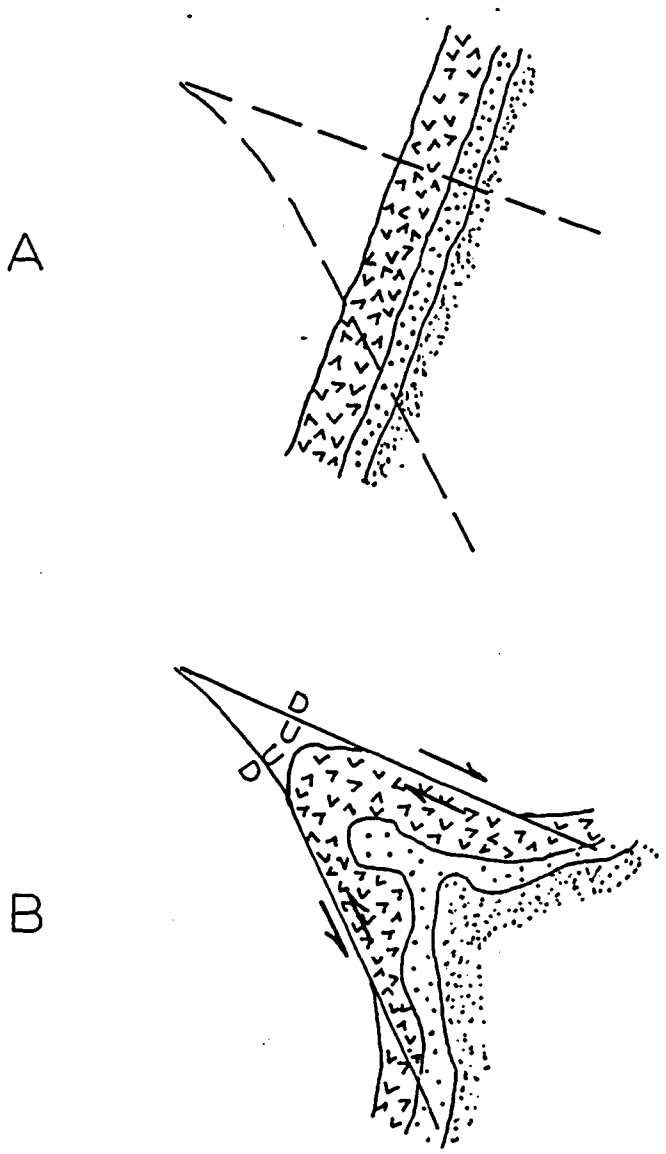

Figure 33. Schematic Illustration of the Structural Evolution of the Bulge: Fault Model. --
(a) Prefault setting.
(b) Activation of WNW and NW faults, and uplift.

the interface lead to mullion or pinch-and-swell fold structures. Smith (1975) points out the structures formed are dependent on the relative rigidity of the thinner bed (schist/gneiss) to the enclosing layers (granodiorite). With an applied compressional strain normal to bedding, boudins or inverse folds will develop; strain parallel to bedding forms normal folds or mullion structures.

The suggestion is advanced that the Bulge and its eastern mirror counterpart at the Copper World Mine, which projects into the quartz monzonite, might represent a pinch-and-swell fold or mega-boudin-like mass formed by northwesterly compression acting on a "thin" layer of schist/gneiss. By inspection of the geologic map on a large scale (Figure 1, in pocket) the canyon thus would appear to constitute a neck to the protrusions. The small-scale, transposed, boudin-like structures seen in Boriana Canyon are consistent with compressive deformational processes. Further regional studies should help to elucidate this interpretation.

Alternative Models

The alternative models for genesis of the Antler and Copper World ores are:

1. Epigenetic hydrothermal replacement of favorable horizons.
2. Sedimentary basinal derivation.
3. Syngenetic-diagenetic sedimentary derivation.

The classic post-metamorphic hydrothermal argument is inconsistent with the lack of crosscutting mineralized features within

ore horizons or within the granodiorite or granite pluton, the absence of alteration effects and permeability "channels" within the pluton or subjacent wallrocks, the textural nature of sulfides and silicates, and the nature of the magnesian alteration horizons.

The sedimentary basin model of the MacArthur River type may be applicable here. However, attention is directed to basalt-rhyolite volcanism in direct association with the Antler ore, the massive nature of the ore, the fibrous silicates probably representing metamorphism of a chloritized conduit assemblage, and the lack of more basinal sediments such as siltstones, dolomites, purple slates, and others in the mine vicinity. Antler ore zone rocks appear generally more volcanic in their geochemical profiles. Arguments involving original grain sizes and textures are invalid, but it should be noted that Cu/Zn/Pb/Ag/minor element ratios of the MacArthur River deposits contrast sharply with those of volcanogenic massive sulfide deposits and the Antler deposit.

The protolith lithology of the Antler wallrocks also eliminates a syngenetic-diagenetic Zambian Copper Belt ore model. Quartz arenites, carbonaceous and silty arenites, and dolomites are host rocks to the Zambian copper deposits. Mineralization is copper, iron, and lesser cobalt, precipitated in a near-shore environment over a large area. Boriana rocks appear to have been basalts, andesites, rhyolite tuffs, and arkosic and pelitic sediments with short narrow horizons of copper, zinc, and iron sulfides deposited in a subaerial volcanic complex.

Conclusions

Evidence for the probable volcanogenic origin of the Antler and Copper World ores is indirect, as transposition during folding has obliterated nearly all primary lithologic features. Mixed igneous-sedimentary protolith of the wallrocks as inferred from petrochemistry, the possible regional correlations in timing, lithology, and tectonic setting with other volcanogenic central Arizona massive sulfides, and comparison with several similar Archean deposits are provocative, but direct proof of a syngenetic origin of the Antler and Copper World lodes is still tentative. However, weakness of other genetic models which might be applied essentially forces adoption of the volcanogenic model by the explorationist.

The stratiform geometry of the sulfide body is deduced from the involvement of tuffaceous and carbonate components with the sulfide-silicate mass and an assumed genetic model of a subaerial vent or volcanic-fumarolic complex. A pipe-shaped geometry of the original orebody that was later tectonically transposed into a flattened body would imply a root zone complex located somewhere off to the south or southwest. If the orebody was solely a stratiform mass precipitated onto the seafloor, the possibility that other ore bodies were emplaced nearby is intriguing, as only two deposits, the Antler and Copper World, have been discovered to date. Step-out exploration into the alluvial-filled valley to the southwest is definitely justified by either conceptual geometry as it is into the terrain between the two deposits.

Further geophysical investigation at the Bulge is also indicated. The copper-iron oxide staining within schists and the cogenetic cordierite-anthophyllite and iron formation bodies hint at mineralization at depth. To date, the Bulge has not been tested by drilling.

An interesting feature at the two mines and in Bulge outcrops is the cordierite-anthophyllite fibrous silicate assemblage. While both minerals can be found separately in middle grade metapelites in many central Arizona belts, the mutual occurrence of the assemblage is indicative of derivation by thermal metamorphism of preexisting chlorite. Recognition of cordierite-anthophyllite rocks ascertains the former presence of rocks containing chlorite, of either hydrothermal or sedimentary origin, that were subsequently metamorphosed. The assemblage, termed "dalmatianite" in the Noranda district of Canada, has been noted in many Precambrian and Mesozoic terrains in the western United States, but the important connection to possible submarine volcanism generation of proto-chlorite often is not made.

Ore reserves developed by the latest series of exploratory drill holes at the Antler Mine show the body to be a substantial deposit of economic interest. Further investigation in the Hualapais and northwestern Arizona for more sulfide bodies is amply justified.

APPENDIX I

ELECTRON MICROPROBE DATA

Cordierite - collected from hilltop above Antler Mine.

Oxide:	Concentration (wt. %):	Stoichiometry:	
Na_2O:	0.10%	Na:	0.0199
K_2O:	0.04	K:	0.0053
CaO:	0.04	Ca:	0.0039
Al_2O_3:	33.39	Al:	3.9580
SiO_2:	49.89	Si:	5.0187
MgO:	8.81	Mg:	1.3212
MnO:	0.01	Mn:	0.0008
Cr_2O_3:	0.00	Cr:	0.0000
FeO:	8.13	Fe:	0.6868
TiO_2:	0.00	Ti:	0.0000
Oxygen:	0.00	O:	18.0000
Total:	100.44%		

Garnet - collected from hilltop above Antler Mine.

Oxide:	Concentration (wt. %):	Stoichiometry:	
Na_2O:	0.04%	Na:	0.0113
K_2O:	0.04	K:	0.0090
CaO:	1.17	Ca:	0.1986
Al_2O_3:	20.73	Al:	3.8773
SiO_2:	37.84	Si:	6.0045
MgO:	4.14	Mg:	0.9788
MnO:	1.28	Mn:	0.1725
Cr_2O_3:	0.01	Cr:	0.0015
FeO:	36.27	Fe:	4.8123
TiO_2:	0.00	Ti:	0.0000
Oxygen:	0.00	O:	24.0000
Total:	101.52%		

Sulfide Ore - B2-1425

	CONCENTRATION (wt. %)										
	Fe	S	As	Cu	Zn	Ag	Ni	Pb	Cr	Co	Total %
Sphalerite:	8.92	31.58	0.07	5.59	52.88	--	--	0.21	--	0.04	99.3
	8.02	30.86	--	0.38	56.12	--	--	0.37	--	0.04	95.8
Chalcopyrite:	30.79	32.71	0.13	34.97	0.41	--	--	--	--	0.10	99.1
	30.96	31.57	0.09	34.80	0.22	--	--	--	--	0.05	97.7
Galena:	0.31	11.32	--	0.24	2.32	0.04	--	83.90	--	0.01	98.1
Pyrite:	46.58	49.32	0.19	--	0.16	--	0.02	--	--	0.12	96.6
	47.08	48.94	0.25	--	0.11	0.03	--	0.05	--	0.19	96.6
Pyrrhotite:	60.75	36.60	0.32	0.21	0.14	--	0.02	0.04	--	0.13	98.3

APPENDIX II

MINERAL ABBREVIATIONS UTILIZED IN TEXT

act = actinolite

alb = albite

and = andalusite

anth = anthophyllite

biot = biotite

cal = calcite

chl = chlorite

cord = cordierite

cpx = clinopyroxene

cumm = cummingtonite

epid = epidote

gedr = gedrite

gt = garnet

hast = hastingsite

hb = hornblende

Kfs = potassium feldspar

mag = magnetite

musc = muscovite

opq = opaque

phlog = phlogopite

po = pyrrhotite

py = pyrite

qz = quartz

ser = sericite

serp = serpentine

sill = sillimanite

trem = tremolite

APPENDIX III

WALLROCK AND FIBROUS SILICATE GEOCHEMICAL DATA

Wallrock sample location:

Drillhole B6 -

1669 - quartz-hornblende-feldspar gneiss (amphibolite)

1684 - hornblende-plagioclase gneiss (amphibolite)

1741 - quartz-biotite-(potassium) feldspar schist

1843 - quartz-biotite-(potassium) feldspar schist

1880 - quartz-biotite schist (hangingwall)

2065 - quartz-biotite schist (footwall)

2114 - quartz-biotite schist

Surface samples -

AM-2: quartz-hornblende-feldspar schist - approximately 30' below Cavalliere granodiorite-amphibolite contact, uppermost drill road west of Antler Mine. NE¼ NW¼ NW¼ NE¼ SE¼, sec. 4, T17N, R16W.

AM-3: quartz-biotite-(potassium) feldspar schist - 100' lower along drill road from AM-2. SE¼ NW¼ NW¼ NE¼ SE¼, sec. 4, T17N, R16W.

AM-4: hornblende-plagioclase gneiss - 3-way drill road intersection, west of Antler Mine. NE¼ NW¼ SW¼ NE¼ SE¼, sec. 4, T17N, R16W.

AM-7: quartz-mica schist - stream cut 150' west of intersection with ranch trail. SE¼ SW¼ NW¼ SW¼ NW¼, sec. 2, T17N,R16W.

AM-8: quartz-biotite schist - 100' south of Antler Mine shaft. NW¼ NE¼ SW¼ NE¼ SE¼, sec. 4, T17N, R16W.

AM-9: quartz-mica schist - along ridge top, approximately 100' south of prospect pits. SE¼ SE¼ SE¼ NW¼ SW¼, sec. 35, T18N, R16W.

Miscellaneous -

AM-5: iron formation - 200' east of Bulge drill road. SW¼ NW¼ NE¼ SW¼ NW¼, sec. 26, T18N, R16W.

AM-6: iron formation - 200' east of Bulge drill road terminus. NW¼ SE¼ NW¼ NE¼ SE¼, sec. 27, T18N, R16W.

Drillhole B6, silicate alteration -

1898 - biotite-anthophyllite silicate alteration

1964 - cordierite-anthophyllite silicate alteration

2004 - anthophyllite silicate alteration with some disseminated sulfides

2054 - massive sulfide ore with biotite-anthophyllite-actinolite silicate alteration

Table 4. Whole Rock Data for the Antler Mine Wallrocks. -- (by X-Ray Assay Labs)

	Sample Number														
Oxide Wt. %	AM2 qhf	AM3 qbf	AM4 hp	AM7 qm	AM8 qb	AM9 qm	B6-1669 qhf	1684 hp	1741 qbf	1843 qbf	1880 qb	2065 qb	2114 qbf	Std.1	Std.1 Known
SiO_2	68.4	76.0	49.5	76.7	76.5	73.9	59.6	49.8	79.0	68.9	75.1	72.8	76.0	68.4	(66.4)
Al_2O_3	12.5	12.2	15.2	12.6	11.6	13.6	15.2	14.7	10.8	12.2	11.5	12.3	10.7	15.3	(14.3)
CaO	6.27	1.44	14.8	0.89	0.47	0.75	5.77	11.8	1.13	1.81	0.18	1.05	1.20	2.25	(2.10)
MgO	2.48	0.14	6.34	0.94	0.63	0.97	1.46	5.59	0.34	1.34	0.99	0.68	0.19	0.86	(0.92)
Na_2O	3.77	3.65	2.95	2.09	1.99	1.38	3.86	3.38	5.04	2.07	0.55	3.12	2.48	2.95	(2.90)
K_2O	0.76	3.59	0.31	2.66	5.53	3.66	0.80	0.83	0.54	3.54	6.85	3.76	3.75	5.32	(5.20)
FeO*	3.6	1.6	7.3	2.2	1.9	3.2	7.5	8.8	2.0	7.5	3.6	4.8	3.8	--	
Fe_2O_3	1.35	1.03	1.99	1.28	1.00	1.72	4.20	3.10	0.69	1.28	0.59	0.62	1.25	3.85(total)	
MnO	0.15	0.16	0.16	0.13	0.15	0.28	0.42	0.16	0.17	0.66	0.43	0.40	0.40	0.06	
TiO_2	0.53	0.16	1.34	0.41	0.16	0.49	0.90	1.58	0.21	0.65	0.21	0.38	0.26	0.65	
P_2O_5	0.10	0.03	0.13	0.09	0.02	0.08	0.38	0.16	0.03	0.09	0.04	0.06	0.03	0.29	
LOI	0.08	0.23	0.38	0.92	0.54	0.69	0.08	0.41	1.69	0.23	0.46	0.38	0.23	0.92	
SUM	95.7	99.4	100.4	98.8	96.3	100.5	100.8	98.8	100.7	101.1	99.1	99.4	98.6	96.7	
Rock type by silica index	rhyodacite	rhyolite	basalt	(pelitic sediment)	rhyolite	(pelitic sediment)	andesite	basalt	rhyolite	rhyodacite	rhyolite	rhyolite	rhyolite		

*Wet chemical analysis by Barringer Research.

Table 5. Trace-Element Data for the Antler Mine Wallrocks. -- (by Barringer Research)

Trace element (ppm)	Sample Number AM2	AM3	AM4	AM7	AM8	AM9	B6-1669	B6-1684	B6-1741	B6-1843	B6-1880	B6-2065	B6-2114
Cr	157	45.4	133	83	50.1	146	175	78.9	57.4	245	77.3	120	157
Ni	69	36	89	39	38	90	115	65	52	184	81	101	137
Zr	80	60	40	88	128	60	78	36	123	99	114	105	128
Sr	168	96.8	151	145	101	75.4	279	293	59.7	114	68.7	75.4	110
Ba	942	1450	993	825	1530	1110	867	946	443	310	1880	1150	1200
Co	5	4	39	14	12	17	29	45	9	29	12	12	15
As	240	240	240	150	250	230	220	230	170	250	260	250	80
Cu	14.5	11.1	3.1	19.6	39.1	187	25.8	5.4	13.4	59.3	26.1	30.1	31.7
Zn	10	40	42	89	478	151	36	55	32	91	202	109	44
Pub	5	5	5	20	50	5	40	10	5	10	55	15	10
Ag	--	--	--	--	--	--	--	--	--	--	--	--	--
Cd	--	--	--	--	--	--	--	--	--	--	--	--	7
V	56.4	5.8	219	33.6	1.7	46.6	13.9	239	7.1	75.3	9.1	28.8	3.4
Be	1.6	2.4	0.5	1.8	0.7	17.5	2.0	0.8	1.3	2.1	0.7	2.4	2.0
Th	--	14	--	17	22	13	6	--	17	16	23	22	46

Table 6. Whole Rock Data for Iron Formations and Silicate Alteration. -- (by Barringer Research)*

Oxide Wt. %	Sample Number AM-5 iron formation	AM-6 iron formation	B6-1898 silicate	B6-1964 silicate	B6-2004 silicate	B6-2054 massive sulfide
SiO_2	(87.8)	(93.6)	68.4	(44.7)	52.0	(41.9)
Al_2O_3	.343	.343	11.2	14.8	4.77	4.31
CaO	.560	1.03	.397	.325	.158	.831
MgO	.783	1.03	5.28	5.59	29.3	3.31
Na_2O	--	0.010	.508	.664	.484	1.11
K_2O	--	0.020	.680	.180	2.07	1.17
FeO	5.1	3.7	9.9	19.6	8.6	9.3
Fe_2O_3	(11.2)	(4.3)	2.7	(3.5)	2.7	(16.6)
MnO	.260	.257	.362	.269	.168	.718
TiO_2	.0196	.0159	.476	.909	.0216	.0794
P_2O_5	--	--	--	0.05	--	--
LOI	N/A	N/A	N/A	1.34	N/A	2.75
Sum	(106.07)	(104.31)	99.90	(90.57)	100.27	(82.09)

Table 7. Trace-Element Data for Iron Formations and Silicate Alteration. -- (by Barringer Research)

Trace element (ppm)	Sample Number AM5	AM6	B6-1898	B6-1964	B6-2004	B6-2054
Cr	150	76.1	198	150	46.8	329
Ni	85	67	118	44	15	183
Zr	--	--	89	90	14	34
Sr	2.9	2.2	28.4	39.9	11.2	8.0
Ba	37	32	1150	1870	618	105
Co	--	--	--	--	--	--
As	--	--	160	210	40	50
Cu	138	29.4	305	74.6	2580	32,000
Zn	39	143	142	68	2050	46,100
Pb	5	5	50	125	425	3550
Ag	--	--	--	--	--	23
Cd	--	--	--	--	--	20
V	11.5	4.1	29.9	53.0	8.9	1.1
Be	0.1	0.7	--	0.1	0.2	0.6
Th	--	--	9	7	--	--

Table 8. Niggli Data for Antler Wallrocks.

Sample Number	mg	al	fm	c	alk	al-alk	k
AM-2	0.47	28.25	30.11	25.77	15.88	12.37	0.12
AM-3	0.08	42.24	14.44	9.07	34.25	7.99	0.39
AM-4	0.55	19.88	38.13	35.20	6.79	13.09	0.06
AM-7	0.32	45.22	26.29	5.81	22.68	22.54	0.46
AM-8	0.28	42.18	21.03	3.11	33.68	8.50	0.65
AM-9	0.26	44.17	31.16	4.43	20.24	23.93	0.64
B6-1669	0.18	28.57	38.15	19.72	13.56	15.01	0.12
B6-1684	0.46	20.02	41.96	29.22	8.80	11.22	0.14
B6-1741	0.18	40.67	18.17	7.74	33.43	7.24	0.66
B6-1843	0.20	30.90	42.42	8.34	18.34	12.56	0.53
B6-1880	0.28	39.47	30.84	1.12	28.56	10.91	0.89
B6-2065	0.17	36.92	39.72	5.73	27.63	9.29	0.44
B6-2114	0.06	36.81	27.68	7.51	28.00	8.81	0.50

Table 9. Ternary Cation Percentage Data for Antler Wallrocks. -- For use with Jensen Cation Plot (Figure 31).

Sample Number	$FeO+Fe_2O_3+TiO_2$	Al_2O_3	MgO
AM-2	19.64	64.16	16.20
AM-3	13.66	85.11	1.23
AM-4	24.20	49.52	26.29
AM-7	16.50	76.26	7.23
AM-8	14.80	79.66	5.54
AM-9	20.45	72.87	6.68
B6-1669	34.11	58.70	7.19
B6-1684	30.23	47.01	22.76
B6-1741	15.35	81.40	3.25
B6-1843	32.32	59.35	8.33
B6-1880	19.61	72.46	7.93
B6-2065	23.63	71.34	5.02
B6-2114	25.51	72.85	1.64

Table 10. Listing of Silicate Alteration Assemblages.

Note: Sulfides not included in estimates.

B1:

1348.5 - 60% anth, 15% biot, 1% act, 1% musc, 4% chl, 10% qz

1350 - 60% anth, 2% chl, 10% qz, 2% Kfs

1351.5 - 12% anth, 5% biot, 1% chl, 65% qz

1353 - 5% anth, 50% biot, 3% phlog, 1% chl, 1% carb, 20% qz

1356 - 10% anth, 25% biot, 5% phlog, 5% musc, 5% chl, 30% qz, 3% alb, 5% Kfs

B3:

1131 - 20% anth, 70% phlog

1137 - 7% anth, 60% act, 20% phlog, 3% chl

B7:

1552 - 40% musc, 56% phlog

1555 - 1% anth, 90% act, 6% gt, 3% cumm

1556 - 85% act

B2:

Horizon 1 -

1248 - 25% biot, 25% phlog, 42% qz, 5% chl, 0.5% calc

1260 - 23% cord, 40% anth, 16% chl, 2% carb, 5% qz, 5% qt

1275.5 - 15% anth, 15% act, 20% ser, 7% chl, 2% carb, 36% qz

1277 - 1% biot, 25% act, 12% ser, 2% chl, 0.5% carb, 53% qz, 5% opq, 5% anth

Table 10, Continued.

B2: (continued)

1289.5 - 7% anth, 10% phlog, 2% biot, 20% act, 3% chl, 1% carb, 45% qz 3% serp

Horizon 2 -

1406 - 1% anth, 17% biot, 7% ser, 4% chl, 57% qz, 1% mag, 3% serp, 7% sill

1412 - 25% biot, 5% musc, 2% chl, 60% qz

1420 - 55% biot, 7% musc, 5% chl, 32% qz, 1% gt

1423 - 1% anth, 55% biot, 1% musc, 1% chl, 35% qz

1435 - 80% biot, 1% musc, 1% chl, 1% carb, 10% qz, 1% gt

1439 - 40% biot, 30% musc, 1% chl, 1% carb, 14% qz, 0.5% gt

1443 - 1% anth, 12% biot, 33% musc, 50% qz, 0.5% gt

B6:

1895 - 50% anth, 37% phlog, 7% chl, 3% qz

1896 - 30% anth, 2% act, 2% biot, 55% phlog, 5% musc, 2% qz

1903 - 5% cord, 47% anth, 2% act, 2% phlog, 5% musc, 5% chl, 35% qz

1908 - 55% cord, 20% anth, 15% chl, 5% qz

1913 - 20% cord, 20% qz, 3% act, 40% anth, 3% chl

1925 - 2% cord, 77% anth, 2% chl, 3% qz, 1% serp

1935 - 35% cord, 42% anth, 10% act, 2% chl, 2% qz, 3% serp

1954 - 3% anth, 32% biot, 2% act, 3% musc, 10% chl, 3% serp

1974 - 25% cord, 55% anth, 2% musc, 3% chl, 10% qz, 3% serp

1984 - 42% anth, 10% gedr,5% phlog, 10% chl, 10% act, 3% ser

1990 - 30% gedr, 55% anth, 7% chl

1995 - 10% gedr, 30% anth, 1% act, 50% phlog, 4% chl

Table 10, Continued.

B6: (continued)

1998 - 75% anth, 5% gedr, 9% phlog, 2% chl, 2% act

2000.5 - 20% gedr, 35% anth, 1% act, 1% chl, 40% phlog

2003.5 - 40% anth, 2% act, 35% phlog

2008 - 25% gedr, 45% phlog, 5% musc, 12% gt, 2% act, 1% carb

2017 - 25% anth, 35% act, 3% cumm

2020 - 20% anth, 30% phlog, 14% act, 5% musc, 1% chl, 8% carb

2025 - 80% phlog, 5% chl, 5% carb

2026 - 3% anth, 30% act, 3% chl, 24% carb, 5% serp

2029 - 40%(?) carb + act(?)

2031 - 50%(?) carb + act(?)

2039 - 78% act, 1% chl, 5% anth, 1% carb, 0.5% sill

2042 - 5% anth, 80% act, 1% carb

2045 - 5% anth, 75% act, 4% chl, 2% carb, 2% sill, 3% serp

2056 - 10% anth, 10% biot, 10% musc, 15% chl, 4% sill, 35% qz, 3% serp, 5% gt

LIST OF REFERENCES

Anderson, C. A., and Nash, J. T., 1972, Geology of the massive sulfide deposits at Jerome, Arizona - a reinterpretation: Econ. Geol., v. 67, p. 845-63.

Anderson, C. A., and Silver, L. T., 1976, Yavapai Series: A greenstone belt: Ariz. Geol. Soc. Digest, v. 10, p. 13-26.

Anderson, P. A., 1979, personal communication.

Anderson, P. A., and Guilbert, J. M., 1979, The Precambrian massive sulfide deposits of Arizona - a distinct metallogenic epoch and province: Proceedings of the Fifth Symposium of the International Association on the Genesis of Ore Deposits, p. 39-48.

Bachinski, D. J., 1976, Metamorphism of cupriferous iron sulfide deposits, Notre Dame Bay, Newfoundland: Econ. Geol., v. 71, p. 443-52.

Barth, T., 1962, Theoretical petrology: New York, John Wiley and Sons, Inc., 416 p.

Brook, D. K., 1974, Relative ages of stratiform sulfide ore and wallrock determined by structural analysis of the Copper Queen mine, Yavapai County, Arizona: Unpub. M.S. thesis, The University of Arizona, Tucson, 60 p.

Chapell, B. W., and White, A. J. R., 1974, Two contrasting granite types: Pac. Geol., v. 8, p. 173-4.

Clark, B. R., and Kelly, W. C., 1973, Sulfide deformation studies: I. Experimental deformation of pyrrhotite and sphalerite to 2000 bars and 500°C: Econ. Geol., v. 68, p. 332-52.

Clayton, R. L., and Baker, A., 1973, Pb-Pb ages of a galena sample from the Bruce Mine, Yavapai County, Arizona: Isochron. West, no. 6, p. 35.

Constantinou, G., and Govett, G. J. S., 1973, Geology, geochemistry, and genesis of Cyprus sulfide deposits: Econ. Geol., v. 68, p. 843-58.

de Rosen-Spence, A., 1969, Genese des roches a cordierite-anthophyllite des gisements cupro-zinciferes de la region de Rouyn-Noranda, Quebec, Canada: Can. Jour. Earth Sci., v. 6, p. 1339-45.

DeWitt, E., 1976, Precambrian geology and ore deposits of the Mayer-Crown King area, Yavapai County, Arizona: Unpub. M.S. thesis, The University of Arizona, Tucson, 150 p.

Evans, B. W., and Leake, B. E., 1960, The composition and origin of the striped amphibolites of Connemarra, Ireland: Jour. Petrol., v. 1, p. 337-63.

Forrester, J. D., 1963, Report on the Bobcat Mining Company property (Copper World Mine) near Yucca, Mohave County, Arizona: private report prepared for the University of Arizona, Tucson, 18 p.

Fraser, J. A., and Heywood, W. W., eds., 1978, Metamorphism in the Canadian Shield: Can. Geol. Surv. Paper 78-10, 367 p.

Gelinas, L., Brooks, C., Perrault, G., Carignan, J., Trudel, P., and Grasso, F., 1977, Chemostratigraphic divisions within the Abitibi volcanic belt, Rouyn-Noranda District, Quebec, in Baragar, W. R. A., ed., Volcanic regimes of Canada: Geol. Assoc. Canada Spec. Paper 16, p. 265-95.

Gilmour, P., 1965, The origin of the massive sulphide mineralization in the Noranda District, northwestern Quebec: Proc. Geol. Assoc. Can., v. 16, p. 63-81.

_____, 1971, Strata-bound massive pyritic sulfide deposits - a review: Econ. Geol., v. 66, p. 1239-44.

_____, 1975, Preliminary feasibility study, Antler Mine, Mohave County, Arizona: private report prepared for Standard Metals Corp., 34 p.

Gilmour, P., and Still, A. R., 1968, The geology of the Iron King Mine: in Ridge, J. D., ed., Ore deposits of the United States, 1933-1967, v. 2: New York, Amer. Inst. Min. Met. Engrs., p. 1238-57.

Goodwin, A. M., 1965, Mineralized volcanic complexes in the Porcupine-Kirkland Lake-Noranda region, Canada: Econ. Geol., v. 60, p. 955-71.

Govett, G. J. S., and Whitehead, R. E. S., 1974, Origin of metal zoning in stratiform sulfides: a hypothesis: Econ. Geol., v. 69, p. 551-56.

Hobbs, S. W., 1944, Tungsten deposits in the Boriana district and the Aquarius Range, Mohave County, Arizona: U.S. Geol. Survey Bull. 940-I, p. 247-65.

Holt, E. B., 1944, Antler Mine in Mohave County, Arizona: Min. Jour., v. 27, no. 19, p. 3-4.

Horikoshi, E., 1969, Volcanic activity related to the formation of the Kuroko-type deposits in the Kosaka district, Japan: Mineral. Deposita, v. 4, p. 321-45.

Hutchinson, R. W., 1973, Volcanogenic sulfide deposits and their metallogenic significance: Econ. Geol., v. 68, p. 1223-46.

Jenks, W. F., 1971, Tectonic transport of massive sulfide deposits in submarine volcanic and sedimentary host rocks: Econ. Geol., v. 66, p. 1215-24.

Jensen, L. S., 1976, A new cation plot for classifying subalkalic volcanic rocks: Ontario Div. Mines Misc. Paper 66, 22 p.

Kessler, E. J., 1976, Rubidium-strontium geochronology and trace element geochemistry of Precambrian rocks in the northern Hualapai Mountains, Mohave County, Arizona: Unpub. M.S. thesis, The University of Arizona, Tucson, 73 p.

Krauskopf, K., 1967, Introduction to geochemistry: New York, McGraw-Hill, 721 p.

Kuno, H., 1953, Formation of calderas and magmatic evolution: Trans. Am. Geophys. Un., v. 34, p. 267-80.

_____, 1966, Lateral variation of basalt magma type across continental margins and island arcs: Bull. Volcanol., v. 29, p. 195-222.

Lane, D., 1979, personal communication.

Large, R. R., 1977, Chemical evolution and zonation of massive sulfide deposits in volcanic terrains: Econ. Geol., v. 72, p. 549-572.

Larson, P. B., 1976, The metamorphosed alteration zone associated with the Bruce Precambrian volcanogenic massive sulfide deposit, Yavapai County, Arizona: Unpub. M.S. thesis, The University of Arizona, Tucson, 98 p.

Leake, B. E., 1964, The chemical distinction between ortho- and para-amphibolites: Jour. Petrol., v. 5, p. 238-54.

Lindgren, W., 1933, Mineral deposits, 4th edition: New York, McGraw-Hill, 930 p.

MacDonald, J. A., 1967, Metamorphism and its effect on sulphide assemblages: Mineral. Deposita, v. 2, p. 200-20.

MacRae, N. D., 1974, Sulfurization of basalt under thermal metamorphic conditions to produce cordierite-bearing rocks: Can. Jour. Earth Sci., v. 11, p. 246-53.

Magnusson, N. H., 1960, Iron and sulfide ores of central Sweden: Int. Geol. Cong., 21st session, 1960. Guide to excursions no. A26 and C21.

Matsukuma, T., and Horikoshi, E., 1970, Kuroko deposits in Japan, a review: in Tatsumi, T., ed., Volcanism and ore genesis: Tokyo, Univ. of Tokyo Press, p. 153-79.

Mauger, R. L., 1973, A geologic interpretation and sulfur isotope study of the Old Dick and Copper Queen massive sulfide deposits, Bagdad area, Arizona (abs.): Econ. Geol., v. 68, p. 1208.

Mookerjee, A., 1976, Ores and metamorphism: temporal and genetic relationships: in Wolf, R. H., ed., Handbook of strata-bound and stratiform ore deposits, v. 4: New York, Elsevier Scientific Publishing Co., p. 203-60.

Nielsen, P. A., 1978, Metamorphism of the Arseno Lake area, Northwest Territories: in Fraser, J. A., and Heywood, W. W., eds., Metamorphism in the Canadian Shield: Can. Geol. Surv. Paper 78-10, p. 115-22.

Oftedahl, C., 1958, A theory of exhalative-sedimentary ores: Geol. Foren. Stockholm Forh., v. 80, pt. 1, #492, p. 1-19.

Putman, G. W., and Burnham, C. W., 1963, Trace elements in igneous rocks, northwest and central Arizona: Geochem. Cosmoch. Acta, v. 27, p. 53-106.

Ramsay, J. G., 1967, Folding and fracturing in rocks: New York, McGraw-Hill, 568 p.

Rasor, C. A., 1946, Loellingite from Arizona: Am. Mineral., v. 31, p. 406-8.

Ridler, R. H., 1970, Relationship of mineralization to volcanic stratigraphy in the Kirkland-Larder Lake area, Ontario: Proc. Geol. Assoc. Canada, v. 21, p. 33-42.

Romslo, T. M., and Wilson, E. D., 1948, Antler copper-zinc deposit, Mohave County, Arizona: U.S. Bur. Mines ROI4214, 14 p.

Salmon, B. C., Clark, B. R., and Kelly, W. C., 1974, Sulfide deformation studies: II. Experimental deformation of galena to 2000 bars and 400°C: Econ. Geol., v. 69, p. 1-16.

Sangster, D. F., 1972, Precambrian volcanogenic massive sulfide deposits in Canada: A review: Can. Geol. Surv. Paper 72-22, 44 p.

Seymour, K. S., and MacLean, W. H., 1977, The geochemistry of possible metavolcanic rocks and their relationship to mineralization at Montauban-Les-Mines, Quebec: Can. Jour. Earth Sci., v. 14, p. 2440-52.

Sillitoe, R. H., 1973, Environments of formation of volcanogenic massive sulfide deposits: Econ. Geol., v. 68, p. 1321-25.

Silman, J. F. B., 1966, Geological and geophysical investigations of the Copper World Mine: private report prepared for Standard Copper Corporation, August, 1966, 21 p.

Silver, L. T., 1965, Mazatzal orogeny and tectonic episodicity (abs.): Geol. Soc. America Spec. Paper 82, p. 185-6.

Simmons, B. D., and the Geological Staff, 1973, Geology of the Millenbach massive sulfide deposit, Noranda, Quebec: Can. Inst. Min. Metall. Bull., v. 66, p. 67-78.

Smith, R. B., 1975, Unified theory of the onset of folding, boudinage, and mullion structure: Geol. Soc. Amer. Bull., v. 86, p. 1601-9.

Spence, C. D., and de Rosen-Spence, A., 1975, The place of sulfide mineralization in the volcanic sequence at Noranda, Quebec: Econ. Geol., v. 70, p. 90-101.

Spitz, G., and Darling, R., 1975, The petrochemistry of altered volcanic rocks surrounding the Louvem copper deposit, Val D'Or, Quebec: Can. Jour. Earth Sci., v. 12, p. 1820-49.

Spry, A., 1969, Metamorphic textures: New York, Pergammon Press, 350 p.

Stanton, R. L., 1972, Ore petrology: New York, McGraw-Hill Book Co., 713 p.

Stanton, R. L., 1976, Petrochemical studies of the ore environment at Broken Hill, New South Wales: Trans. Inst. Min. Met., v. 89, p. B33-46, B118-42, B221-33.

Stensrud, H. L., 1979, personal communication.

Still, A. R., 1974, Review of geology and recommendations for exploration, Antler Mine and adjacent areas, Mohave County, Arizona: private report prepared for Standard Metals Corporation, 34 p.

Tatsumi, T., and Clark, L. A., 1972, Chemical composition of acid volcanic rocks genetically related to formation of Kuroko deposits: Jour. Geol. Soc. Japan, v. 78, p. 191-201.

Tatsumi, T., and Watanabe, T., 1971, Geological environment of formation of the Kuroko deposits: Soc. Min. Geol. Japan, Spec. Issue 3, p. 216-20.

Upadhyay, H. D., and Smitheringale, W. G., 1972, Geology of the Gullbridge copper deposit, Newfoundland: Volcanogenic sulfides in cordierite-anthophyllite rocks: Can. Jour. Earth Sci., v. 9, p. 1061-73.

Vahatalo, V. O., 1953, On the geology of the Outokumpu ore deposit in Finland: Bull. Comm. Geol. Finlande 164.

Van De Kamp, P. C., 1968, Geochemistry and origin of metasediments in the Haliburton-Modoc area, southeastern Ontario: Can. Jour. Earth Sci., v. 5, p. 1337-72.

Vokes, F. M., 1969, A review of the metamorphism of sulphide deposits; Earth Sci. Rev., v. 5, p. 99-143.

Webb, W. F., 1979, Precambrian geology and ore deposits near Poland Junction, Yavapai County, Arizona: Unpub. M.S. thesis, The University of Arizona, Tucson, 113 p.

Whitmore, D. R. E., 1969, Geology of the Coronation copper deposit: in Symposium on geology of Coronation Mine, Saskatchewan: Geol. Surv. Can. Paper 68-5, p. 37-53.

Whitten, E. H. T., 1966, Structural geology of folded rocks: Chicago, Rand-McNally, 663 p.

Wilson, E. D., 1939, Pre-Cambrian Mazatzal revolution in central Arizona: Geol. Soc. Amer. Bull., v. 50, p. 1113-64.

Winkler, H. G. F., 1967, Petrogenesis of metamorphic rocks, second edition: New York, Springer-Verlag, 237 p.

_____, 1976, Petrogenesis of metamorphic rocks, fourth edition: New York, Springer-Verlag, 334 p.

2 pieces in pocket

FIGURE 2. GEOLOGIC MAP OF THE ANTLER MINE AND VICINITY, MOHAVE COUNTY, ARIZONA: PHOTO-LINEARS

Scale = 1 : 6000

500′ 0 500′ 1000′ 1500′ 2000′ 2500′

1″ = 500′

0 100 200 300 400 500m.

1cm. = 60m.

CONTOUR INTERVAL = 200′

by
SYVER W. MORE
– 1979 –

Reference: Wabayuma Peak 7.5′
Creamery Canyon 7.5′
Cedar Valley Mining District

LEGEND

POST-PRECAMBRIAN

- Quaternary alluvium

PRECAMBRIAN

- db — Diabase
- p — Pegmatite
- ag — Antler granite
- cgd — Cavalliere granodiorite
- qmo — Quartz monzonite
- im — Injection migmatite
- qm — Quartz-muscovite schist
- qb — Quartz-biotite schist
- qbf — Quartz-biotite-feldspar schist/gneiss
- qhf — Quartz-hornblende-feldspar gneiss
- hp / hp′ — amphibolite — Hornblende-plagioclase gneiss; (′pseudofragmental texture)

- Massive fibrous silicates
- Quartz-magnetite formation
- Secondary roads
- Mineshaft
- Prospect

SYMBOLS

- Geologic contact, dashed where inferred
- Foliation orientation
- Antiform / Synform
- Overturned antiform / synform
- Shear zone
- Fault, showing relative displacement.
- Photo-linear defined structures

Other symbols as per convention.

MORE, S.W., M.S. THESIS, 1980, DEPT. OF GEOSCIENCES, UNIV. OF ARIZONA.

Copper World Mine

Antler Mine

Joshua Fault

Ocotillo Fault

Soguaro Fault

Breccia

conglomeratic section

FIGURE 1. GEOLOGIC MAP OF THE ANTLER MINE AND VICINITY, MOHAVE COUNTY, ARIZONA.

Scale = 1 : 6000

500' 0 500' 1000' 1500' 2000' 2500'

1" = 500'

0 100 200 300 400 500m.

1cm.=60m.

CONTOUR INTERVAL = 200'

by
SYVER W. MORE
– 1979 –

Reference: Wabayuma Peak 7.5'
Creamery Canyon 7.5'
Cedar Valley Mining District

LEGEND

POST-PRECAMBRIAN

- Quaternary alluvium
- db — Diabase
- p — Pegmatite
- ag — Antler granite
- cgd — Cavalliere granodiorite
- qmo — Quartz monzonite

PRECAMBRIAN

- im — Injection migmatite
- qm — Quartz-muscovite schist
- qb — Quartz-biotite schist
- qbf — Quartz-biotite-feldspar schist/gneiss
- qhf — Quartz-hornblende-feldspar gneiss
- hp / hp' — Hornblende-plagioclase gneiss; ('pseudofragmental texture) — amphibolite

- Massive fibrous silicates
- Quartz-magnetite formation
- Secondary roads
- Mineshaft
- Prospect

SYMBOLS

- Geologic contact, dashed where inferred.
- Foliation orientation
- Antiform / Synform
- Overturned antiform / synform
- Shear zone
- Fault, showing relative displacement. (U / D)

Other symbols as per convention.

MORE, S.W., M.S. THESIS, 1980, DEPT. OF GEOSCIENCES, UNIV. OF ARIZONA.